MATERIALS SCIENCE AND ENGINEERING

A Publication of the University of Miskolc

Volume 39, Number 2 (2014)

CONTENTS

LINEAR VISCOELASTIC PROPERTIES OF ASPHALT MASTICS USING CREEP-RECOVERY TECHNIQUE

RÓBERT GÉBER[1]–A. APKARYAN[2]–S. KULKOV[3]–LÁSZLÓ A. GÖMZE[4]

In the present work, we deal with the rheological properties of asphalt mastics made with mineral fillers, as well as with the relation of fine grain fillers to bitumen. The utilization of dolomite can (potentially) reduce the current use of limestone in Hungarian road construction. By testing different fillers, various asphalt mastic mixtures has been created, in which the effects of type, grain size and quantity (volume fraction) of the fillers could be observed at the same time. Rheological tests were performed on the mastics in the linear viscoelastic region (LVE) to describe the behaviour of asphalt pavements in summer. For the analysis of the creep-recovery features, the behaviour of the mastics has been described with the four-parameter Burgers model where the parameters were numerically defined. In view of the results, we could conclude that the coarse grains in the mastics increase the elasticity of the mixtures in each case and consequently reduce the deformation developed under the effect of load as well as the amount of deformation remaining from recovery. It has also been proved that with the use of limestone, minor deformations developed, which is attributable to the fact that limestone creates a stronger relation with the binder.

Keywords: asphalt mastics, creep, filler, recovery, rheology

Introduction

Asphalt mastics, which is the mixture of bitumen and filler, is the most important component of asphalt concretes. It affects both the cohesion between coarse grains (i.e. the load-carrying capacity of the layer) and the strength and stiffness of the pavement [1, 2]. A fundamental point in the (composite) structure formed with bitumen is the origin of the mineral filler [3, 4]).

The behaviour of asphalt pavements also depend on the type of loading as well as on temperature [5]. Therefore, pavements are considered as viscoelastic material systems during their entire life-cycle, which means that viscous and elastic properties are simultaneously present. It is possible to study the properties of binder-and-asphalt-mixtures under linear viscoelastic circumstances and to reveal the relationships between them [6, 7].

Creep-recovery test is a suitable technique to analyse the viscoelastic properties of different materials such as asphalt mastics. One of the most common rheological model that describes the total deformation of a viscoelastic system due to constant loading (creep) and unloading (recovery) is the four parameter Burgers model (Fig. 1, Eqs. (1) and (2)) [8].

---

[1] University of Miskolc, Institute of Ceramics and Polymer Engineering
    3515 Miskolc-Egyetemváros, Hungary
    femgeber@uni-miskolc.hu
[2] Tomsk State University of Control Systems and Radioelectronics
[3] Tomsk State University Institute of Strength Physics and Materials Science SB RAS
[4] University of Miskolc, Institute of Ceramics and Polymer Engineering
    3515 Miskolc-Egyetemváros, Hungary
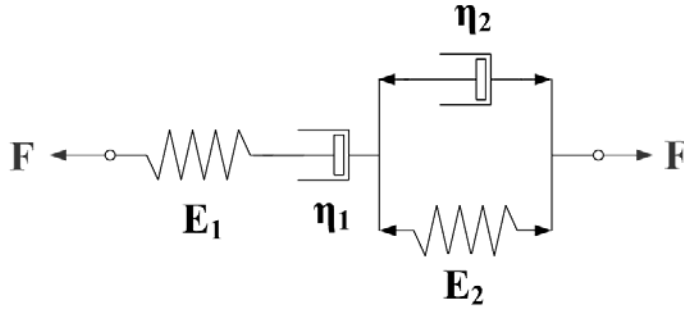
Figure 1. Burgers model

Burgers equation in creep stage:

$$\varepsilon_{sum}(t) = \frac{\sigma_0}{E_1} + \frac{\sigma_0}{\eta_1} \cdot t + \frac{\sigma_0}{E_2} \cdot \left(1 - e^{-\frac{E_2}{\eta_2} \cdot t}\right)$$

(1)

where:

ε_{sum}: the sum of elastic deformations [–]
σ_0: constant shear stress [Pa]
E_1 and E_2: elastic moduli of two spring elements of the Burgers model [Pa]
η_1 and η_2: viscosity of two dashpot elements of the Burgers model [Pa·s]
t: loading time [s]

Burgers equation in recovery stage:

$$\varepsilon_{sum} = \varepsilon_0 + \dot{\varepsilon} \cdot t_2 + \varepsilon_1 \cdot (1 - e^{\frac{-t_2}{\lambda_2}})$$

(2)

where:

ε_{sum}: the sum of elastic deformations [–]
ε_0: instantaneous deformation at recovery stage [–]
ε_1: delayed deformation at recovery stage [–]
$\dot{\varepsilon}$: shear rate [s^{-1}]
t_2: time at the end of recovery stage [s]
λ_2: retardation time [s]

There are another two other parameters that properly describe the deformations of the material system: recovered part and permanent deformation (Fig. 2).

Figure 2. Representation of the parameters "recovered part" and "permanent deformation"

The most widely used filler is limestone, and Hungary is rich in good quality mineral resources of it. Industrial requests, however, urge on the use of another type of mineral dolomite, which might reduce the current use of limestone. The need for the utilization of dolomite in road construction has enco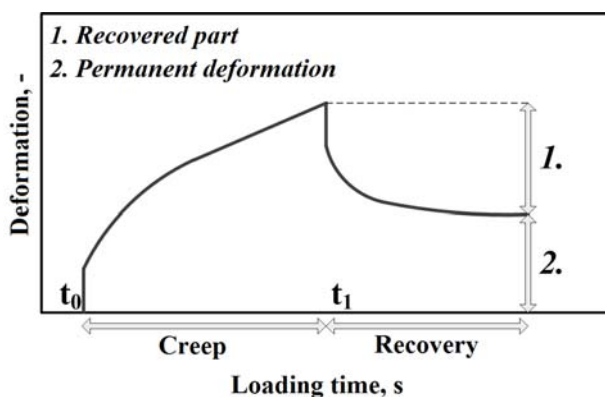uraged this research work and gave us impetus for further investigations. Given the above, the aims of this research were the followings:

- By the use of fillers, various asphalt mastic mixtures have been created, in which the effect of two fillers of different grain size and quantity (volume fraction) was be observed at the same time. Rheological tests were performed on the mastics to describe the behaviour of asphalt pavements in summer.
- Creep-recovery tests made it possible to fit the viscoelastic rheological model with the test results, which provided a well-based mathematical description of the processes in asphalt mastics during constant loading and unloading. With this method, it was also possible to define the exact rheological model and the model parameters.
- With the measuring methods used, our research has set forth to investigate rutting, the typical defect of pavements.

1. Sample preparation and experimental procedures

Mineral materials were prepared with the following methods in all cases. Raw materials − limestone /Mexikóvölgy/ and dolomite /Pilisvörösvár/ − were available in bags in bulk state. Dolomite was supplied in two different ranges (d<0.3 mm and d<0.045 mm, respectively) previously fractioned by the manufacturer. Our purpose was to create units of the mineral materials that are smaller than a given grain size. Thus, the raw mineral materials were fractioned into two different fractions (d<0.063 mm and d<0.045 mm) using standard sieves. The fractions were then dried to weight-constancy in a drying chamber. After cooling, the samples were hermetically sealed in containers to avoid moisture uptake until further investigation. The physical properties of the fillers are shown in Table 1.

Physical properties of the fillers

Filler	Mineral composition	Bulk density (g·cm^{-3})	BET specific surface area of fractions (m^2·g^{-1})
Limestone (*Mexikóvölgy*)	CaCO$_3$ (100 wt%)	2.717	d<0.045 mm: 1.11
			d<0.063 mm: 1.02
Dolomite (*Pilisvörösvár*)	MgCa(CO$_3$)$_2$ (100 wt%)	2.842	d<0.045 mm: 1.10
			d<0.063 mm: 0.38

To determine particle size distribution, laser granulometric tests of the fractioned fillers were made with a Horiba LA-950V2 instrument using wet method. In order to dispergate the mineral fillers, 0.5 ml of sodium-pyrophosphate was added to each sample and ultrasonic treatment was applied for 1 minute.

During the research work, asphalt mastic samples were prepared with the use of two mineral fillers abundantly available in Hungary (limestone from Mexikóvölgy and dolomite from Pilisvörösvár), and from standard bitumen (Százhalombatta) with a penetration grade of 50/70. The filler to mastics volumetric ratios (i.e. filler volume/mastics volume; F/M ratio) were selected as 5%, 13% and 20%.

The mineral fillers were mixed with bitumen at a temperature of 160 °C with 500 rpm mixing speed in a mixer. With these options/under these conditions, voidless, particle-filled asphalt mastics were produced (Table 2.).

Composition of the tested asphalt mastics

No.	Mixture	Binder	Type of filler	Particle size	F/M ratio
1	Bitumen		–	–	–
2	LS_45μm_005				0.05
3	LS_45μm_013			d<0.045 mm	0.13
4	LS_45μm_020		Limestone (*Mexikóvölgy*)		0.20
5	LS_63μm_005				0.05
6	LS_63μm_013	B50/70 bitumen (*Százhalombatta*)		d<0.063 mm	0.13
7	LS_63μm_020				0.20
8	D_45μm_005				0.05
9	D_45μm_013			d<0.045 mm	0.13
10	D_45μm_020		Dolomite (*Pilisvörösvár*)		0.20
11	D_63μm_005				0.05
12	D_63μm_013			d<0.063 mm	0.13
13	D_63μm_020				0.20

A Haake RheoStress RS80 dynamic shear rheometer with a standard 25 mm diameter parallel plate (or plate-plate) testing geometry was used to determine the LVE properties of asphalt mastics by creep-recovery method.

Considering the particle size of the tested mineral fillers, the gap size of the rheometer was set at 1.5 mm. The rheological tests were performed at 60 °C considering the pavement temperature in summer. During the research program, creep-recovery tests were performed on the mastics samples within the linear viscoelastic (LVE) region, therefore the applied shear stress was $\tau_0 = 1$ Pa. A loading time of $t_1 = 60$ s (creep) and an unloading time of $t_2 = 180$ s (recovery) were chosen, as recommended by the literature [5, 9, 10].

2. Results and discussion

2.1. Laser granulometric tests of mineral fillers

A large amount (~25%) of fine grains was detected with laser granulometric tests. Grains under the size of 10 microns are decisive from the viewpoint of the role of these fillers in asphalt mixtures. In dolomite (d<0.063 mm), however, the amount of these fine grains hardly reached 1%. At the same time, in the d<0.045 mm fraction, the presence of grains under the size of 10 microns was highly significant (~38%). Figure 2. shows the results of particle size distribution tests.
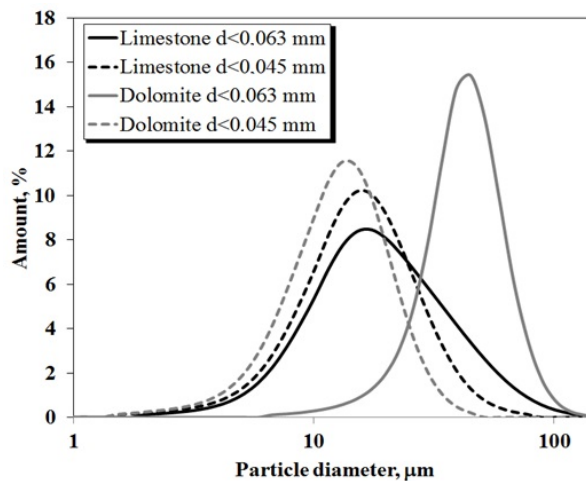
Figure 2. Particlesize distribution of fillers

2.2. Creep-recovery tests of asphalt-mastics

In view of the results, it was concluded that the presence of coarse grains in the mastics increased the elasticity of the mixtures (in each case) and thus decreased the deformation developed under the effect of load and the deformation remaining from recovery. It was also proved that with the use of limestone, minor deformations would develop due to the stronger binding of limestone to the binder. The results of creep-recovery tests are shown in Figure 3 and Table 3.

Recovered part and permanent deformation

Sample	Recovered part (%)	Permanent deformation (%)
Bitumen	54.27	45.73
LS_45μm_005	40.24	59.76
LS_45μm_013	43.42	56.58
LS_45μm_020	72.69	27.31
LS_63μm_005	77.98	22.02
LS_63μm_013	49.04	50.96
LS_63μm_020	50.55	49.45
D_45μm_005	11.11	88.89
D_45μm_013	13.35	86.65
D_45μm_020	31.70	68.30
D_63μm_005	36.25	63.75
D_63μm_013	27.51	72.49
D_63μm_020	16.57	83.43

Figure 3. Results of the creep-recovery tests

Conclusions

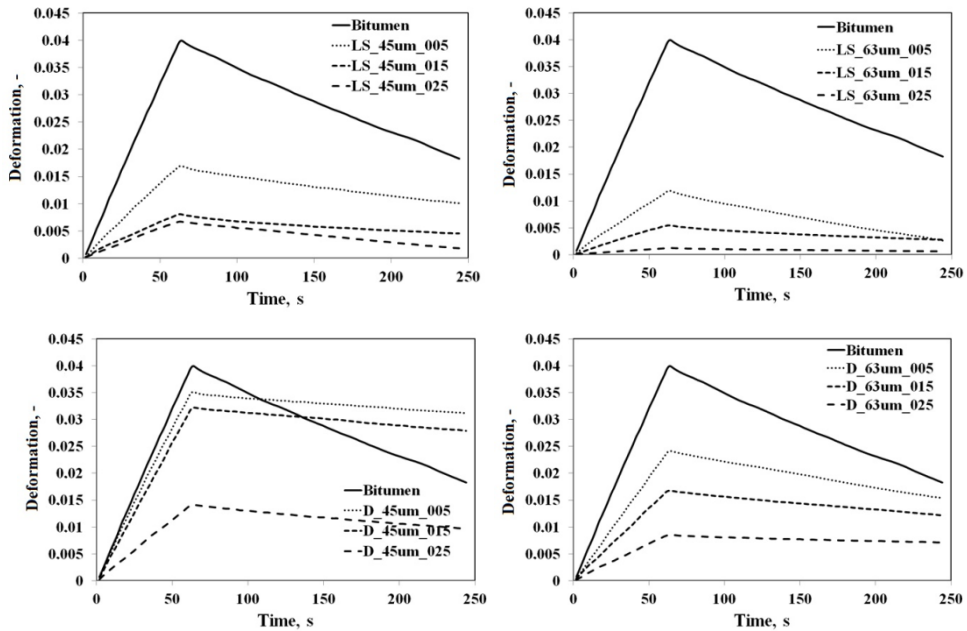Based on the analysis of creep-recovery features, this study has set forth to describe the behaviour of mastics with the four-parameter Burgers model. In view of the results it was stated that the elasticity of the mixtures increases and consequently, the deformation under load and that remaining from recovery reduces with the fraction of coarse grains in the mastics. It has also been proved that the use of limestone leads to minor deformations due to the stronger binding relation of the limestone with the binder.

Acknowledgements

References

[1] Grabowski, W.–Wilanowicz, J.: The structure of mineral fillers and their stiffening properties in filler-bitumen mastics. *Materials and Structures,* Vol. 41. pp. 793–804 (2008).
[2] Aljassar, A. H.–Metwali, S.–Ali, M. A.: Effect of filler types on Marshall stability and retained strength of asphalt concrete; *The International Journal of Pavement Engineering,* Vol. 58, No. 1, pp. 47–51 (2004).
[3] Gezentsvey, L. B.: *Road asphalt concrete;* Moskva, Stroynadat (1960).
[4] Lesueur, D.: The colloidal structure of bitumen: Consequences on the rheology and on the mechanisms of bitumen modification. *Advances in Colloid and Interface Science,* Vol. 145, pp. 42–82 (2009).
[5] Chen, J.: Rheological properties of asphalt-mineral filler mastics; *Journal of Materials, Concrete Structures and Pavements,* Vol. 36,. No. 571, pp. 269–277 (1997).
[6] Buttlar, W. G.–Roque, R:: Evaluation of empirical and theoretical models to determine asphalt mixtures stiffnesses at low temperature. *Association of Asphalt Paving Technology,* Vol. 65, pp. 99–141. (1996).
[7] Kavussi, A.–Hicks, R. G.: Properties of bituminous mixtures containing different fillers. *Journal of Association of Asphalt Paving Technologists.* Vol. 66, pp. 153–186 (1997).
[8] Liu, Y.–You, Z.: Determining Burger's Model Parameters of Asphalt Materials Using Creep-Recovery Testing Data. *Pavements and Materials: Modeling, Testing and Performance*, pp. 26–36 (2008).
[9] Kim, H.–Lee, J.–Amirkhanian, S.: Rheology investigation of crumb rubber modified asphalt binders. *KSCE Journal of Civil Engineering,* Vol. 14, pp. 839–843 (2010).
[10] Liu, C.–Wu, S.–Liu, Q.–Zhu, G.: Rheological characteristics of aged asphalt binder. *Journal of Central South University of Technology,* Vol. 15,. pp. 298−301 (2008)

EXTRACTION OF TIN FROM OXIDIZED SOLDERING DROSS BY CARBOTHERMIC REDUCTION AND ACID LEACHING

ZOLTÁN HARANGI[1]–TAMÁS KÉKESI[2]

The melting of soldering scrap originating from the electronic industry produces *inter alia* oxide dross, composed mainly of SnO_2, which is resistant to the lixiviants most commonly used for hydrometallurgical treatment. We have investigated the possibility of converting this SnO_2 into a soluble form by carbothermic reduction using coke powder in the 800–1000 ^{o}C temperature range. The raw material for the experiments was obtained by increasing the SnO_2 concentration in the dross skimmed from the tin bath by further oxidation at high temperature. The treated dross and the products were examined with scanning electron microscopy and X-ray powder diffraction (XRD). The efficiency of the treatment was determined by leaching the reduced material with boiling 6 mol dm^{-3} HCl solution. The obtained solutions were analyzed by atomic absorption to determine the dissolved portion of tin content. Under optimized conditions, it was possible to reach conversion rates higher than 90% of the originally insoluble tin-dioxide content.
Keywords: soldering waste, tin dioxide, carbothermic reduction, solubility

Introduction

The soldering and surface coating technologies applied in the electronic industry generate a layer of oxidized dross at the surface of the tin melt. It is removed periodically by skimming and it contains a large amount of entrapped metal. According to a novel process [1–2], the metallic component is separated by re-melting the primary dross and after skimming, the molten metal is cast into anodes for electrorefining. During this re-melting step a significant amount of secondary oxide dross is skimmed off the surface of the metal bath. The aim of this research is to find a method which can facilitate the recycling of tin from that oxide based heterogeneous waste material. However, the SnO_2 matrix is highly refractory [3]. It is rather difficult to dissolve either in acids or in bases [4]. This difficulty can be overcome by applying a preliminary reduction to achieve the conversion of SnO_2 into the soluble metallic or the lower state oxide forms. As it is shown in Fig. 1, the thermodynamic conditions would allow the reduction of SnO_2 by carbon in standard states (applying unit value relative partial pressure of CO_2) above approximately 700 ^{o}C. The required reaction is, however, more likely to occur through an indirect mechanism, with CO acting as the effective reducing reagent. Not only kinetic but also thermodynamic feasibility is more beneficial in this way. Even in a CO/CO_2 gas mixture of unit partial pressure ratio, the process is possible at temperatures above 400 ^{o}C. The reducing CO gas can be produced by the initial oxidation of the coke particles and the subsequent Boudouard-reaction. However, the latter step – as commonly known – requires

---

[1] University of Miskolc, Institute of Metallurgy and Foundry Engineering
   3515 Miskolc-Egyetemváros, Hungary
[2] University of Miskolc, Institute of Metallurgy and Foundry Engineering
   3515 Miskolc-Egyetemváros, Hungary
   kekesi@uni-miskolc.hu

temperatures higher than 800 ^{o}C. Besides thermodynamics, the kinetics of the reaction may require the application of even higher temperatures.
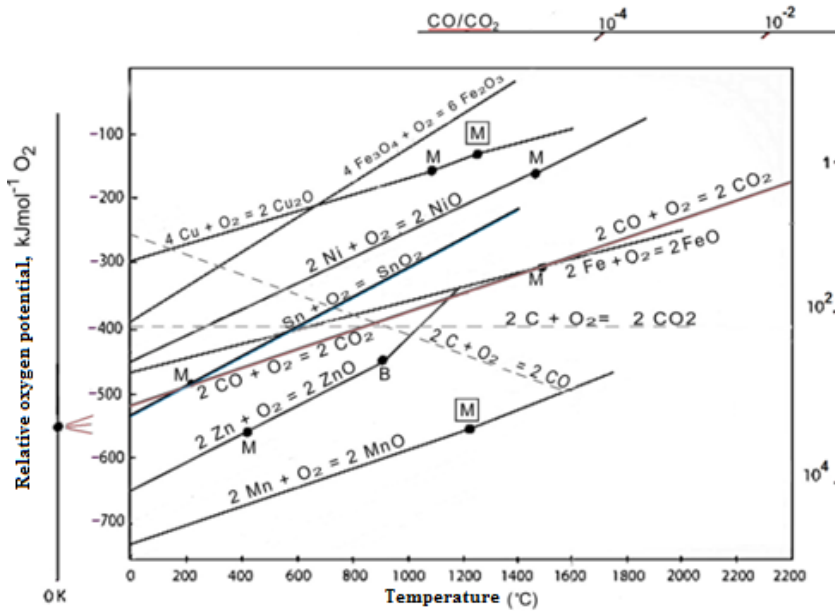

Figure 1. The relative oxygen potential of the reactions

Mitchell and Parker [5] reduced pure stannic oxide with anthracite and graphite powder. They demonstrated that the reaction is practically possible in the temperature range of 800 to 1000 ^{o}C, yet the reaction rate was strongly dependent on temperature. At 1000 ^{o}C, the whole conversion process required only 5 minutes; at 800 ^{o}C it took more than half an hour. The rate of recovery was found proportional to the used proportion of carbon in the 1–3 C/SnO_2 mol ratio range, but the final carbon consumption corresponded to the overall reaction expressed as:

$$SnO_{2(s)} + C_{(s)} = Sn_{(l)} + CO_{2(g)} \tag{1}$$
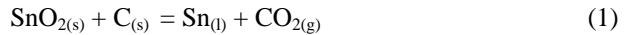
The main steps of the reaction can be assumed as:

$$C_{(s)} + O_{2(g)} = CO_{2(g)} \tag{2}$$
$$C_{(s)} + CO_{2(g)} = 2\ CO_{(g)} \tag{3}$$
$$SnO_{2\ (s)} + CO_{(g)} = SnO_{(s,g)} + CO_{2(g)} \tag{4}$$
$$SnO_{(s)} + CO_{(g)} = Sn_{(l)} + CO_{2(g)} \tag{5}$$
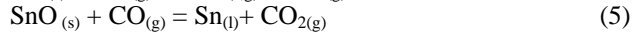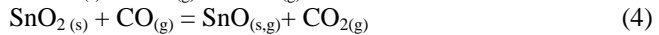
This assumed mechanism explains for the strong change in the conversion rates observed in the experiments referred as the temperature was increased to 1000 ^{o}C.

According to the thermodynamic consideration, such a reduction has the potential to produce metallic tin. However, tin will be embedded in a dispersed form in the residual material. Therefore, hydrometallurgical processing – implying a hydrochloric acid leaching

and a subsequent extraction from the tin chloride solution by electrowinning [1, 2] –seems indispensable.

1. Experimental Materials and Procedure

By heating up the soldering waste material – the primary dross – over the liquidus temperature of the metal, the contained metallic and non-metallic components can be separated. After careful skimming, the removed secondary dross was oxidized at 700 ^{o}C in a crucible furnace to convert most of the still remaining metallic portion into tin-dioxide. The oxidized material was ground and attrited in a ceramic mortar, then the brittle oxide particles were separated from the residual metal by passing the powder through a 0.2 mm sieve. In this way, by increasing the concentration of SnO_2 in the tested material, we obtained results that more clearly reflected the behavior of the oxide fraction of the dross. The main steps of the dross pre-treatment are shown in Fig. 2. The fine powder used as the raw material for the leaching tests was examined in different ways. The scanning electron microscope (SEM) image and the relevant energy dispersive X-ray spectrum (EDS) are shown in Fig. 3.
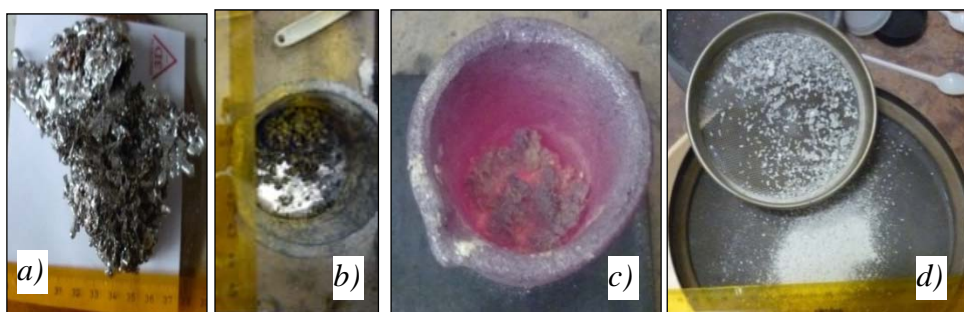

Figure 2. Pre-treatment of the soldering tin dross to produce the raw material for testing
a – raw dross, b – extracted metal and secondary dross, c – oxidation, d – fine oxide powder
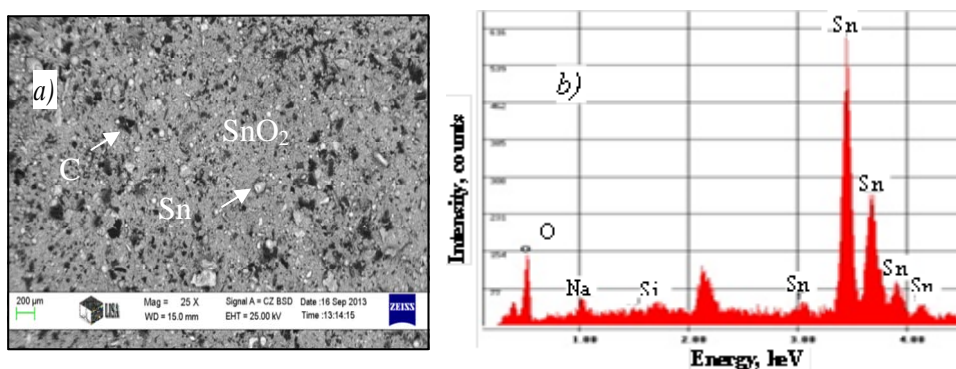

Figure 3. The SEM image (a) and EDS spectrum (b) of the pre-treated SnO_2 powder

According to both the SEM and EDX examinations, the oxidized fine powder obtained from the pre-treatment of the tin dross contained mainly tin and oxygen. The phase composition of the material was examined by X-ray diffraction (XRD), the result is given in the diffractogram of Fig. 4.
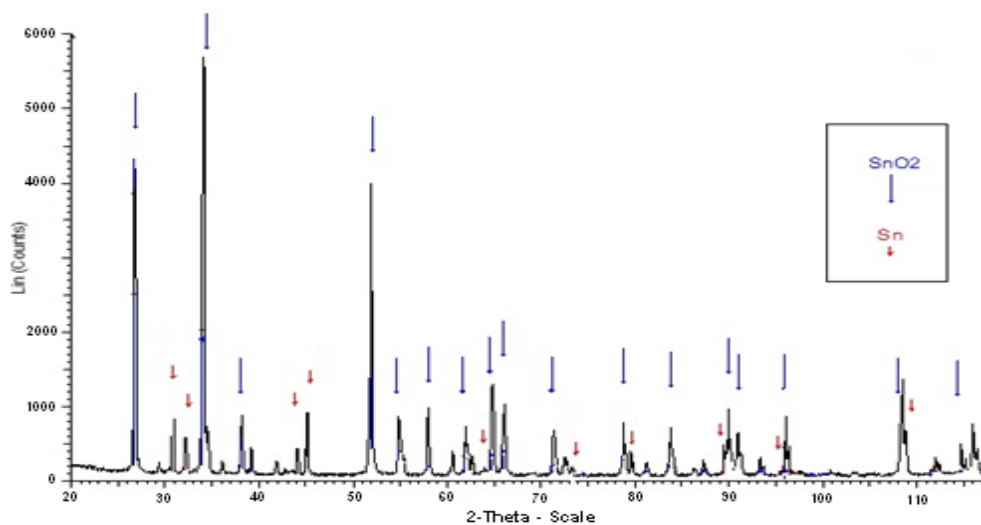
Figure 4. X-ray diffraction pattern of the treated tin dross

The elemental analysis regarding the metal content was carried out by applying inductively coupled plasma atomic emission spectrometry (ICP-AES) method after a complete digestion procedure. The results are given in Table 1, which also includes the composition of the metal bath obtained at the first step (Fig. 2*b*) in the pre-treating procedure.

Table 1

Elemental analysis of the examined SnO_2 powder and the metal bath

Material	Concentration, mass percent						
	Ag	Cu	Fe	Ni	Pb	Zn	Sn
Oxidized dross	0.0101	1.29	0.044	0.030	0.0190	1.32	**71.6**
Metal bath	0.0059	1.72	0.022	0.012	0.0056	0.0068	**~98**

A minor amount of metallic tin was still found in the oxidized and mechanically separated fine SnO_2 powder. This was determined from the measured volume of the hydrogen gas that evolved during the dissolution of tin in hot 6 mol dm^{-3} HCl solution:

$$Sn + 2HCl = SnCl_2 + H_2 \qquad (6)$$

The released hydrogen was collected in a gas burette connected to the reactor, and the volume was converted to standard conditions at room temperature so as to determine the concentration of the metallic tin in a sample of mass m_{sample} (g):

$$c_{Sn} = \left[\sum_i \left(V_i \frac{p_o - \rho g h_i - p_{H_2O}}{p_o} \right) \cdot \frac{298}{T} \cdot \frac{119}{2 \cdot 24 \cdot 1000} \right] \cdot \frac{100}{m_{sample}} \qquad (7)$$

where c_{Sn} is the tin concentration in mass percent, V_i is the partial volume of the gas collected (cm^3), ρ is the density of the solution (kg m^{-3}) and p_{H2O} is the vapour pressure of the solution (Pa) at a height of h_i (m) above the level of the solution in the reactor. The temperature of the system is T (K). Performing this analysis with the necessary repetitions, the remaining metal concentration in the oxidised dross was found to be 16 mass %. In actual practice, however, the metal content of the dross would be definitely higher, which nonetheless causes no difference in the suitability of the hydrometallurgical processing route. The original metal content will behave the same way as the metal obtained by the reduction of the dross.

In order to determine the kinetically efficient range of the intended reaction, preliminary investigations were also carried out by derivatography. The pre-treated oxide based pulverized raw material was charged in the corundum crucible of the C-MOM type derivatograph either directly or mixed with coke. Controlled heating was carried out in contact with air. The results are given in Fig. 5.
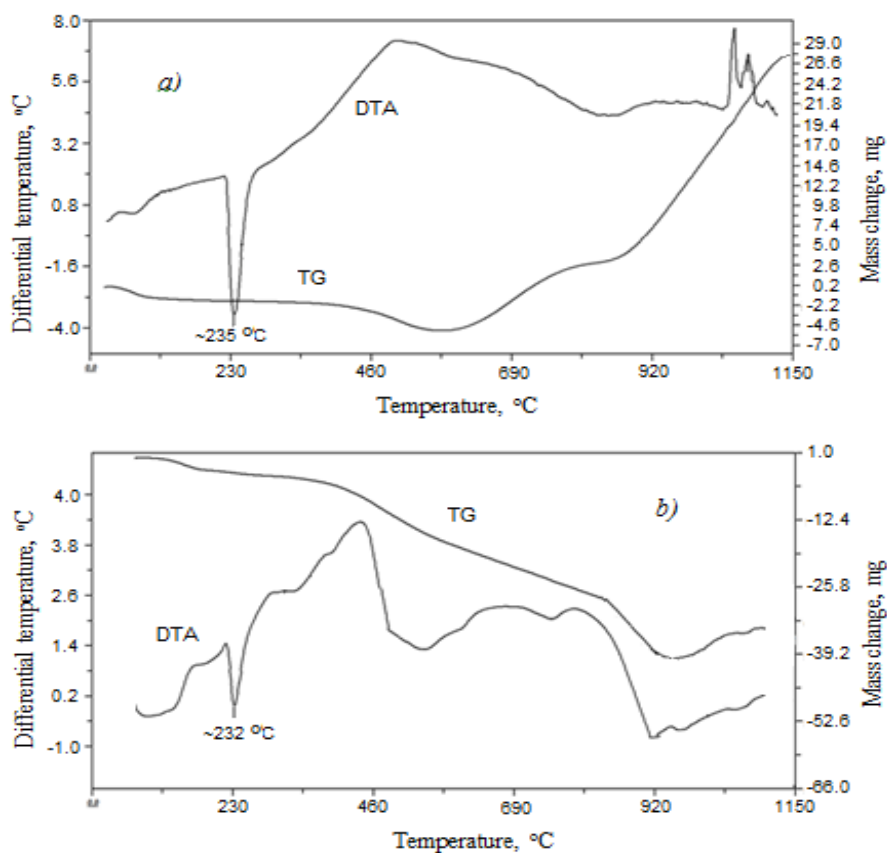

Figure 5. Derivatograms of pre-treated dross (a) and that of the dross-carbon mixture (b)

The obtained derivatograms implied the presence of metallic tin through a sharp negative DTA-peak at ~230 ^{o}C. As can be seen in Fig. 5a, after the initial drying, there was no noticeable variation in the mass (shown by the TG curve) of the oxidised raw material until approx. 600 ^{o}C was reached. Subsequently to that, the mass increased slightly at first, then (above approx. 900 ^{o}C) more rapidly, showing the gradual formation of tin dioxide. When the raw material was mixed with carbon, as shown in Fig. 5b, the mass slightly but continuously decreased until approx. 400 ^{o}C due to the formation of sub-oxides from the initial reduction steps. The effect of oxygen removal may be coupled with the evaporation of volatile species. At higher temperatures, especially in the 800–1000 ^{0}C range, the weight loss indicating the reduction process intensified. The derivatogram of the mixed material showed less heat effect on the DTA differential temperature curve at the melting point of the metal. This results from the dilution of the dross in the sample by the added carbon. However, the mass loss caused by the reduction process (Fig. 5b – TG) even slightly exceeded the mass increase resulting from the oxidation of the unmixed starting material (Fig. 5a – TG), indicating that the molar amount of the oxide was higher than that of the metal in the dross. It can also be seen in Fig. 5b that the carbon content of the mixture got consumed by the reduction process and the unavoidable aerial oxidation by the time the 920 ^{o}C was reached. After this point, the oxidation of the reduced metal could take place.

The experimental carbothermic reduction of the pre-treated secondary dross was carried out in a Heraeus TIK 6.5/8 furnace, applying the temperature range suggested by the relevant literature [5] and by the preliminary test results (i.e. derivatography). The starting material was the oxidized and finely ground dross mixed with coke powder (87% C) in a ceramic mortar (in a way to yield a stoichiometric excess of carbon approximately 10 times). The mixture was charged in a clay graphite crucible. The parameters are summarized in Table 2.

Table 2.

Parameter setting of the carbothermic reduction experiments

Sample mass, g	Reagent mass, g	Temperature, ^{o}C	Reduction time, min
5	4.63	800	30
			60
			120
		1000	30
			60
			120

The product of the carbothermic reduction was ground and screened with a 0.45 mm sieve. The fine and coarse fractions were leached separately in 6 mol dm^{-3} HCl solution close to boiling temperature. The obtained solutions were analysed for tin and for some other significant elements by ICP-AES.

2. Experimental Results and Discussion

The carbothermic reduction of the pre-treated tin dross under milder and stronger conditions produced the material illustrated by Fig. 7. The presence of metallic tin is prominent in the electron micrographs. In Fig. 7a, the metal beads formed at 800 ^{o}C in 0.5 h reduction time are only 1–5 μm in diameter and almost uniformly dispersed. On the other

hand, higher temperature and longer residence time resulted in metal beads with larger diameters. Fig. 7*b* shows that when the material is kept for a longer time at the higher temperature, the dispersion of the reduced metal remains principally the same, but almost 50 μm diameters might as well arise due to the merging of smaller tin droplets. Besides the dominance of tin, the EDS spectrum of the product indicates the presence of a possibly silicate material which may derive from the ash content of the coke and to a lesser extent from the crucible. The macrophotograph in Fig. 7*d* demonstrates that the metal content is very dispersed though still recognizable to the bare eye and the material crumbles easily.
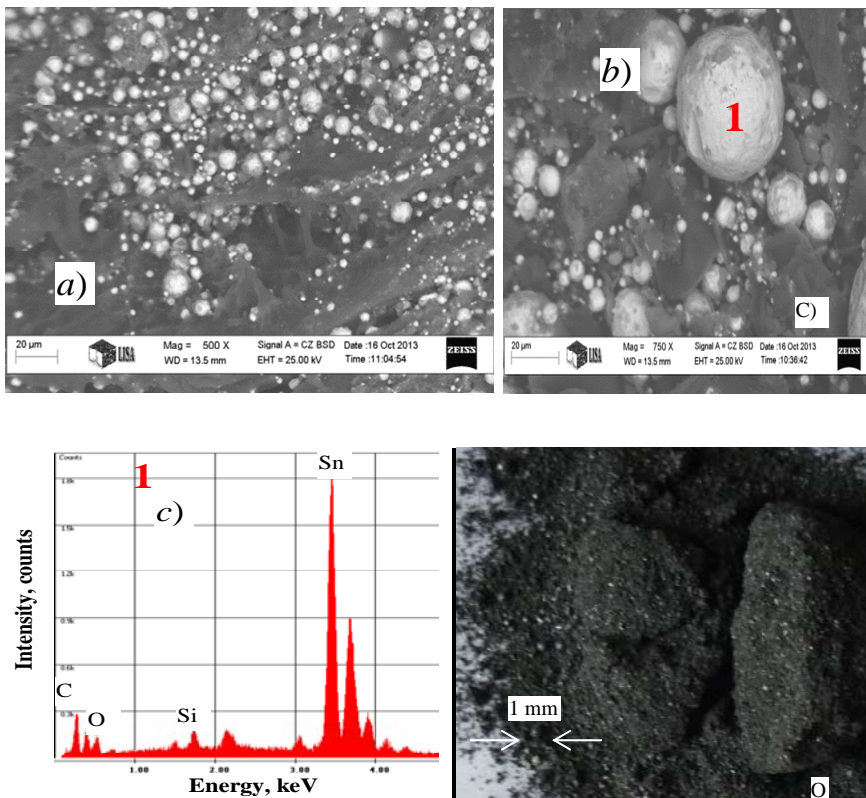
Figure 7. SEM images of the products of carbothermic reduction at 800 ^{o}C for 0.5 h (a), and at 1000 ^{o}C for 2 h (b), together with the corresponding EDS spectrum (c) and the macrophotograph of the fine material obtained

The XRD spectrum in Fig. 8 proves that the major phase in the reduced material is Sn, although some tin sub-oxides and a minor amount of SnO_2 can also be detected. The ratio of the metallic phases was found to be increasing with the temperature and time of the reduction. The results of the elemental analysis of the products obtained during the reduction process are given in Table 3.

Figure 8. XRD spectrum of the material obtained from the carbothermic reduction of the pre-treated tin dross (1000 ^{o}C, 2h)

Table 3

The analysis of the products from carbothermic reductions

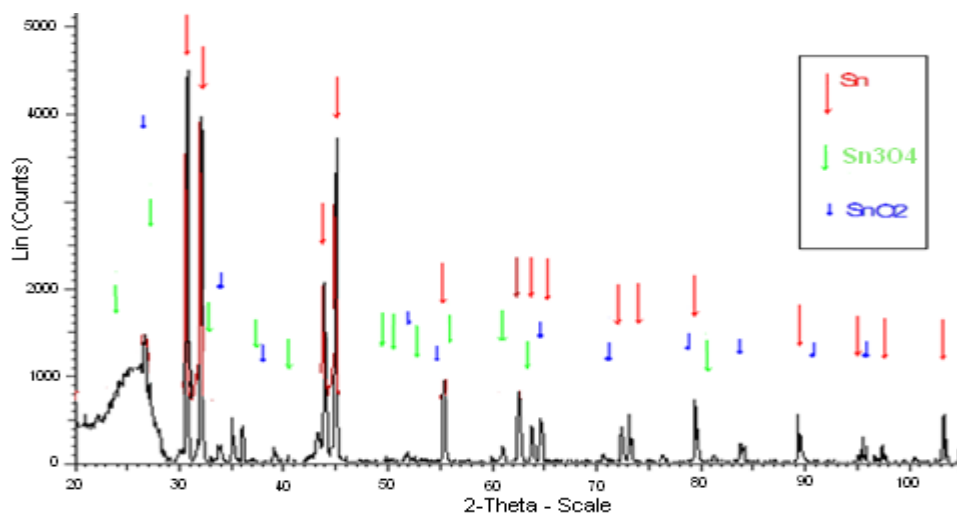| Reduction temp. / time, ^{o}C / h	Fraction		Concentration, %						
	Particle type	Mass, g	Sn	Al	Cu	Fe	Ni	Pb	Zn
1000 / 2	Fine	3.42	**86.1**	0.084	2.04	0.84	0.076	0.041	0.024
	Coarse	1.35	**36.2**	0.81	0.62	1.41	0.063	0.016	0.046
1000 / 1	Fine	3.71	**84.7**	0.084	2.08	0.85	0.079	0.041	0.032
	Coarse	1.27	**31.3**	0.87	0.45	1.85	0.11	0.017	0.062
1000 / 0.5	Fine	3.7	**83.4**	0.21	1.88	0.68	0.046	0.037	0.023
	Coarse	1.15	**31.2**	0.69	0.55	1.31	0.043	0.019	0.049
800 / 2	Fine	3.58	**84.1**	0.23	2.08	0.44	0.033	0.021	0.022
	Coarse	0.84	**39.5**	1.37	0.56	1.87	0.092	0.018	0.102
800 / 1	Fine	3.56	**88.9**	0.22	2.16	0.42	0.053	0.028	0.018
	Coarse	0.69	**33.1**	0.59	0.37	1.77	0.045	0.014	0.061
800 / 0.5	Fine	3.9	**82.2**	0.17	1.96	0.33	0.033	0.021	0.024
	Coarse	0.7	**47.6**	0.69	1.01	2.04	0.087	0.018	0.084

Most of the iron and aluminium contamination – collected from the coke, the crucible and the mortars – appeared in the coarse fraction, while the copper content of the tin dross remained mostly in the fraction composed of the fine particles. This may indicate that the coarse fraction is mostly attributable to the original metal content of the pre-treated tin dross, whereas the reduced metal can be found principally in the fine particles. Since the

applied conditions do not facilitate the coalescence of the reduced metallic tin, most of it remains in the fine powder fraction.

The leaching of the reduced products with hot 6 mol dm^{-3} HCl solution resulted in the dissolution of the metallic tin according to reaction (6). The presence of metallic tin was also detectable from the observed intensive gas evolution. Any partially reduced tin sub-oxide also transfers into solution. Only little undissolved residue was observed to remain in the reactor, mostly corresponding to the residual SnO_2 content and the silicate impurity entrapped in the material during the heating and grinding steps. The ICP-AES analytical results demonstrated the expected solubilisation of tin by the devised reduction procedure. In order to assess the overall efficiency of the process, the extracted amount of tin was compared to the analysed total tin content (71.6%) of the pre-treated dross in the form of the oxidised fine powder (Fig. 3*d*), expressed in Table 1. Efficiency is the ratio of the tin content obtained in the solution to that in the starting material used for the reduction-leaching procedure. The recoveries yielded by reduction carried out with different parameters are given in Fig. 9.
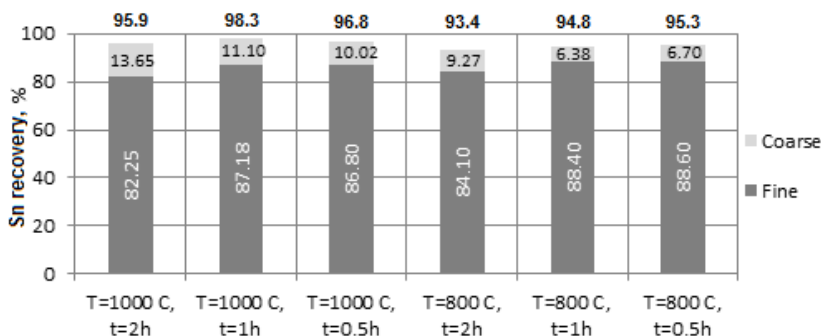
Figure 9. Recoveries of tin in the fine and corse fractions of the reduced material.

Since the starting material of the reduction-leaching procedure also contained 16% metallic tin, conversion efficiency has to be expressed with reference to the remaining amount of oxidised tin, corresponding to 55.6% of the starting mass. Conversion efficiencies are accordingly given in Table 4.

Table 4

Tin recovery from the dross by 6M HCl leaching after different reducing steps

Reduction Temp., ^{o}C / time, h	1000/2	1000/1	1000/0.5	800/2	800/1	800/0.5
Sn conversion, %	94.7	97.8	95.9	91.5	93.3	93.9
Average Sn conversion, %		96.1			92.9	

The shortest testing time (0.5 h) was practically sufficient for reduction. At 800 ^{o}C, increasing time resulted in slightly but continually decreasing recovery. This tendency recurred with respect to the shortest and longest times also at 1000 ^{o}C. Prolonged heating resulted in losses caused by unfavourable re-oxidation locally at the surface of the charge, where the reducing effect was weak and volatile monoxide or inert dioxide could arise by

partial reduction or re-oxidation. Increased temperature, however, could raise the efficiency of reduction. The conversion rates obtained at the same temperature for different times can be considered practically parallel results within the error margin, since the reduction process virtually reached its full scale after the first 30 minutes.

Conclusions

The oxide content of the dross obtained from the melting of soldering scrap is resistant to common known acids and bases. However conversion of the SnO_2 to acid soluble form by carbothermic reduction has proved practically viable. Experiments have been carried out to examine the feasibility and the characteristics of this method using coke powder as the reducing agent for various durations of heating at different temperatures in a feasible range determined by preliminary derivatography. Examination of the product by direct SEM, EDS XRD techniques pointed at the formation of metallic tin and some sub-oxides. The converted material was leached with hot 6 mol dm^{-3} HCl solution. ICP-AES analysis of the pre-treated fine oxidized powder starting material and the obtained solutions was used to express the recovery and conversion rates. With carbothermic reduction it was possible to convert the oxidized tin of the dross into acid soluble form with an efficiency of 93–96% depending on the conditions applied. The optimum parameters of reduction with coke powder were found to be 1000 ^{o}C temperature and 0.5 hour duration. The effect of increased reduction time is negligible because unfavorable re-oxidation and evaporation may also occur at the surface. Decreasing the temperature to 800 ^{o}C slightly reduces process efficiency (by ~ 3%) of reductions carried out in the 0.5–2 h time range. Metallic tin was formed as finely dispersed particles, amenable to hydrometallurgical extraction. Although carbothermic reduction with cheap coke powder is efficient in converting the SnO_2 content of the tin dross into soluble form, but the subsequent leaching of the metal requires the use of boiling 6 mol dm^{-3} HCl solution in a closed system.

Acknowledgement

References

[1]   Rimaszéki, G.–Kulcsár, T.–Kékesi, T.: Application of HCl solutions for recovering the high purity metal from tin scrap by electrorefining. *Hydrometallurgy*, 125–126, (2012) 55–63.

[2]   Rimaszéki, G.–Kulcsár, T.–Kékesi, T.: Investigation and optimization of tin electrorefining in hydrochloric acid solutions. *J. Appl. Electrochem.* 42, (2012) 573–584.

[3]   Wright, P.: *Extractive Metallurgy of Tin.* Elsevier Press, 1967.

[4]   Stephen, H.–Stephen, T.: *Solubilities of Inorganic and Organic Compounds.* Vol. 1, Macmillan, New York, 1963.

[5]   Mitchell, A. R.–Parker, R. H.: The Reduction of SnO_2 and Fe_2O_3 by solid carbon. *Minerals Engineering,* 1. (1988) 53–66.

COMPUTER SIMULATION OF THE HEATING PROCESS OF FUSED CAST REFRACTORY BLOCKS

TAMÁS KOÓS[1],–ISTVÁN SZŰCS[2],–LÁSZLÓ GYULAI[3]

After the solidification process of fused cast refractories – used for glass melting furnaces – the sprue is cut off with a cutting machine in wet operation. Then, the cavity is sealed with refractory concrete. The aim of our research was to determine the most important parameters (e.g. gas permeability) for the safe application of the refractory concrete used for the sealing of the solidification hole. In order to validate the permeability test results, test blocks were made from fused cast alumina-zirconia-silicate (AZS) material equipped with pressure and temperature sensors. The investigations revealed that the gas permeability of the sealing material allows the steam (evolving from the moisture contained by the concrete and from the water trapped in the shrinkage cavity) – which can cause damage to the refractory block – to flow out safely during the first heat-up of the fused cast blocks.

In order to better understand the heating process and the temperature field inside the refractory blocks a numerical model was created with ANSYS FLUENT software. More articles revealed that the accuracy of the results depends largely on the choice of material properties [1][2]. The differences between the temperature values calculated by the computer model and those measured with thermocouples during the tests are within the acceptable limits of industrial practice. Based on the experiences we constructed a model of a real-size AZS block built into a glass furnace with insulation layers. In the case of the industrial block we can declare: the gauge pressure in the cavity is not likely to cause damage to the refractory blocks by itself.

Keywords: fused cast refractory, shrinkage cavity, refractory concrete, gas permeability, simulation

Introduction

A fused cast refractory block is usually built-in so that it contains the shrinkage cavity, which is formed during solidification. It has the same properties and durability yet lower costs than the block that has no porosity or cavity.

Two glass melting furnaces built of these types of blocks had problems during the first heat-up operation. When the furnace temperature reached about 350 °C, one brick was damaged and broke out of the lining of both equipment. It was claimed that the steam coming from the moisture content of the concrete or from the water trapped in the shrinkage cavity caused the damage. In our previous paper we reported on the gas permeability and thermogravimetry tests of the refractory concrete. The aim of the research was to determine the following parameters:

---

[1] University of Miskolc, Department of Combustion Technology and Thermal Energy
 3515 Miskolc-Egyetemváros, Hungary
 tuzkt@uni-miskolc.hu
[2] University of Miskolc, Department of Combustion Technology and Thermal Energy
 3515 Miskolc-Egyetemváros, Hungary
 tuzsi@uni-miskolc.hu
[3] University of Miskolc, Department of Combustion Technology and Thermal Energy
 3515 Miskolc-Egyetemváros, Hungary
 tuzgyl@uni-miskolc.hu

- the mass and heat changes during the first heat-up with thermogravimetry; the gas permeability of the refractory concrete;
- the gauge pressure in the cavity covered with refractory concrete during the first heat-up of the refractory block;
- the temperature measured in the shrinkage cavity.

The permeability tests were made on cores made of refractory concrete used for the construction of the two furnaces. The cavity temperature and gauge pressure tests were performed on test blocks (see *Figure 1*) with the same thickness as the real-size blocks. The main test results were as follows (see also on our previous paper [3]):

- the refractory concrete is not impervious;
- when the temperature inside the furnace and along the interior surface of the refractory is 250–260 °C, the hole has a temperature of approximately 100 °C;
- around 100 °C (i.e. the boiling point of water), the steam can leave from the hole at low gauge pressure levels without causing any damage.

During the heat tests of the refractory test blocks, only the furnace temperature and the interior temperature of the shrinkage cavity could be measured with reliable accuracy. A computer model using finite element analysis was used for the more detailed, complex study of the temperature field in the refractory blocks and in the shrinkage cavity created by the unilateral heating technique. This allowed for making a comparison between the temperature inside the cavity of the test block and temperature values obtained from the simulation. The temperature field of an industrial-size block with insulation layers were generated with the same method too.

1. Examination of the temperature in the shrinkage cavity

In order to simultaneously determine the possible temperature and gauge pressure values in the shrinkage cavity, test blocks from regular production sealed with refractory concrete were used for the laboratory measurements.
The test objects had the following composition:

- fused cast alumina-zirconia-silicate (AZS) refractory blocks (Al_2O_3 = 66 %, ZrO_2 = 21%, SiO_2 = 12 %, $Na_2O+Fe_2O_3$ = 0,4%) [4];
- for the sealing layer: refractory concrete using mixing ratios of standard production: made from cement Almatis CA 25-R (Al_2O_3 = 81 %, CaO = 18%, SiO_2 = 12%, Na_2O = 0,6%, Fe_2O_3+MgO = 0,6%) [5], AZS powder and 16%(m/m) of water.

These were 170 x 250 x 120 mm blocks (with the same thickness as the industrial-size fused cast blocks). In order to simulate the conditions within the shrinkage cavity, 80 mm deep and 60 mm diameter cylindrical cavities were made in the test objects with a core drill. This opening was sealed with a thick layer of concrete (made of Almatis CA 25-R cement and AZS powder). A thin copper mesh was placed inside the cavity 30 mm below the opening so that the thickness and position of the refractory concrete could be accurately set.
The temperature within the shrinkage cavity was measured with NiCr-Ni thermocouples built into the refractory concrete sealing. The gauge pressure of the steam evolving inside

the shrinkage cavity was regulated with a copper tube. A differential pressure sensor was connected to the outer end of the copper tube with a thick, transparent PVC tube. Silicone oil (heat-resistant up to 350 °C) was applied inside the external part of the copper tube and the PVC tube in order to transmit pressure and prevent the steam from condensation or compression.

Six test blocks were placed in an electric resistance furnace and heated up to 350 °C at a rate of 5 °C/h (recommended for the refractory blocks during the first heat-up) from the backside.

A schematic of the measurement setup is shown in Figure 1.
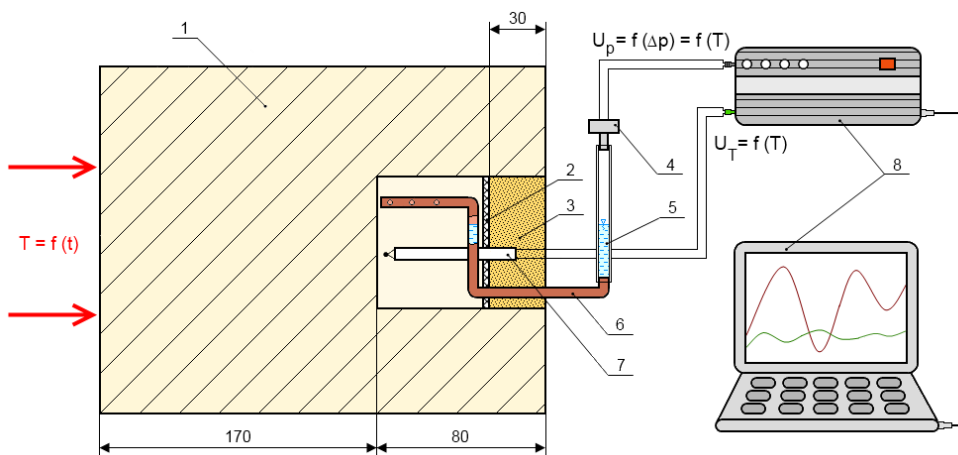
Figure 1. Schematic illustration of the measurement setup for the monitoring of gauge pressure and temperature in the shrinkage cavity
1– refractory block; 2– positioning copper mesh; 3– refractory concrete; 4– pressure sensor; 5– heat-resistant silicone oil; 6– copper tube; 7– thermocouple; 8– data collector

We measured the temperature and the pressure in the hole during the heating up process.

The gauge pressure (with pressure sensor Figure 1/4) and temperature (with thermocouple Figure 1/7) was monitored and registered throughout the test with a computerized data collector (Figure 1/8).

Temperature values in the shrinkage cavities of the 6 blocks are displayed as a function of time in Figure 2.

Figure 2. Temperature values registered in the shrinkage cavities of the refractory sealed test blocks as a function of heating time

The temperature values measured in the shrinkage cavities provided the base data for comparison with the computational simulation.

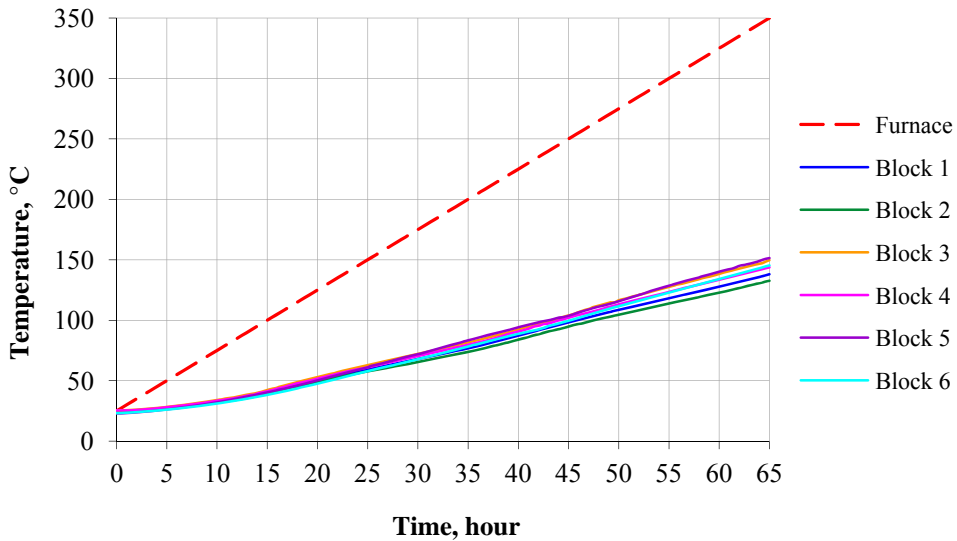## 2. Temperature distribution in the refractory block and in the shrinkage cavity obtained by computational simulation

Temperature was measured only at two points during the laboratory experiment: one point inside the furnace and one inside the shrinkage cavities. In order to map the whole temperature field in the fused cast refractory block and to show the effect of the cavity on temperature distribution a computational simulation of the heating process of the test blocks was made with FLUENT numerical simulation software. It also provided an opportunity to draw a comparison between the cavity temperatures actually measured in the laboratory and calculated with the program. Based on the experiences, we created the temperature contour map of a real-size AZS block.

2.1. Simulation of the laboratory test block

The dimensions of the model are the same as those of the laboratory test blocks. Temperature specific physical parameters required to run the computer program (density, specific heat capacity, thermal conductivity etc.) were obtained from catalogue databases and tables [4][7]. The dimensions of the refractory block, shrinkage cavity and the sealing layer used for the model are shown in Figure 3. The computational grid required for the numerical solution of the model is shown in Figure 4.
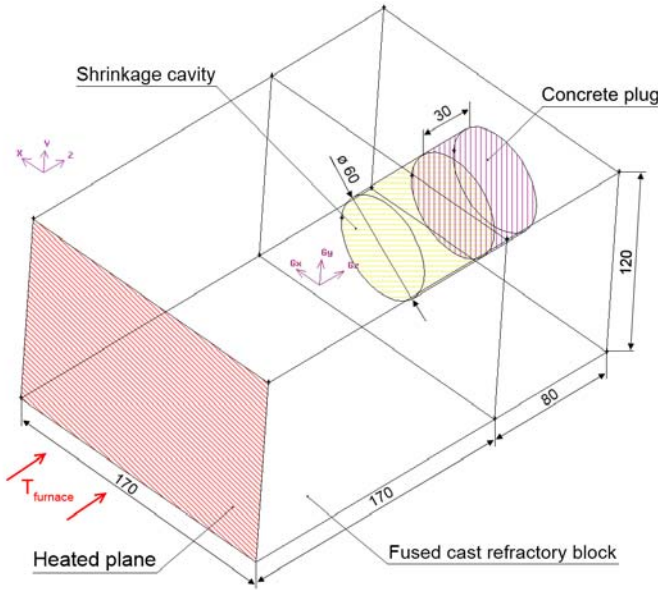
Figure 3. Dimensions of the laboratory test block model
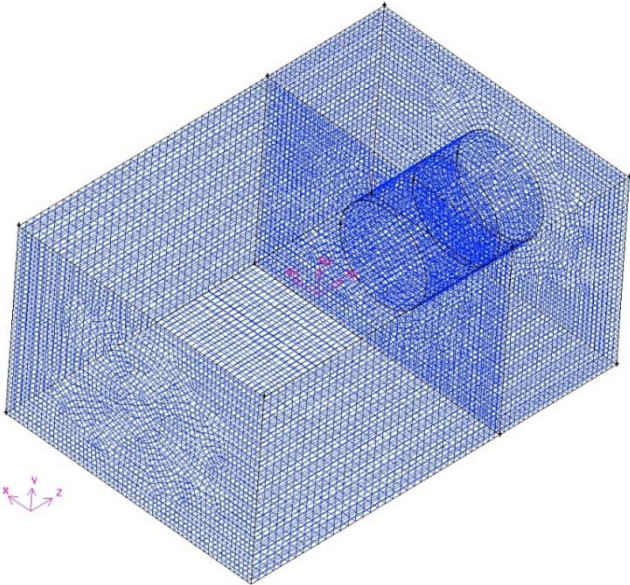
Figure 4. Computational grid of the laboratory test block

The temperature distribution of the sample at a furnace temperature and interior surface temperature of 350 °C of the refractory block is shown in Figure 5. The temperature curve characterising the central axis of the heated test object is shown in Figure 6.
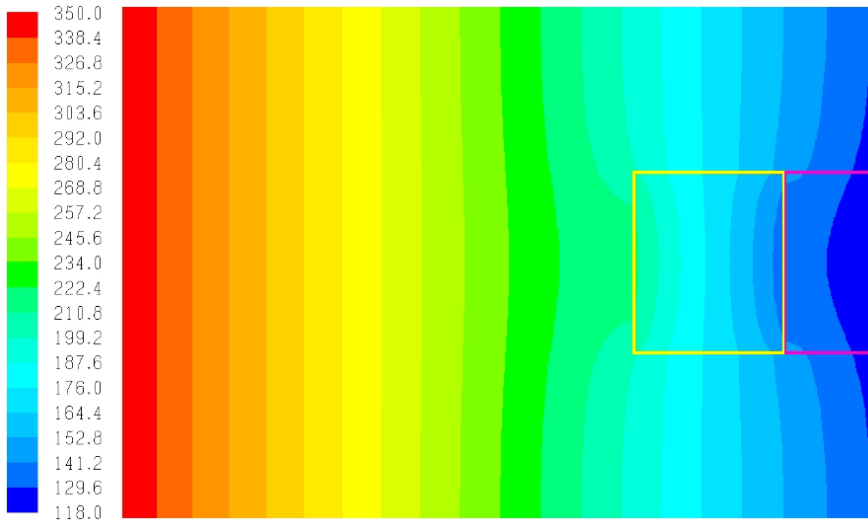
Figure 5. Temperature contours in the cross-section of the laboratory test block calculated with simulation at an interior surface temperature of 350 °C
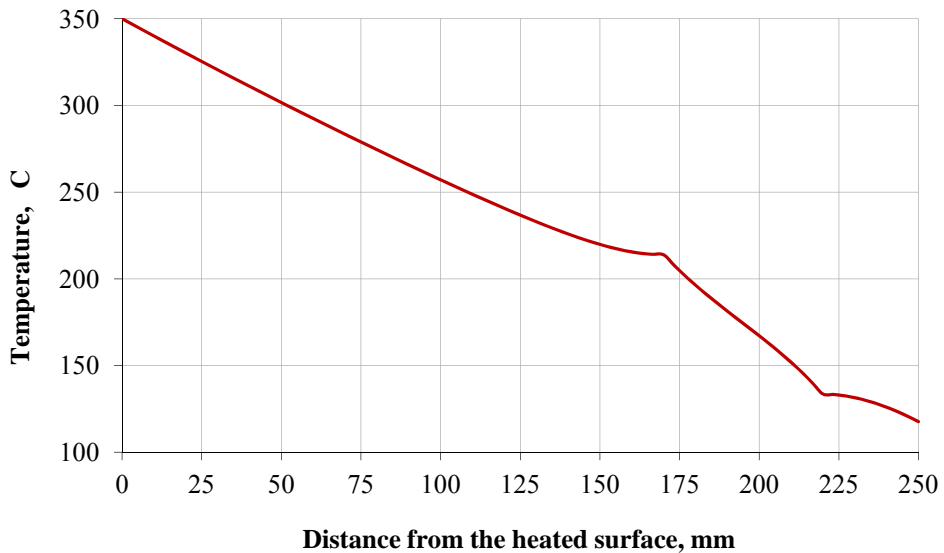
Figure 6. Temperature along the central axis at the end of the heating process as a function of distance from the heated surface calculated with simulation

The difference between the measured cavity temperature and the computer calculated value at the furnace temperature of 350 °C is approximately 10 °C as seen in Figure 7.
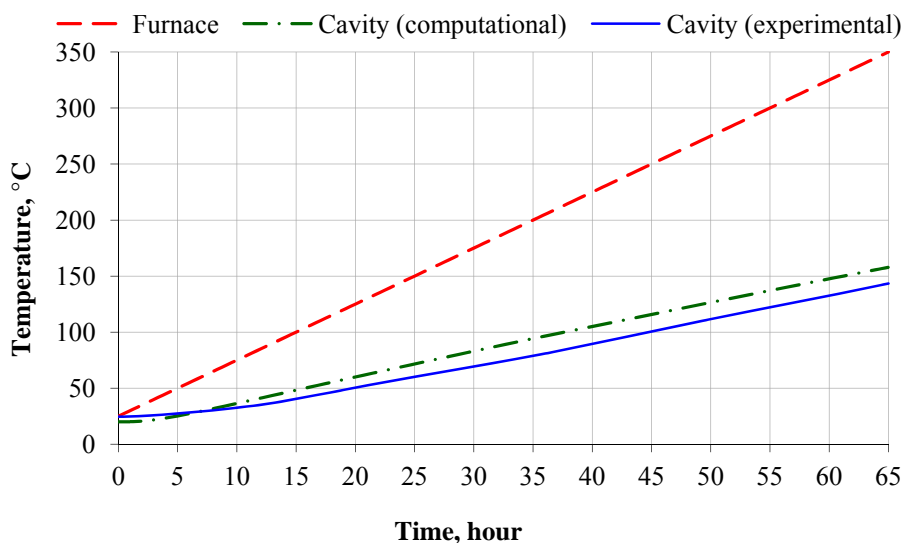
Figure 7. Comparison of experimental average shrinkage cavity temperature and computed cavity temperature as a function of heating time

The temperature distribution diagrams show the heat insulating effect of the gas phase inside the cavity, which has low heat conductivity. An inhomogeneous temperature field is formed around the cavity, slightly but not completely compensated by lateral heat transfer. The differences between the temperature values determined by the computer model and those measured in the cavities are within the acceptable limits of industrial practice.

2.2. Simulation of the industrial block

Temperature distribution in an industrial-size block was also calculated by the software. The simulated block had the dimensions of 700 x 300 x 250 mm, which is the exact size of the fused cast block damaged in the two glass melting furnaces mentioned above. The model has insulating brick layers like when it is built in. The geometry of the model contains shrinkage cavity sealed with refractory concrete and closed shrinkage defects (also known as shrinkage porosity) based on the casting defects of the AZS block shown in Figure 8. The blocks were made with a special casting method that ensures that the shrinkage cavities are located in the middle of the sidewall opposite to the hot sidewall near the surface.

Figure 9 shows the schematic illustration of the model. The computed temperature distribution of the insulated AZS block is shown in Figure 10. The temperature curve characterising the central axis of the heated test object is shown in Figure 11.
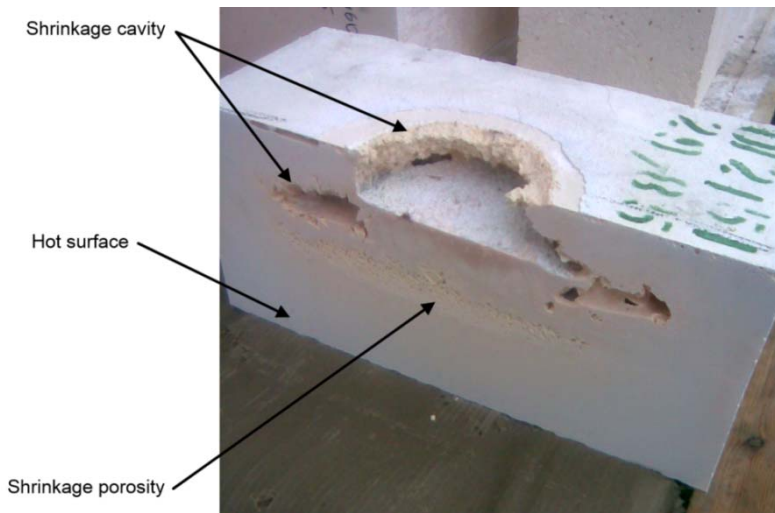
Figure 8. The fused cast refractory block cut in half with shrinkage defects
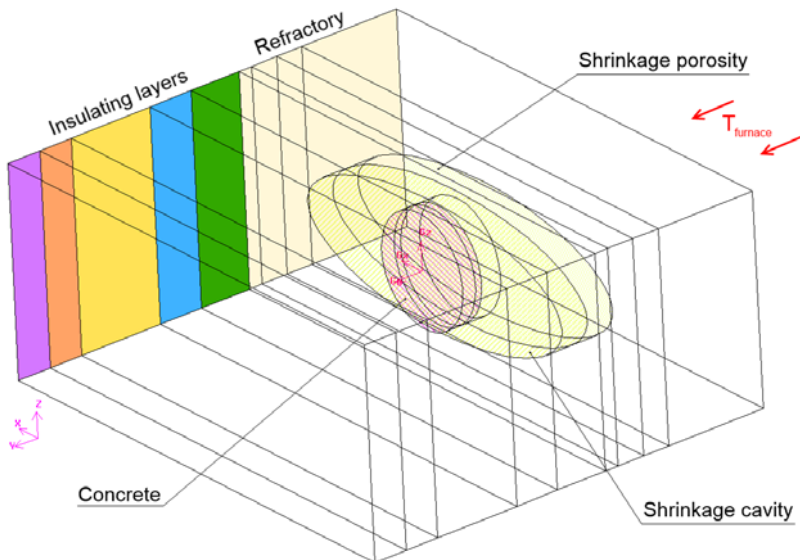
*Figure 9. The industrial block model with insulating layers, casting defects
and concrete sealing*

The insulating layers allow the cavity to reach the temperature level of 300 °C, so that we can declare: the gauge pressure in the cavity is not likely to cause damage to the refractory blocks once the steam has already flowed out from the shrinkage cavity through the concrete layer. For safety sake it is recommended to turn the blocks in a downward position after cutting, thus, the residual water (deriving from the wet cutting process) will freely drip out from the shrinkage cavity.
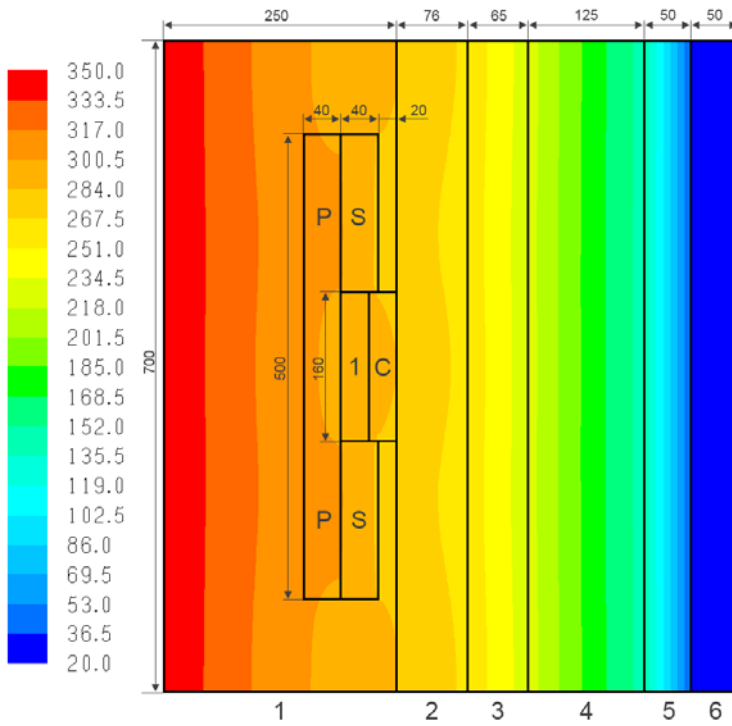
Figure 10. Temperature contours of industrial block (at 350 °C inside)
Types of layers: 1 fused cast refractory; 2 S 60; 3 OFL 116; 4 SL 8P-140; 5 KFM 1400;
6 SASI-Platte; P shrinkage porosity; S shrinkage cavity; C refractory concrete
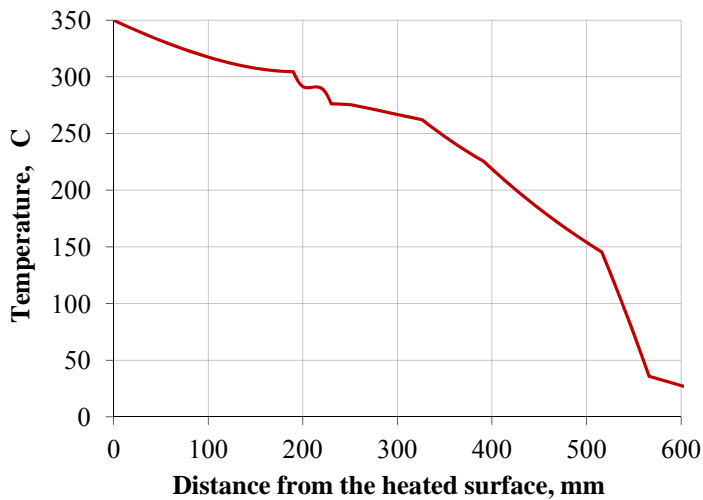
Figure 11. Temperature along the central axis at the end of the heating process
as a function of distance from the heated surface

Conclusions

In order to determine the temperature distribution in the fused cast refractory blocks during the first heat-up to 350 °C (which is temperature of damage in blocks of the glass furnaces) computational simulations were made with ANSYS FLUENT numerical simulation software. This provided an opportunity for comparison between the cavity temperature measured during the permeability laboratory tests and calculated with the program. Moreover, base data could be obtained for the simulation of a real-size refractory block.

Based on the computer simulation the following can be stated:

- the temperature distribution diagrams show the heat insulating effect of the gas phase inside the cavity, which has low heat conductivity;
- due to significant differences in the technical parameters of the block, the gas phase in the cavity and the concrete, an inhomogeneous temperature field is formed around the cavity, slightly but not completely compensated by lateral heat transfer;
- the differences between the temperature values determined by the computer model and those measured in the cavities of the test blocks are within the acceptable limits of industrial practice (approx. 10 °C);
- in the case of a real-size block the insulating layers allow the cavity to reach the temperature level of 300 °C, so that we can declare: the gauge pressure in the cavity is not likely to cause damage to the refractory blocks once the steam has already flowed out from the shrinkage cavity through the concrete layer, which has a quite good permeability;
- by turn the blocks in a downward position after cutting, the residual water (deriving from the wet cutting process) will freely drip out from the shrinkage cavity, thus, the damage of the blocks can be definitely avoided.

Acknowledgements

References

[1]   Petroni, L.–Boussuge, M–Ryckelynck, D.: Numerical simulation of the cooling-down of high-zirconia fused-cast refractories. *Journal of the European Ceramic Society,* Volume 32, Issue 15, November 2012, pp 3941–3947.

[2]   Madi, K.–Forest, S.–Boussuge, M.–Gailliègue, S.–Lataste, E.–Buffière, J.–Bernard, D.–Jeulin, D.: Finite element simulations of the deformation of fused-cast refractories based on X-ray computed tomography. *Computational Materials Science,* Volume 39, Issue 1, March 2007, pp 224–229.

[3]   Szűcs I.–Koós T.–Tóth J.: Determination of the Gas Permeability of Hydraulic Bonded Refractory Concrete. *Materials Science and Engineering,* Vol. 39, No. 1, Miskolc University Press, 2014, pp 59-67.

[4]   MOTIM Fused Cast Refractories Ltd.: *Catalogue of Fused Cast Refractory Blocks.* 2012.

[5]   Almatis GmbH: Data sheet of "Calcium Aluminate Cements."

[6]   *Schacht, Charles A. (ed.):Refractories Handbook*, CRC Press, 2004, 499 p.

[7]   Raznjevic, Kuzman: *Handbook of Thermodynamic Tables & Charts.* McGraw-Hill Book, 1976.

SUSTAINABLE REUSE OF HEAVY METAL CONTAMINATED BROWNFIELD LANDS BY PHYTOEXTRACTION

HELGA KOVÁCS[1]–JÓZSEF PAULOVICS[2]– KATALIN SZEMMELVEISZ[3]

Polluted industrial sites, particularly brownfield lands, are a source of major problems all over Europe, thus the remediation of these areas is a matter of interest for economists, urban development officers, environmental protectionists, engineers and promoters of sustainable growth.

Various definitions are given in the literature for "*brownfield lands*". The term generally denotes heavily contaminated, degraded, desolate locations, the utilization of which is hampered by adverse environmental factors (e.g. the presence of hazardous substances, obsolete industrial or commercial facilities etc.). Based on these criteria, a number of contaminated sites can be identified as *brownfields* in Hungary.

One of the viable solutions of remediating disused lands with metal-contaminated soil – that is a subclass of brownfield lands – is the *in-situ* planting of wooden species capable of metal uptake. This type of cleanup technique is called *phytoextraction* and is considered a simple, feasible and environmentally effective method to restore extensive areas at the outskirts of industrial settlements. When phytoextraction is applied, an additional benefit to site recovery is the potential energy use of the harvested plants. In this way, even the share of renewables (biomass) in the domestic energy mix can be increased. However, the energy utilization of biomass from plant-based remediation raises hot issues of environmental safety. The most important question is whether the solid combustion residues of this type of such fuel still contain hazardous heavy metals. In order to qualitatively assess the environmental risk of the combustion wastes, we performed scanning electron microscopy analysis on ash and fly ash samples by using an AMRAY 1830 I type SEM instrument and with DX4 EDAX EDS type microprobe.

The results show that the heavy metal content of the combusted fuel is detectable both in the ash and in the fly ash carried by the flue gas. This sets certain ecological constraints to the applicability of the technology. In other words, the sustainable reuse of heavy metal contaminated brownfield lands via the plantation of energy crops seems to be a plausible yet limited option, where the (technical) conditions for the safe combustion of the respective biomass need further specification.

Keywords: brownfield lands, ligneous plants, heavy metal, SEM, ash, fly ash

1. Introduction

So far no systematic database on the exact size and number of inland brownfields has been compiled by Hungarian authorities. Some estimates and surveys are, nonetheless, available. A total area of 3520 hectares is reported in a nation-wide record [1], while another survey keeps record of 240 contaminated sites from three Eastern-Hungarian regions, with a total area of 4500 hectares [2]. Recently, Váti Ltd. has made an estimate of 12000 hectares of brownfield lands in Hungary. The apparent mismatch of these figures

---

[1] University of Miskolc, Department of Combustion Technology and Energy Affairs,
   3515 Miskolc-Egyetemváros, Hungary
   kovacs.helga@uni-miskolc.hu
[2] Bay Zoltán Nonprofit Ltd. for Applied Research, Institute for Logistics and Production Engineering,
   3515 Miskolc-Egyetemváros, Hungary
   jozsef.paulovics@bayzoltan.hu
[3] University of Miskolc, Department of Combustion Technology and Energy Affairs,
   3515 Miskolc-Egyetemváros, Hungary
   tuzszemt@uni-miskolc.hu

derives partly from the lack of proper reporting regulations. Data are provided on a voluntary base, thus, many proprietors feel encouraged to evade site restoration liabilities by giving scanty or defective information on the actual state of their lands (concerning environmental risks). Therefore, the actual size of abused land is presumably far above the estimated level.

The problem of sustainably reusing heavy metal contaminated brownfields left behind by general industrial restructuring is still unsolved in Hungary. Under given conditions, the plantation and controlled combustion of energy crops would mean a feasible response.

1.1. The accumulative potential of plants – phytoremediation

The effect of heavy metals on soil and crops

The list and definition of heavy metals is neither uniform, nor standard. Due to the diversity of contexts, the International Union of Pure and Applied Chemistry (IUPAC) labelled the category as "meaningless and misleading" [3]. Nevertheless, the term heavy metals is still widely used in the literature.

Based on general consensus, Zn, Cu, Co, Cr, Ni, Cd, Hg, Pb [4] are considered to be the most important heavy metals; some of them (e.g. Zn, Cu) are essential nutrients, others are harmful to living organisms, even at very low concentrations [5–6].

Whether the concentration of trace elements in a given ecological environment should be regarded as "natural" or "toxic" depends partly on the given plant culture. In any case, metal bioavailability is a necessary precondition for the vegetal growth and development of plants, thus also vital for the crops grown on contaminated lands.

Toxic metals are partly extracted from contaminated soil by plants [7]. The uptake capacity of a plant largely depends on the biological characteristics of the given species [8–10]. Certain "hyperaccumulators" are capable of absorbing and storing high levels of heavy metals without any apparent sign of toxicity, nevertheless, the biologicalmechanism of phytoextraction is not free of environmental risks [5–6].

Remediation/clean up technologies

Depending on the actual situation, several cleanup technologies are available for remediation – the most suitable method is always selected and applied with respect to site-specific properties. We can differentiate between *in situ* and *ex situ* methods, implying on-site removal or off-site disposal processes.

In situ recovery includes bioventing, phytoremediation, soil washing and soil ventilation. These techniques require good soil permeability and a uniform distribution of the pollusive substance.

Ex situ methods include composting, separation, incineration/combustion, thermal desorption and pyrolysis. These processes are less sensitive to soil permeability and to inhomogeneity or uneven metal distributions. Extensivity and high costs, however, mean a great drawback to application.

Whenever organic or inorganic pollutants are removed, converted or consolidated by ways of phytoremediation, it is essential that the metal-accumulating plants in no way could become part of the food chain. Each cleanup technology has a double function: the damage control and the sustainable reutilization of the deteriorated lands.

There are different forms of phytoremediation, among them phytoextraction, phytostabilization, phytodegradation and rhizofiltration. Phytoextraction is a subprocess of phytoremediation in which plants capable of accumulating hazardous elements, are used to remove inorganic contaminants, particularly heavy metals, from soil and water [7], [11]. The heavy metals are extracted by the plant, and concentrated in the roots or sequestered in the above-ground plant parts (twigs, sprouts). At maturity, the metal-enriched biomass is harvested.

Some examples of phytoremediation are given in Table 1.

Table 1

. In situ remediation of heavy metal contaminated sites in the US [11] Meers, E.–Ruttens, A.–Hopgood, M. J.–Samson, D.–Tack, F. M. G.: Comparison of EDTA and EDDS as potential soil amendments for enhanced phytoextraction of heavy metals. *Chemosphere,* 58 (2005) 1011–1022.

[12]

Site and responsible organization	Applied Technology	Contaminants
Dearing, Kansas, 1998	Phytoremediation	Pb, Zn, Cd
Trenton, New Jersey Site, 1998	Phytoremediation	Heavy metals
Radford Army Ammunition Plant, Virginia, 1997	Phytoremediation	Heavy metals

All the listed research organizations conduct scientific investigation on soil contaminants, incl. heavy metals (Cd, As, Zn etc.).

2. Laboratory experiments: methodology

Subsequent to the componental analysis of the selected soil and wooden biomass samples, a series of combustion experiments were performed in a small-scale wood stove in order to obtain ash and fly ash samples from the respective biomass. Then the chemical composition of the solid burning residues was analysed.

Soil and biomass chemical analysis

The chemical composition of the soil and biomass samples was determined with ICP spectrometry, using a Varian 720 ES type Inductively Coupled Plasma-Optical Emission Spectrometer.

The samples were prepared by digestion and dissolution in high purity concentrated nitric acid at 130 °C for 120 min, in a Teflon (PTFE) acid digestion bomb. After cooling, the solution was filled up to a final volume of 50 cm^3.

Combustion experiments

The combustion experiments were performed in a closed-chamber wood stove. The equipment used – a so-called "Alicante" product by Fireplace Ltd. – was suitable for burning both wood and brown coal briquette. Three-phase airflow was provided by the double-row nozzle system inserted in the refractory chamber wall, with changing intensity rate adjusted to exhaust ventilation. Additional air supply – from either or both directions – was controlled through the valves at the upper and lower rim of the front door. Flue gas

exited through a rear flue outlet with injector tee connection. The sampling points were set along the length of the flue pipe directly connected to the stove. With respect to fluctuating soot levels (due to the periodic cycles of *feed-in* and *burning*), wet absorption method was used for the determination of solid particulate pollutants. The test procedure was designed to resemble the real combustion process, including fuel feeding. Consequently, two-stage sampling was applied, with phases of "smooth burning" and "soot formation".

The SEM analysis of solid burning residues (ash, fly ash)

For the general analysis of ash composition, the DX4 EDAX EDS microprobe of an AMRAY 1830 I Scanning Electronmicroscope was used. The measurement results are presented below. Sample surface topography was identified on the basis of SEM micrographs, compositional data were calculated from the acquired spectra.

3. Experimental results

The Mátra region is long since notable for the mining of metal ores. The explorations in Gyöngyösoroszi in 1926 marked the beginning of large-scale industrial lead and zinc ore mining (from mines "Peter–Paul" and "Charles"), with mineral processing from 1950 on. The excavated ore had been crashed on site, then enriched through flotation process. Sphalerite (zinc sulphide) and galena (lead sulphide) were separated in powdered form, then smelted abroad. Subsequent to the processing of the four main products – lead, copper lead, zinc and pyrite in high-purity powdered form – the refuse ore was transported to a flotation spoil bank through a pipeline system.

3.1. Chemical analysis of the sampled wooden species

Among the woody plants, the most frequently applied energy crops are fast growing, short rotation species, such as acacius, willow or to a lesser degree birch, alder, maple and elm. Relative to biomass yield and heavy metal content, acacius, poplar and birch were selected for sampling from the respective brownfield land. Oak and pine – two of the most widespread species typically present in Hungarian native forests, particularly in the specified region – were also chosen for analysis.

The selected species are: *False Acacia* (Robinia pseudoacacia), *Trembling Aspen* (Populus tremula), *Silver Birch* (Betula pendula), *Scots Pine* (Pinus sylvestris), *Pendunculate Oak* (Quercus robur).

Table 2

Heavy metal content of the tested specimen (quantitative results)

Sample type	Zn	Cu	Cd	Pb	Mn	Cr	Ni	Co	Fe
	mg/kg								
Birch	396	10.9	14.9	42.7	209	213	236	15.9	499
Pine	61.2	10.9	8.9	< 10	117	310	278	23.7	665
Acacia	76.8	11.0	11.0	12.0	22.9	45.9	59.0	12.0	857
Oak	47.6	32.7	10.9	< 10	206	813	556	24.8	2346
Poplar	274	16.0	19.0	< 10	58.0	191	94.9	19.1	673

In Table 2, excessive heavy metal contents (respective of each of the given elements) are indicated with blue for the tested species. The comparative results are summarized in Fig. 1.
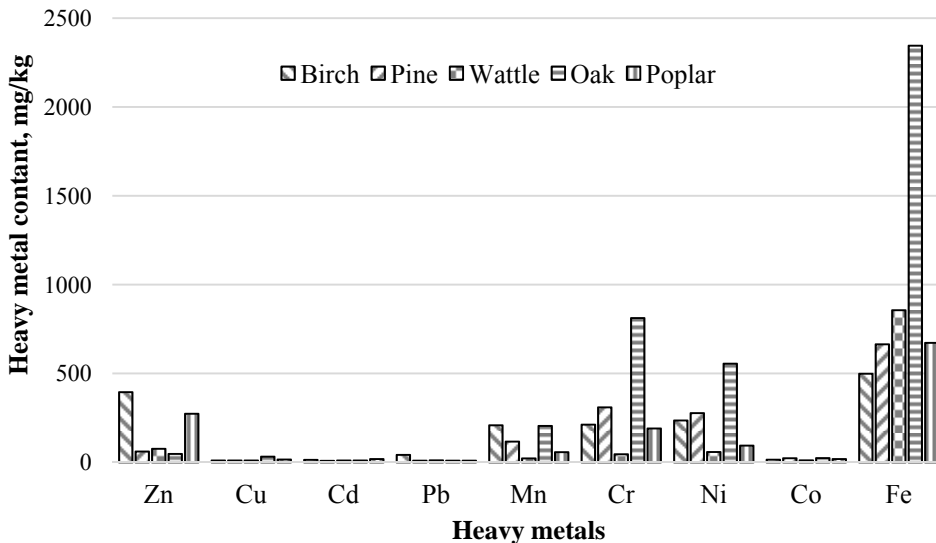

Figure 1. Heavy metal content of the tested woody samples

The results show the actual heavy metal content of the tested biomass samples. Since the test pieces had been sampled from differently contaminated sites, these figures are not informative of the typical accumulative potential of the given species.

3.2. *Soil chemical analysis of the sampling site*

Soil samples were obtained from the defined target areas, and the heavy metal content of the samples was determined. The analysis results presented in Table 3 are representative of the *status quo* (current state) of the respective area. The data suggest that the pollusive metals are unevenly distributed along the sampling sites.

Compliant with the existing legislation, the assessment and evaluation of site-specific soil contamination shall regard the total elemental composition of the target area. Accordingly, the results presented in Table 3 indicate the total heavy metal content of the tested soil samples – which does not correspond to the actual bioavailability of metals for remediation.

By comparing the results of Table 3 with the limit values, it can be concluded that the *soil sample 2* from *site B* is currently the least contaminated among the target areas. The tested soil samples reliably prove that the respective sites are seriously contaminated with heavy metals, thus, they should be identified as brownfields.

*Total heavy metal content of the tested soil samples, and limit values for the disposal
and discharge of metal and metalloid pollutants in geological media,
mg/kg (dry matter)*

Total heavy metal content	site A		site B		site C	Limit value
	1	**2**	**1**	**2**		
	mg/kg					
Zn	495	640	2599	110	5028	200
Cu	223	275	327	67	1113	75
Cd	8	10	20	6	28	1
Pb	1651	3542	752	24	9169	100
Cr	87	94	101	88	66	75
Ni	14	20	25	24	19	40
Co	28	17	20	24	11	30
Fe	45300	65800	29800	35700	72300	–
Ba	687	657	365	477	405	250

Annex 1 to Joint Decree *No.* 6/2009. *(*IV. 14.*)* KvVM-EüM-FVM *of the Hungarian
Government on limit values established for the protection of groundwater
and the geological medium, 2009*

3.3. Heavy metals in the ash

In the following section, the electronmicroscopic images of two ash samples are analysed. Fig. 2 shows the 100 μm resolution micrograph of ash obtained from the combustion of birch briquette. Compositional analysis was conducted at two salient/characteristic points of the respective sample. The highest value of heavy metal concentration was detected at point 1, where the sample contained 63.29% m/m of iron.
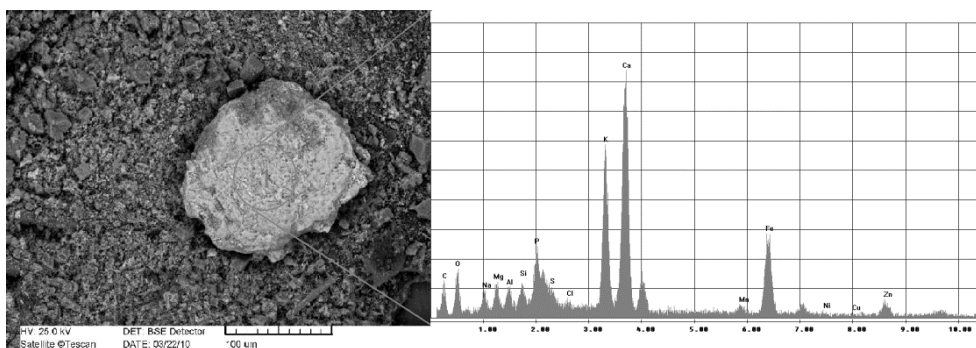
Na	Mg	Al	Si	P	Cl	K	Ca	Mn	Fe	Cu	Zn
% m/m											
3.88	1.07	1.8	1.52	<DL	0.16	4.32	1.68	0.92	63.29	0.12	6.8

*Figure 2. SEM micrograph of the ash produced from the experimental combustion of
birch briquette, with the spectrum and compositional data measured at point 1*

Fig. 3 shows a 50 µm resolution micrograph of the ash produced from the combustion of poplar briquette containing 1.45% m/m of Zn.
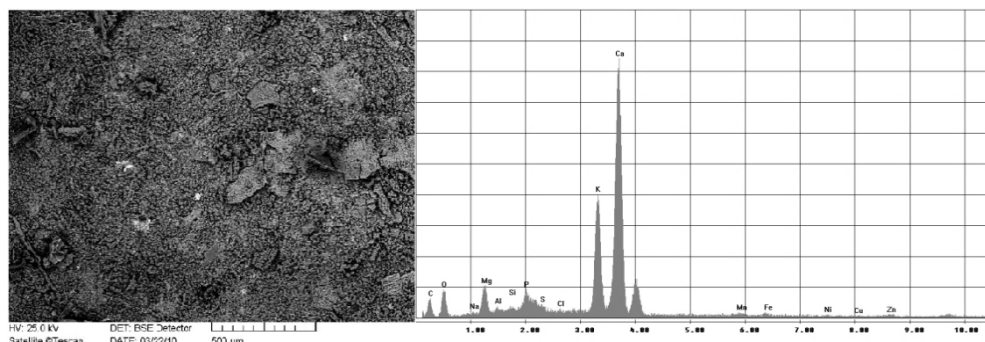
Na	Mg	Al	Si	P	Cl	K	Ca	Mn	Fe	Cu	Zn
% m/m											
0.56	4.85	0.5	0.36	1.89	0.2	14.0	35.12	0.76	0.83	0.47	1.45

Figure 3. SEM micrograph of the ash produced from the experimental combustion of poplar briquette, with the measured spectrum and compositional data

Table 5 summarizes the average composition of the ashes produced from the combustion experiments. The data are calculated from the analysis and evaluation of the SEM images and from the spectra acquired for the biomass samples.

Table 5

Elemental composition of the ash samples, based on the EDS analysis of the combusted biomass

Sample	Na	Mg	Al	Si	K	Ca	Mn	Fe	Cu	Zn
	% m/m									
Birch column	8.97	2.98	0.61	0.94	12.80	18.7	2.10	0.42	0.46	11.8
Pine column	0.33	2.42	2.17	0.78	17.73	31.2	1.52	0.70	0.81	1.06
Acacius column	0.36	1.37	0.54	0.37	13.28	32.1	0.53	17.2	0.54	0.61
Oak column	0.40	2.68	0.86	0.43	19.91	34.5	1.51	0.41	0.56	0.75
Poplar column	1.18	3.90	0.61	0.73	12.47	34.1	0.43	0.78	0.41	1.87
Birch briquette	2.03	2.72	1.71	1.16	10.92	21.6	1.34	17.9	0.26	4.49
Pine briquette	0.91	2.94	2.23	2.11	12.15	20.7	2.57	12.1	0.37	1.08
Acacius briquette	0.43	2.77	0.64	0.76	16.42	33.7	0.45	0.83	0.52	0.98
Oak briquette	0.51	2.66	0.55	1.09	9.10	28.2	1.79	6.81	0.60	0.98
Poplar briquette	0.82	5.45	0.35	0.28	17.46	29.7	0.76	0.57	0.57	7.99

Based on the results it can be concluded that the heavy metals accumulated in the biomass fuel are traceable in the ashes. The exact amounts can be determined from further chemical-compositional analyses.

3.4. Heavy metals in the fly ash

In the following section, the electronmicroscopic images of two fly ash samples are analysed. Fig. 4 shows the 100 μm resolution micrograph of a fly ash sample produced from the combustion of an oak column. Compositional analysis was conducted at three salient points of the respective sample. The highest value of heavy metal concentration was detected at point 2, where the sample contained 76.26% m/m of iron.
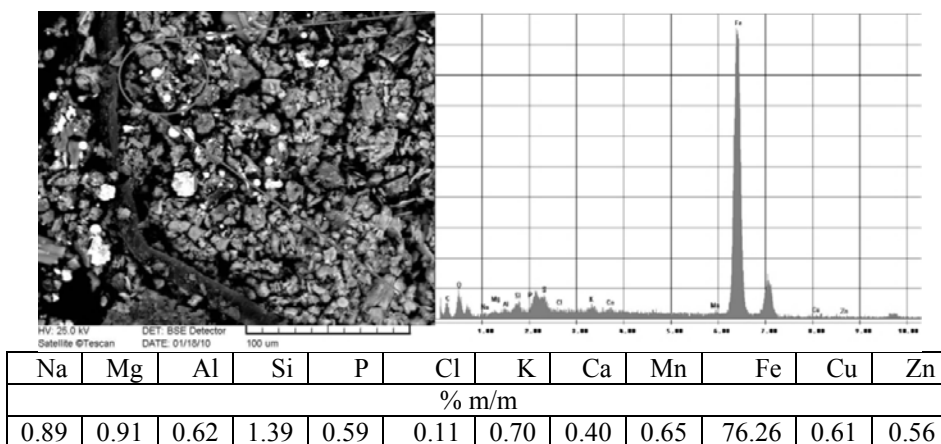

Na	Mg	Al	Si	P	Cl	K	Ca	Mn	Fe	Cu	Zn
% m/m											
0.89	0.91	0.62	1.39	0.59	0.11	0.70	0.40	0.65	76.26	0.61	0.56

Figure 4. SEM micrograph of the fly ash (particulate matter in the flue gas) sampled from the experimental combustion of an oak column, with the measured spectrum and compositional data at point 2

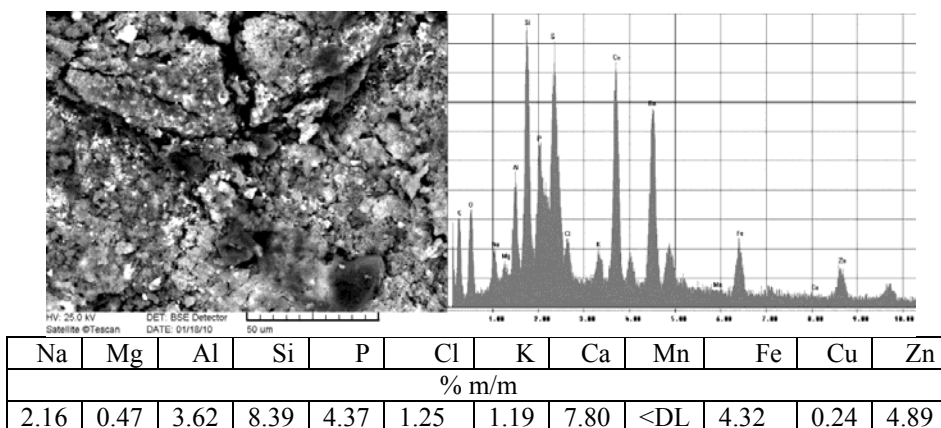| Na	Mg	Al	Si	P	Cl	K	Ca	Mn	Fe	Cu	Zn
% m/m											
2.16	0.47	3.62	8.39	4.37	1.25	1.19	7.80	<DL	4.32	0.24	4.89

Figure 5. SEM micrograph of the fly ash (particulate matter in the flue gas) sampled from the experimental combustion of a pine column, with the measured spectrum and compositional data

Fig. 5 shows a 50 µm resolution micrograph of solid residual particles in the flue gas sampled from the experimental combustion of a pine column. The sample contained 4.89% m/m of Zn and 23.45% of m/m Ba.

Table 6 summarizes the average composition of the fly ash samples produced from the combustion experiments. The data are calculated from the analysis and evaluation of the SEM images and the spectra acquired.

Table 6.

Elemental composition of the fly ash samples, based
on the SEM analysis of the combusted biomass

Sample	Na	Mg	Al	Si	K	Ca	Mn	Fe	Cu	Zn
	% m/m									
Birch column	2.5	0.3	0.7	4.9	4.8	2.4	0.2	0.5	0.2	2.7
Pine column	6.7	0.3	0.5	4.7	11.9	7.6	0.3	2.4	0.2	0.3
Acacius column	2.0	0.7	0.6	1.9	22.9	7.3	0.2	0.1	0.3	0.9
Oak column	1.0	1.0	0.7	2.6	15.0	8.4	0.4	3.3	0.1	1.0
Poplar column	2.0	0.6	0.6	2.4	17.1	4.4	0.4	2.0	0.3	2.1
Birch briquette	4.6	0.7	0.3	2.9	25.9	5.0	0.2	1.2	0.4	0.7
Pine briquette	4.0	0.7	0.6	6.7	10.1	4.8	0.1	2.3	0.4	2.2
Acacius briquette	1.5	0.6	0.4	2.0	6.9	4.0	0.3	1.9	0.4	0.3
Oak briquette	1.4	1.3	0.8	5.3	12.3	15.3	0.8	0.7	0.7	1.8
Poplar briquette	2.4	0.6	0.8	3.5	14.1	3.7	0.3	2.3	0.4	2.5

The results demonstrate the potential hazards of the flue gas produced from the combustion of the respective biomass. As it can be seen, considerable amounts of toxic metals (Cu, Fe, Mn, Zn) are adsorbed on the surface of the fly ash particles. An additional environmental risk is set by the stream released from the outlet pipe at a temperature of 450–500 °C, since the steam-gas phase of the hot flue gas also contains metal compounds. The assessment of the expected impact needs further investigation. It seems to be certain, however, that any emissions from the combustion of heavy metal contaminated biomass are potentially subject to strict environmental control and regulation. The cooling of the released flue gas or the installation of a flue gas cleaning device/purging system would be recommended for safe operation.

Conclusions

The reutilization of various types of brownfields, including the sustainable reuse of heavy metal contaminated sites are recently coming into the focus of attention. It seems a viable option to grow energy crops on polluted soils, thereby accumulate high levels of the hazardous metals in plant tissues.

This paper presents the results of SEM analyses performed on the combustion residues of contaminated biomass samples. The figures are indicative of the heavy metal content of the respective samples, yet they do not provide exact quantitative data for the separate determination of each elemental component. For more detailed analysis, destructive measurements and chemical testing is required.

It is essential to get a thorough knowledge of the composition of the burning residues, with special respect to the level and distribution of heavy metals. Due to the presence of toxic metals in the ashes and the flue gas of the combusted biomass, the treatment and disposal of such waste is a matter of environmental concern.

Acknowledgements

References

[1]   KörnyezettudományiKözpont, Barnamezős Adatbázis, http://www.ktk-ces.hu/ barnamezo_ adatbazis.html

[2]   *Biofiom project,* zárótanulmány. Bay Zoltán Alkalmazott Kutatási Közhasznú Nonprofit Kft.

[3]   Duffus, John H.: „Heavy metals" a meaningless term? (IUPAC Technical Report) *Pure Appl. Chem.*, 2002, Vol. 74, No. 5, pp. 793–807 doi:10.1351/pac200274050793

[4]   Láng I. (2007): *Környezetvédelmi lexikon*. Akadémiai Kiadó, Budapest 2007.

[5]   Xiangdong Li–Chi-sun Poon–Pui Sum Liu: Heavy metal contamination of urban soils and street dusts in Hong Kong. *Applied Geochemistry*, Volume 16, Issues 11–12, August–September 2001, pp. 1361–1368.

[6]   Hall, J. L.: Cellular mechanisms for heavy metal detoxification and tolerance. *Journal of Experimental Botany*, Volume53, Issue 366, pp. 1–11.

[7]   Muhammad Nazmin Bin Yaapar–Intan Ndhirah Binti Masri–Nuradliza Binti Baharom–Yeow Jiing Shyi–Hanafi B Mohd Ali: *Biology-Online.org*. Article published on 23 June 2008.in http://www.biology-online.org/articles/phytoremediation-a-lecture/phytoextraction.html (20. 07. 2011)

[8]   Lehoczky É.–Szabados I.–Marth, P.: Cd content of plants as affected by soil Cd concentra-tion. *Comm. in Soil Science and Plant Analysis*. 27 (5–8) pp. 1765–1777.

[9]   Lehoczky É.–Szabó L.–Horváth Sz.: Cadmium uptake by lettuce (Lactuca sativa L.) in different soils. *Comm. in Soil Science and Plant Analysis*, 29 (11–14) pp. 1903–1912.

[10]   Lehoczky É.–Marth, P.–Szabados I.–Palkovics M.–Lukács P: Influence of soil factors on the accumulation of cadmium by lettuce. *Commun. of Soil Sci. and Plant Anal*. 31 (11–14) pp. 2425–2431.

[11]   Meers, E.–Ruttens, A.–Hopgood, M. J.–Samson, D.–Tack, F. M. G.: Comparison of EDTA and EDDS as potential soil amendments for enhanced phytoextraction of heavy metals. *Chemosphere,* 58 (2005) 1011–1022.

[12]   FRTR Remediation Technologies Screening Matrix and Reference Guide http://www. frtr. gov/matrix2/top_page.html

ENERGY EFFICIENCY ENHANCEMENT IN THE HOT ROLLING MILL

ERIKA KUN[1]–TAMÁSNÉ SZEMMELVEISZ[2]

Hungarian steel producer ISD Dunaferr Ltd. is a pioneer in implementing integrated iron and steel processing technology in large-scale domestic industrial production. The product portfolio ranges from pig iron through BOF steel manufacturing to hot- and cold-rolled coils and sheets, steel profiles and shaped steel sections. The reported gross energy consumption of the Company Group is 30 PJ per year, which accounts for nearly 30% of the total annual costs. The bulk of energy expenditures are realized as fuel costs to accommodate primary fuel needs (i.e. coke) for the conversion of iron, nonetheless, considerable sums are spent on electricity and natural gas supply too. In order to retain the company's favorable market position and economic competitiveness, the careful use of energy resources – including the reduction of process-specific energy consumption and improving energy efficiency – seems to be a key factor.

In terms of specific energy consumption, the hot rolling process largely contributes to the total energy input required for the smooth operation of the plant. Roll forming mills have the highest electricity needs, and considerable heat energy is consumed by continuous slab reheating furnaces.

With a view to ensure effective operation and enhanced performance, ISD Dunaferr Company Group has set forth to increase its production capacity by 20%. The streamlining of energy use and the rationalization of energy costs are considered to be crucial milestones on the way forward.

Keywords: hot rolling, energy efficiency, data mining

Introduction

Integrated steel production, that is the production technology used by ISD Dunaferr Company Group and its predecessors, dates back to the 1950s. The iron and steel processing units started operating one by one, the Hot Rolling Mill (HRM) was put into operation in 1960. Accordingly, today a more than 50-year-old rolling facility is expected to compete with other recently established hot rolling systems. In order to remain competitive, the company needs to implement continuous improvements in the production technology, yielding high quality marketable products at low production costs, with special respect to energy costs. Compared to Europe's other integrated steel production companies, the Dunaferr hot rolling mill is one of the biggest energy consumers in the region. Besides the tremendous amount of fuel required to operate the reheating furnaces, the electricity needs of the metal forming process is also massive.

This paper gives an overview of our ongoing research concerning the energy reduction potentials of the HRM, with respect to the diversity of the production portfolio.

[1] ISD POWER Kft.
2400 Dunaújváros, Hungary
kun.erika@isdpower.hu
[2] University of Miskolc, Department of Combustion Technology and Thermal Energy
3515 Miskolc-Egyetemváros, Hungary
tuzszemt@uni-miskolc.hu

1. Hot rolling and ways of reducing energy consumption

1.1. Hot rolling process

With regard to the gross energy requirements of integrated iron and steel technology, hot rolling (Fig. 1) can be identified as one of the most energy-intensive steel manufacturing processes, with an electrical energy need of about 30% of the total energy consumed.
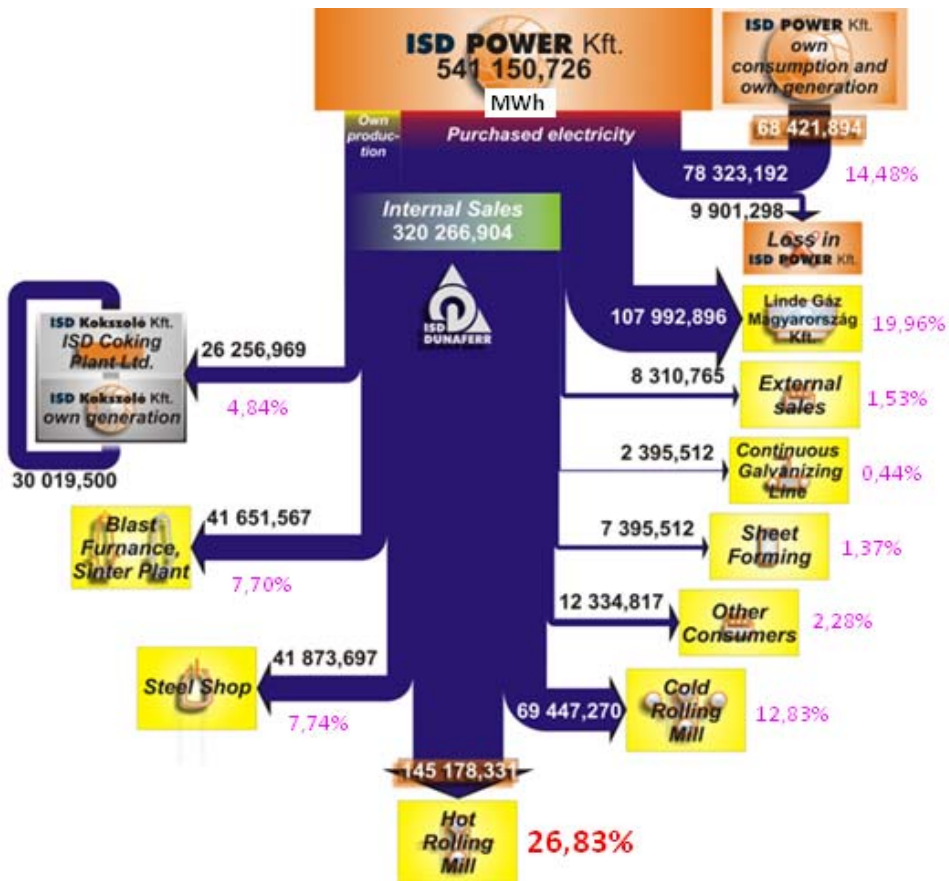

Figure 1. Electricity consumption of ISD Dunaferr Company Group
Source: ISD Dunaferr Directorate of Energy

The aim of the hot rolling process is to produce coils or sheets (for further processing) that fit the preliminary set size and quality demands.

Rolling is a specific case of forging done with rotating rolls [1].

The term 'hot rolling' describes a process when mainly metals are formed at temperatures above the recrystallization temperature. When applied to low carbon steel, the

1. Hot rolling and ways of reducing energy consumption

1.1. Hot rolling process

With regard to the gross energy requirements of integrated iron and steel technology, hot rolling (Fig. 1) can be identified as one of the most energy-intensive steel manufacturing processes, with an electrical energy need of about 30% of the total energy consumed.
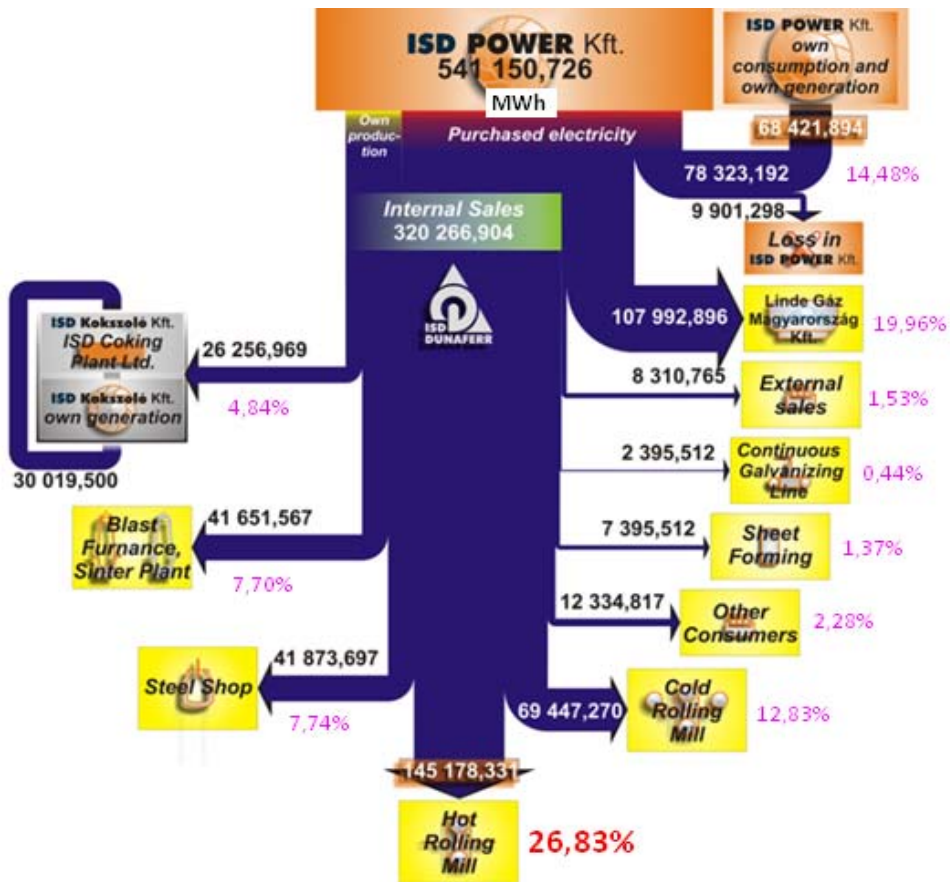

Figure 1. Electricity consumption of ISD Dunaferr Company Group
Source: ISD Dunaferr Directorate of Energy

The aim of the hot rolling process is to produce coils or sheets (for further processing) that fit the preliminary set size and quality demands.

Rolling is a specific case of forging done with rotating rolls [1].

The term 'hot rolling' describes a process when mainly metals are formed at temperatures above the recrystallization temperature. When applied to low carbon steel, the

Along with a decrease in the target discharging temperature of slabs, the necessary amount of heat – thus, the quantity of the combusted fuel used for reheating – will decrease as well. On the other hand, higher deformation resistance due to lower slab temperatures causes greater deformation torque resulting in higher electricity consumption. The two trends are controversial, which means that in principle an optimal forming temperature should be found, where the sum of the energy needs of reheating and forming can be minimized [4].

The aim of this research is to examine whether such an optimization could be realized in the HRM of ISD Dunaferr Company Group, and what the boundary conditions of feasibility are.

This task is rather challenging given that a number of variables and unknown, sometimes unpredictable values has to be taken into consideration as risk factors in the future optimization attempts. In this case, simplification is a must. The next chapter introduces a way to simplify the operation of the HRM and to transform the operational scheme into a simple Energy Management Model.

Chapter 3 reveals a calculation-based approach, Chapter 4 introduces a "Data Mining approach" for calculating the energy consumption of the process.

1.3. Energy Management Model

System (management) modelling was made to carry out examinations regarding the possibilities of energy consumption reduction and to define the technical parameters for optimal operation and for the reduction of unit energy needs. The ultimate aim was to achieve decreased energy costs (being fully aware of the fact that energy management is not separable from energy costs).

An energy management system should be defined for the smallest individual settlement unit. Herein, the great energy consuming processes in the HRM are treated as one single individual settlement unit [5].
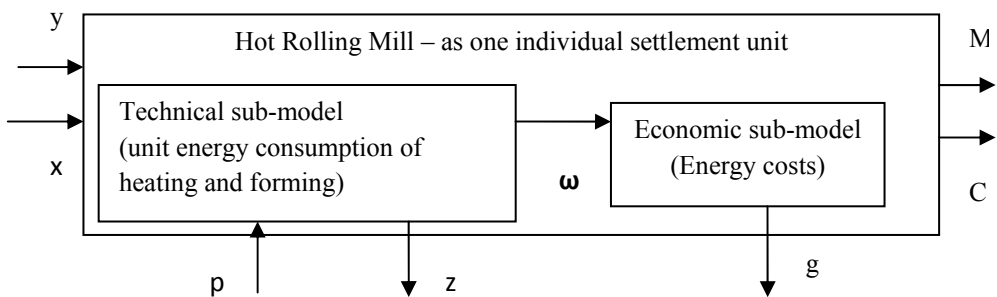

Figure 2. Energy management model of the hot rolling mill

Modelling starts with the definition of the limits of the system. The research focuses on the great energy consuming processes of the HRM, where the limits are: the fuel supply and combustion systems of the furnaces (walking beam and pusher type), the horizontal and vertical stands of the rougher, the drives and motors, the coil box, the 6-stand continuous

finishing line with drives and motors, the laminar cooling device and the down-coiler with its motor.

Table 2 reveals the input and interim parameters of the model.

The model's target function (i.e. the linear combination of each consumption unit) can be displayed in the following form:

$$C = a^T * E = [a_1 \quad a_2 \quad a_n] \begin{bmatrix} E_1 \\ E_2 \\ E_n \end{bmatrix}, \text{where}$$

$a_1, a_2 \ldots a_n$: weighting factors,
$E_1, E_2 \ldots E_n$: energy consumption (per unit).

Table 2

Variables of the energy management model of the hot rolling mill

Variables, short description	
p: fixed data: the values from the main task of the process, criteria of the target function	– forming temperature of the target quality – heating characteristics/velocity assigned to a given quality – minimum discharging temperature – acceptable maximum forces at the rolling equipment – electrical limit values on motors – maximum torque values at rolling drives
y: environmental values: data describeing the effect on the environment	– heating values of coke oven gas and natural gas (average value for a given period of time) – average electricity and natural gas prices
x: optional value variable: variables with at least 2 different values that the task could be performed with, considering the limiting criteria	– discharging temperature – way of reheating
ω: technical values determining the operation of the economic sub-model	– unit energy consumption for each energy resource
M: sensitivity matrix	– how the 'y' environmental variables influence the target function
z and **g** parameters	– interim values of model calculation

In this case we presume that the operation of the technical sub-model determines the result of the economic sub-model. (Given this particular technology, "energy cost-driven production" would be hard to imagine.) Our further aim is to specify cases, if there is any, when the economic sub-model would define the operation of the technical sub-model, thus the direction of relationship would be altered.

2. Study on energy consumption: calculating energy needs

2.1. Reheating

To describe the efficiency of the reheating process in terms of energy consumption, the heat balance of the furnace can be used. The simplified heat balance can be described with the following equation:

$$Q_{in} = Q_e + Q_{fg} + Q_s + Q_w + Q_r$$

where: Q_{in}:   heat of combustion (of the fuel);
            Q_e: enthalpy of the steel,
            Q_{fg}:   sensible heat (loss) in the flue gas,
            Q_s: heat loss in the cooling water (skid loss);
            Q_w: wall (heat) loss;
            Q_r: heat loss due to openings and other unaccounted heat loss.

The discharging temperature is set with respect to the deformation capability and the required structure of the material. As regards the HRM of ISD Dunaferr Company Group, the minimum target discharging temperature of the slabs is 1200 °C.

3.2. Electricity need of the forming process

The following formula can be used to characterize the electricity needs of the forming process:

$$W_{el} = W_w / \eta_L / \eta_{Ma} / \eta_M * k_A$$

where $W_w = V * k_{wm} * \varphi_h$, unit work of deformation,
         φ_h magnitude of deformation in the direction of the biggest deformation,
         k_{wm} medium deformation stress,
         η_L coefficient of friction in bearings,
         η_{Ma},   efficiency of the drives,
         η_M efficiency of the motors.

The electricity consumption of hot rolling depends on the following factors:
- quantity of material (to be processed),
- forming temperature,
- forming velocity,
- geometry of the workpiece,
- geometry of the forming zone,
- method of widening,
- friction conditions between the workpiece and the forming tools.

3. Study on energy consumption – "data mining"

Data mining: the extraction of hidden predictive information from large databases. ISD Dunaferr Company Group does not have an integrated energy management system. Ø Energy-related data are measured and collected in different databases.

In view of the energy features of the hot rolling technology, the following databases are available:

Availability of energy-related data (by ISD Dunaferr)

Combustion fuel measurements		
Coke oven gas	Metered at the point of delivery	Minute resolution time series
Natural gas	Metered at the point of delivery	Minute resolution time series
Electricity data		
Measurements at the point of delivery of HRM	Load and consumption	Quarter of an hour resolution average load time series
Metering of the forming tools	Data Acquisition System of the HRM	Discreet measurement series, collectable to each slab rolled

The hot rolling mill has its own data acquisition system to collect all the information necessary for quality management purposes. This database is a thorough collection of the technical parameters of rolling, with data e.g. on the applied torque(s), the maximum width and height of the strip, the temperature distribution along the strip, maximum applicable linear reduction; the temperature of coiling, the length and weight of the strip and the coil, cropping etc. Among the above listed data we find a few energy-related ones, like the power supply for roughing (horizontal and vertical drives) or the electricity need of the continuous finishing line.

The "excavation"/extraction/deduction of hidden correlations from the large database and the analysis of the data influencing the energy needs was done with the tool called RapidMiner. With data mining, the following issues have been/can be examined:

1. Data related to the forming process and deformations
   a) the chemical composition of the workpieces, the production portfolio,
   b) temperature characteristics of the workpieces during processing, target temperature after rolling and before down-coiling,
   c) the torque of the forming tools,
   d) the power consumption of the forming tools.
2. Power consumption associated with different deformation strengths;
3. Power consumption assigned to different target qualities;
4. Ø Combustion variables assigned to average and extreme power consumption values.

Following the data mining process, the research process presented above shall be accomplished by setting correlations between electricity consumption and the technical parameters of the process (quality, size, temperature), which will determine the steps of our further investigations.

Acknowledgement

References

[1]   VOITH, M.: *A képlékenyalakítás elmélete*, Miskolci Egyetemi Kiadó, Miskolc, 1998, pp. 65.
[2]   KUN, E.: *Energy efficiency enhancement of the hot rolling mill*, MicroCad 2014.
[3]   SPITTEL, T.–HENSEL, A.: *Rationeller Energieeinsatz bei Umformprozessen*. Leipzig, 1983.
[4]   BRAUN, G.: *Az acél szélesszalag meleghengerlési technológia tervezésének újszerű alapelvei*. PhD-értekezés; Kerpely Antal Anyagtudományok és technológiák Doktori Iskola, Miskolc, 2003.
[5]   BALIKÓ, S.: Az energiagazdálkodási model. *Energiagazdálkodás*, 52. évf. 3. sz. (211) pp. 3–5.

EFFECT OF SILVER CONTENT ON THE PROPERTIES OF LEAD-FREE SOLDERS

ALÍZ MOLNÁR[1]–IBOLYA KARDOS[2]–ISTVÁN MOLNÁR[3]–ZOLTÁN GÁCSI[4]

According to the new RoHS Directive 2011/65/EU of the European Union on the restriction of hazardous materials for environmental reasons, the application of lead-containing solders in electronic devices should be avoided. It follows that Hence, there is an increased interest in lead-free solders to ensure the reliable operation of electronic devices under extreme conditions (e.g. high temperature, vibration) and to overcome/surpass the limits of resilience in lead-containing solders [1].We studied the relationship between silver content (1%, 2%, 3%, 4%) and the structural-mechanical properties of SAC alloys.
Keywords: soldering alloy, lead-free, SAC

Introduction

As of July 1, 2006, it is forbidden to use lead-containing solders in the production of electronic devices. Electronic products to be installed in vehicles are exempt on a temporary basis. Even though lead-free solders are long since known in production technology, eutectic tin-lead solders – already used some thousand years ago – have undoubtedly taken the leading role and become widespread in the production industry. With lead being phased out, there is, however, a strong interest in lead-free solders, particularly in eutectic Sn-Ag and Sn-Ag-Cu (SAC) alloys. Instead of 183 °C, that is the melting point of the eutectic Sn-37% Pb alloy, these materials have a melting point of approx. 221 °C. This property allows for higher application temperatures [2]. Newly introduced lead-free solders have to comply with several application requirements such as: no substances potentially harmful to human health are contained; long-term availability of material components; material compatibility with the technologies and electric components currently in use; easy solvability of repair issues, price competitiveness and comparability to that of Sn/Pb alloys [3].

---

[1] University of Miskolc, Faculty of Materials Science and Engineering
  Institute of Physical Metallurgy, Metalforming and Nanotechnology
  3515 Miskolc-Egyetemváros, Hungary
  femaliz@uni-miskolc.hu
[2] ISD Dunaferr Zrt.,
  2400 Dunaújváros, Hungary
  kardos.ajbolya@gmail.com
[3] University of Miskolc, Faculty of Materials Science and Engineering
  Institute of Physical Metallurgy, Metalforming and Nanotechnology
  3515 Miskolc-Egyetemváros, Hungary
  femtanasz@gmail.com
[4] University of Miskolc, Faculty of Materials Science and Engineering
  Institute of Physical Metallurgy, Metalforming and Nanotechnology
  3515 Miskolc-Egyetemváros, Hungary
  femtangz@uni-miskolc.hu

Out of SAC alloys, alloys with nearly eutectic composition containing 3.0 to 4.0 weight% silver and 0.5 to 1.0 weight% copper are the most common [1, 2]. *Che* et al. [4] studied a SAC alloy with 1%, 2% and 3% silver, with particular emphasis on the relationship of silver content and mechanical properties such as elongation, conventional yield strength and tensile strength. They determined that higher silver content is associated with higher strength. Increased silver content reduces the formability of solder joints and consequently shortens the service life of electronic components. This statement corresponds to the test results reported by *Amagai*, M. et al. [5]. Accordingly, materials with low silver content are targets for use wherever possible. The silver content of the alloy clearly affects the volume fraction of the Ag_3Sn intermetallic phase formed and the size of tin grains. As a result at elevated Ag levels, a well-dispersed intermetallic phase and small tin grain size can be detected in the microstructure of the solder, which allows for higher strength properties strength and higher resistance to fatigue. All this is confirmed by *Terashima* et al. [6] who, based on the results of thermal fatigue examinations stated that solders with higher silver content have a higher fatigue life.

1. Experimental

The studied samples involved commercially available and widely used SAC105, SAC205, SAC305 and SAC405 solders. For the preparation of the test pieces, two kinds of mold were used, as shown in Figures 1 and 2. The first mold (*Figure 1*) is appropriate for the casting of a cylindrical body, which can be processed into a standard (DIN-EN-50125) tensile test piece. The second (*Figure 2*) is suitable for the preparation of coin test pieces that are used for microscopic examination and hardness tests.
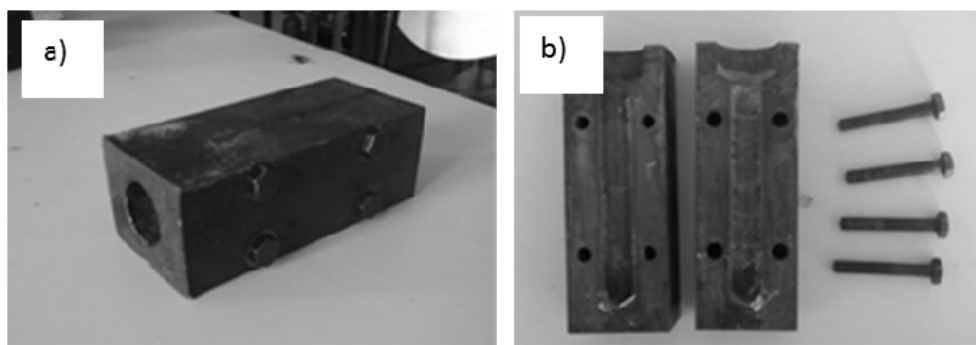

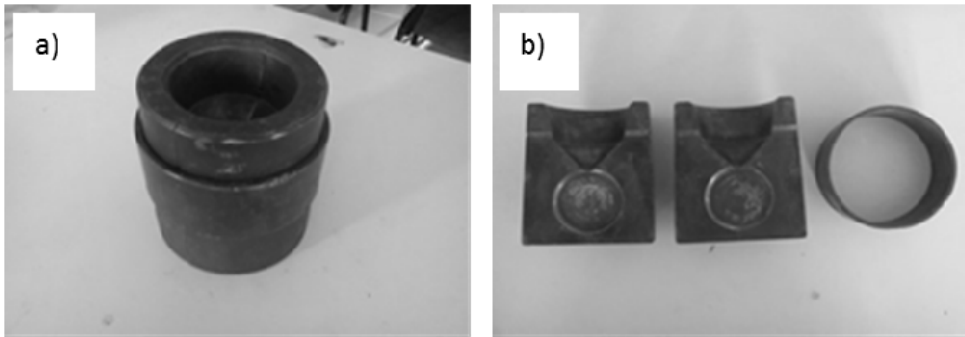*Figure 1. Mold for tensile test pieces before casting (a) and dismantled (b)*

Figure 2. Mold for coin test pieces before casting (a) and dismantled (b)

The melting and casting parameters for the casting process were the following.

Melting and casting parameters

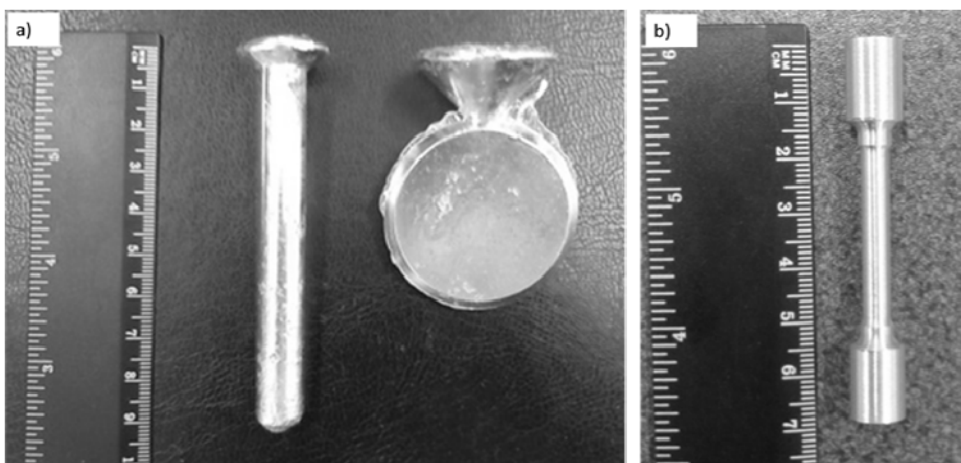| Parameter	Value
Melting temperature	350 °C
Mold preheating temperature	230 °C
Holding time before the first casting	30 min
Melting time for the second and third casting	10 min
Mold preheating time for the first casting (minimum)	1 hour
Mold preheating time for the second and third casting	7 min

As-cast pieces are shown in *Figure 3*.

Figure 3. Casted tensile test piece and coin test piece (a), machined tensile test piece (b)

The chemical composition of the studied specimens (Table 2) was determined using inductively coupled plasma (ICP) spectrometry.

<div align="right">*Table 2*</div>

<div align="center">*Composition of the studied solders*</div>

Specimen ID	Elements (%)						
	Sn	**Ag**	**Cu**	**Bi**	**Pb**	**Sb**	**Zn**
SAC105	98.3273	1.15	0.514	< 0.005	0.0015	0.0011	0.0011
SAC205	97.2499	2.21	0.511	0.0010	0.0012	0.0167	0.0102
SAC305	96.156	3.35	0.485	< 0.005	0.0020	0.0012	0.0008
SAC405	95.1727	4.28	0.536	< 0.005	0.0032	0.0013	0.0018

2. Results

The proper preparation of test pieces (from solders) is a necessary prequisite for optical microscopy analysis. For specimen grinding, SiC abrasive paper was used. In this case, the grinding step was completed with the application of P1000 grade abrasive paper. Grinding was followed by polishing, where the specimens were subject to surface modification by various grade cloths and diamond suspensions of various particle size. Polishing started with woven cloth and a 9 μm diamond suspension, then a 3 μm suspension. Next, fleecy cloth was applied with a 3 μm diamond suspension again. Eventually, final polishing was performed using colloidal silica gel on a fleecy cloth. Colloidal silica gel contains negatively charged SiO_2 parts of a pH between 8 and 11, which softly etches the surface of the specimen, therefore the primary ß-Sn dendrites and the $Sn-Ag_3Sn$ and $Sn-Cu_6Sn_5$ eutectics between dentrites could be made clearly visible in the studied specimens.

Optical microscopy analyses were carried out using a Zeiss Observer Z1m light microscope and AxioVision Rel. 4.8 software. *Figure 4* presents the optical micrographs of the ground-polished specimens at a magnification of 100x. The micrographs affirm the observations described in the literature about the scarce appearance of tiny Ag_3Sn intermetallic particles besides relatively large primary ß-Sn grains in the solder matrix of SAC105 (solders). A smaller quantity of primary ß-Sn dendrites are present in the SAC205 specimen, surrounded several tiny Ag_3Sn intermetallic particles in a random pattern. In the SAC305 alloy, Ag_3Sn forms a connected network around the primary ß-Sn. Here, primary ß-Sn grain size is, again, much smaller. In the SAC405 solder, the Ag_3Sn intermetallic particles are well-dispersed in the matrix, with the lowest inter-particle distances and the poorest quantity of primary ß-Sn grains.

To determine the surface area share of primary ß-Sn in the specimens, 20 visual fields were examined for each specimen using digital image analysis with AxioVision imaging software. The optical micrographs of SAC105 and SAC205 specimens were captured with bright-field illumination, then measurements were carried out (on these micrographs) by means of the AxioVision imaging software. This software offers the possibility of gray and binary image transformations. First, contrast and brightness adjustment was applied to the gray image, then noises were removed using sigma filter. Subsequently, the objects were

separated from the background (i.e. detection). In the binary image generated so, the tiny undetected areas were added to the detected objects using the so-called „Fill Holes" operation. Next, computational measurements were carried out. In case of SAC305 and SAC405 specimens, white light illumination was insufficient, thus, a dark field contrast procedure was applied. In doing so, we obtained images of proper quality for the digital image analysis whereby the primary β-Sn was distinguishable from the Sn-Ag$_3$Sn and Sn-Cu$_6$Sn$_5$ eutectics. The measurement was basically performed in a way similar to the previous two cases. The micrographs captured by the AxioVision imaging software with dark field illumination were passed on to contrast and brightness adjustment then filtering (Sigma filter). Following this, detection was performed and the unwanted detected objects were removed, finally measurements were executed. *Figure 5* shows the measurement results clearly confirming the observations from the optical micrographs, namely: with the increase of silver content, the surface area share of eutectic increases.
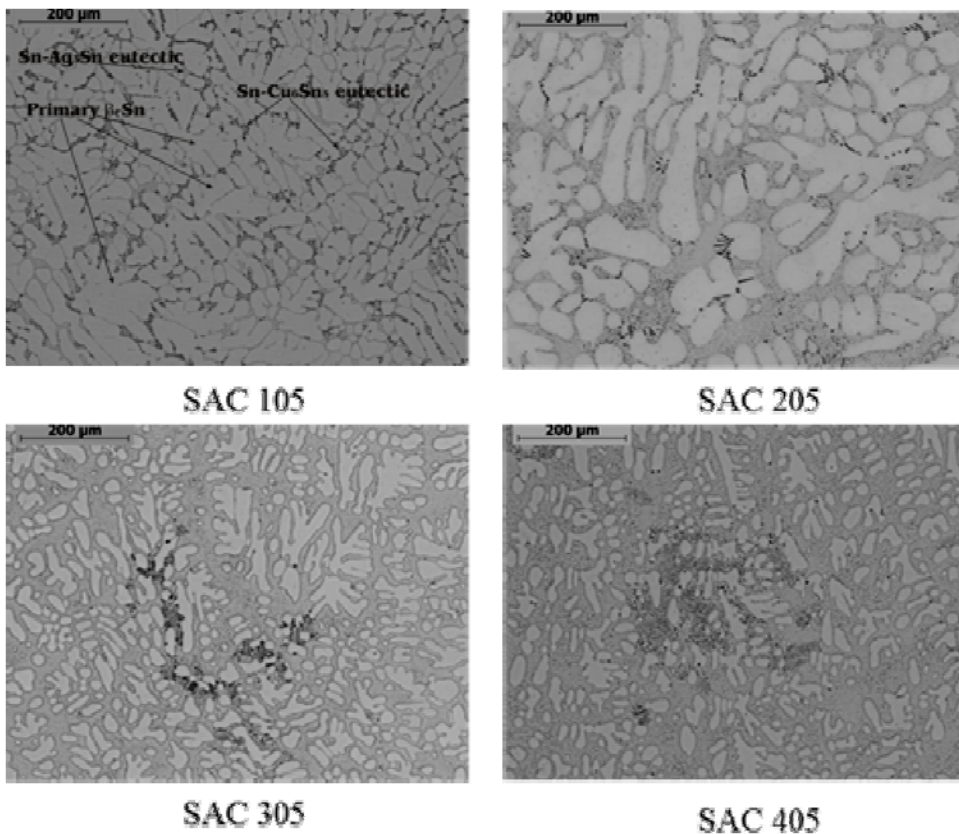
Figure 4. Optical micrographs of SAC 105, SAC 205, SAC 305 and SAC 405 specimens (original magnification: 100x)
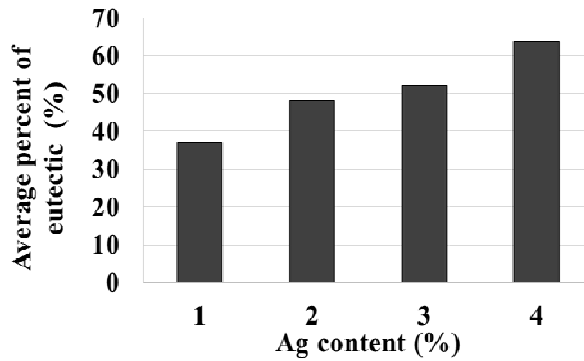
Figure 5. Variation of the surface area share of eutectic determined by digital image processing vs. silver content

Microhardness tests were performed using an Tukon 2100B apparatus, which operates on Vicker's principle. The analysis required ten measurements per specimen, with a load of 0.5 kg and a load time of 10 s.

The results of microhardness testing can be seen in *Figure 6*. Observably, as the silver content increases, the hardness of the solder rises, which is probably due to the growing number of Ag_3Sn intermetallic particles formed in the bulk material.
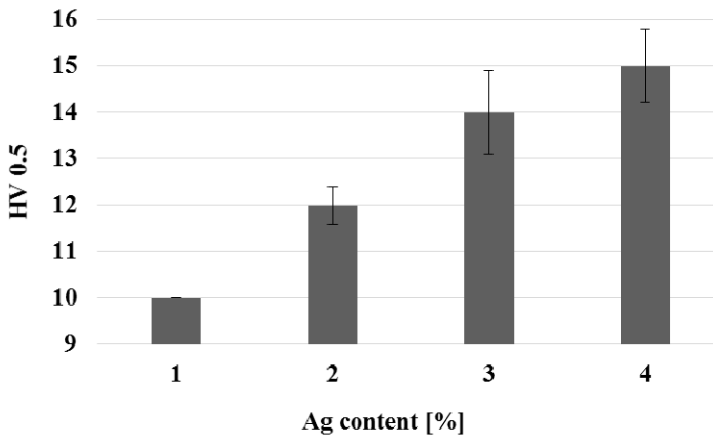

Figure 6. Variation of microhardness test values vs. increasing silver content

Tensile tests were performed at room temperature using an Instron 5982 type universal material testing machine, with a tensile speed of 3 mm/min. Based on the tensile test results (*Figure 7*) it can be stated that both tensile and yield strength rises with increasing silver content, except for the SAC405 specimen, where there is a minimal decline in yield strength compared to the SAC305 specimen.
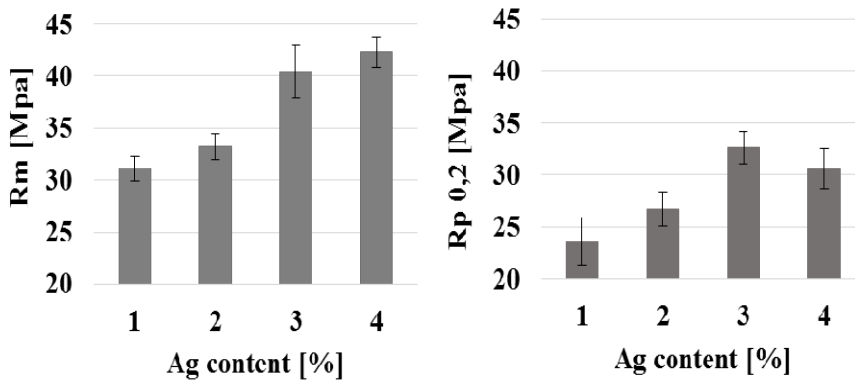
Figure 7. Variation of tensile strength and conventional yield strength values vs. increasing silver content
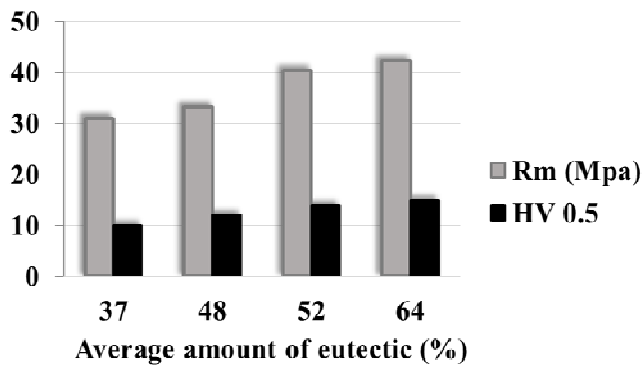

Figure 8. Effect of the quantity of eutectic on the studied parameters

Summary

In this paper, we studied the variation of microstructural and mechanical properties of SAC (Sn-Ag-Cu) lead-free solders vs. silver content (1%, 2%, 3%, 4%).

Based on the image analyses of optical micrographs it can be concluded that in the bulk material of lead-free SAC alloys, the quantity of Ag_3Sn rises with the silver content. Higher silver content results in an increased number of Ag_3Sn intermetallic particles and the reduced formation of primary ß-tin. It follows from this and the results of mechanical tests that the presence of small intermetallic particles improves the strength of solder. Therefore, both the Young's modulus and yield strength increase. The increase in the quantity of eutectic leads to also higher hardness values, which are confirmed by results in the professional literature [1–6] as well.

Acknowledgments

References

[1]   Eur-lex.europa.eu, Available: http://eur-lex.europa.eu
[2]   Böyük, U.–Marasli, N.: The microstructure parameters and microhardness of directionally solidified Sn–Ag–Cu eutectic alloy. *Journal of Alloys and Compounds*. 485, pp. 264–269 2009.
[3]   http://autotechnika.hu/uploads/files/archiv/2004/01/26-27.pdf, *Kötéstechnika. Ólommentes forraszanyagok.* pp. 26–27, 2004/1.
[4]   Che, F. X.–Poh, E. C.–Zhu, W. H.–Xiong, B. S.: Ag Content Effect on Mechanical Properties of Sn-xAg-0.5Cu Solders. *2007 9th Electronics Packaging Technology Conference,* pp. 713–718, 2007.
[5]   Amagai, M.: A Study of Nano Particles in SnAg-Based Lead Free Solders for intermetallic Compounds and Drop Test Performance. *Proc 56th Electronic Components and...,* pp. 1170–1190, 2006.
[6]   Kariya, Y.–Hossi, T.–Terashima, S.–Tanaka, M.–Otsuka, M.: Effect of Silver Content on Shear Fatigue Performance of SnAgCu Flip Chip Interconnects, J. Electron Mater., Vol 33., pp. 321–328, 2004.

PHYSICAL AND CHEMICAL ANALYSIS OF CANTEEN WASTES FOR SYNGAS PRODUCTION

GÁBOR NAGY[1]–ÁGNES WOPERA[2]–TAMÁS KOÓS[3]

This paper studies the physical and chemical properties of different types of food substance generally involved in the daily menu of a university canteen. The data obtained from proximate analysis (i.e. elemental composition, moisture and ash content) suggest that the tested food samples are suitable for synthesis gas production but should be mixed with dry matter from additional resources to make the process commercially viable.
Keywords: canteen waste, synthesis gas production, proximate analysis

Introduction

Apart from discarded food, considerable amounts of food processing or kitchen waste (i.e. remains from meal preparation) are generated in the daily practice of canteens. These are often disposed of as municipal waste in landfill sites. An economically beneficial alternative to landfill disposal is the energy utilization of food waste. Different technical solutions are available: biogas production (through biodegradation), combined waste incineration and synthesis gas production by pyrolysis/gasification.

A detailed study on the physical-chemical properties of canteen waste helps predicting whether the given feedstock/raw material is suitable for thermochemical conversion.

The exhaust gases produced from the pyrolysis/gasification process can be utilized directly as a fuel or, subsequent to purification, as a secondary raw material for the chemical industry. Therefore, the thermal conversion of food and canteen waste is likely to be of considerable economic importance in the long run.

Continuous feedstock supply is one of the most critical factors in the smooth operation of a syngas process plant (besides high initial investment costs). Considering the limited availability of food waste, it seems necessary to combine this feedstock with complementary raw material sources.

1. Synthesis gas production

Synthesis gas is a special gas mixture produced from the thermochemical conversion (pyrolysis, gasification) of different fuels like coals, biomass or wastes. It consists primarily of carbon monoxide and hydrogen (and to a lesser extent other organic components). Industrially generated syngas is target for various uses by the energy industry and the chemical industry, as illustrated in Figure 1 [1].

----

[1] University of Miskolc, Department of Combustion Technology and Thermal Energy
  3515 Miskolc-Egyetemváros, Hungary
  nagy.gabii86@gmail.com
[2] University of Miskolc, Department of Combustion Technology and Thermal Energy
  3515 Miskolc-Egyetemváros, Hungary
  tuzdb@uni-miskolc.hu
[3] University of Miskolc, Department of Combustion Technology and Thermal Energy
  3515 Miskolc-Egyetemváros, Hungary
  tuzkt@uni-miskolc.hu

The actual composition of the synthesis gas depends on the initial material, the gasifying medium, the time spent by the feed in the distinctive gasification zones and on process temperature and pressure. Relative to these factors, various pollutants may occur in the produced gas, which need to be removed lest they would cause adverse effects during industrial use.
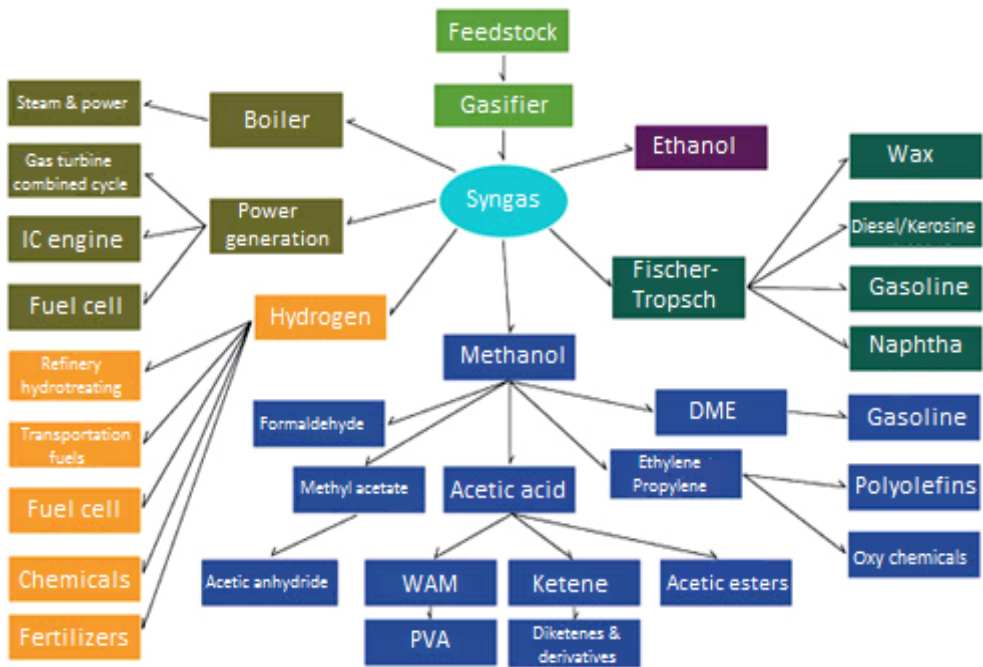

Figure 1. Flow chart of industrial syngas use

2. Materials

It is well-known from the literature that food materials (meat, vegetables, fruits etc.) are basically made up of water, fats, proteins and carbohydrates (Table 1). These building blocks can be broken down into elemental components like carbon, hydrogen and oxygen, which combine into the hydrogen and carbon monoxide fractions of the process gas.

Table 1

Basic parameters of food materials (expressed in weight percent) [2, 3, 4]

Parameter		Quantity
Moisture content	%	60–90
Oil or fat content (relative to dry matter)	%	0,1–50
Proteins (relative to dry matter)	%	0–41
Carbohydrates (relative to dry matter)	%	0,1–80

The parameters of ready-made dishes substantially differ from that of the initial food substances (particularly in moisture and oil/fat content). The scarcity of literary data on the elemental composition of prepared meals made it necessary to conduct investigations and lay the base – by ways of quantitative analyses – for experimental syngas production.

Due to excessive water content, soups were precluded from the experiments – only main courses were tested. The samples selected for testing were meals that occur on a daily base in university canteens, e.g. stews, fried and cooked meats, side dishes.

The data were first locally evaluated, then placed in a wider context. Estimates on the provision of feedstock were necessary to investigate the large-scale applicability of the proposed method (i.e. the pyrolysis/gasification of food waste in). Since the remains of ready-made food are not available in large enough quantities for industrial production0 – in Hungary, the total amount of canteen waste is about 220,000 tonnes per year [5] – supplementary raw material resources (like food preparation wastes) should be added to make gasification economically viable.

Subsequent to representative sampling, moisture content was determined using a Mettler Toledo HB43-S type moisture analyser. The samples were dried at a temperature of 105 °C until weight constancy was reached.

The dry samples were then pulverized in a mortar and loaded into a Carlo Erba EA 1108 type elemental analyser for compositional determination. The measurement method was based on the complete and instantaneous oxidation of the samples by flash combustion (thereby organic and inorganic substances could be converted into combustion products). The resulting combustion gases passed through a reduction furnace and were swept into a chromatographic column by the carrier gas (helium). The gas species (CO_2, H_2, N_2, H_2S) were separated in the column and detected by a thermal conductivity detector which gave an output signal proportional to the individual components of the mixture.

Finally, ash content was determined by heating the pulverized samples up to 830 °C in an electrical furnace. After being kept at constant temperature for 3 hours, the combusted samples were cooled in a desiccator, then weighed. From the obtained measurement data, weight loss was calculated.

3. Analysis results

The moisture content of the ready-made food samples are represented in Figure 2. The results of elemental analysis and ash content values are summarized in Table 2.

As seen from Figure 2, the moisture content of the distinctive food samples tended to vary on a wide range (23.4-85.4%). The measured values gave a mean average of 59.6%, which was assumed too high to effectuate reasonable syngas yields. Low moisture is critical for process performance, since most thermochemical reactions take place once the water has evaporated from the feed.
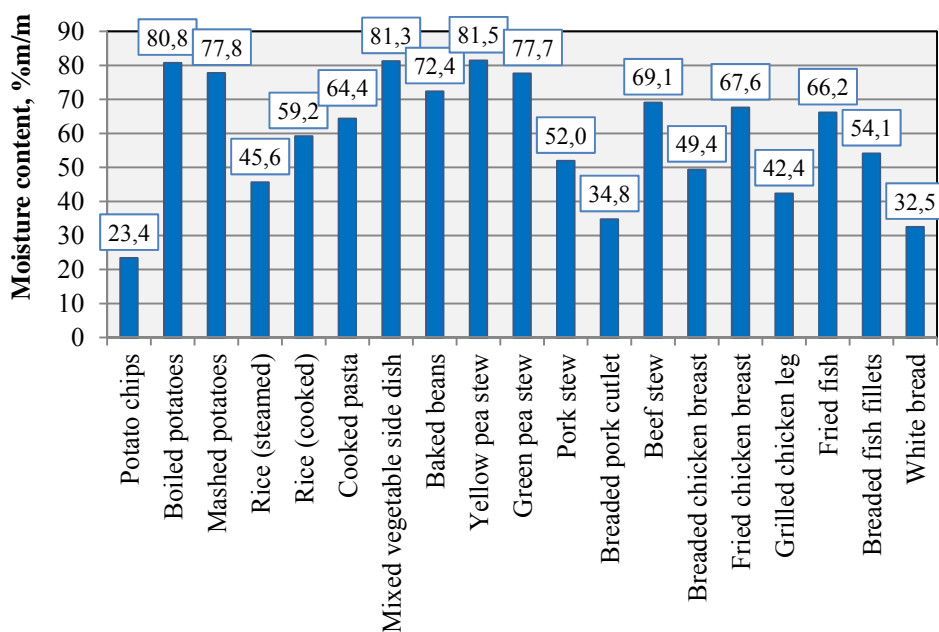
Figure 2. Percent moisture content of ready-made meals

Ash content and elemental composition of dry food waste samples

Samples	Elemental composition of dried samples, %m/m					Ash content, %m/m
	Nitrogen	Carbon	Hydrogen	Sulphur	Oxygen	
Potato chips	0.56	43.97	7.58	0.08	44.80	3.01
Boiled potatoes	2.00	36.67	6.53	1.66	49.81	3.33
Mashed potatoes	1.41	44.48	7.29	0.91	42.46	3.45
Rice (steamed)	1.13	41.13	6.90	1.58	48.10	1.16
Rice (cooked)	0.70	42.08	7.01	1.98	47.04	1.19
Cooked pasta	2.24	42.97	7.00	2.06	44.52	1.21
Mixed vegetable side dish	2.10	40.44	8.66	2.13	42.43	4.24
Baked beans	3.18	43.26	6.76	2.01	40.46	4.33
Yellow pea stew	2.76	42.56	7.05	2.11	43.08	2.44
Green pea stew	2.30	44.16	7.38	1.84	41.30	3.02
Pork stew	8.23	52.74	7.87	0.94	26.91	3.31

Samples	Elemental composition of dried samples, %m/m					Ash content, %m/m
	Nitrogen	Carbon	Hydrogen	Sulphur	Oxygen	
Breaded pork cutlet	5.74	53.91	8.25	3.25	26.91	1.94
Beef stew	13.53	46.22	9.18	2.72	24.02	4.33
Breaded chicken breast	6.18	49.50	7.75	2.83	30.56	3.18
Fried chicken breast	13.30	48.48	9.59	2.68	20.77	5.18
Grilled chicken leg	7.89	53.31	8.35	3.48	23.77	3.20
Fried fish	12.91	49.69	9.50	3.12	19.33	5.45
Breaded fish fillets	8.19	51.45	10.17	2.99	23.25	3.95
White bread	1.90	44.02	7.07	2.80	42.65	1.56
Average	**5.07**	**45.84**	**7.89**	**2.17**	**35.90**	**3.13**

The following conclusions can be drawn from Table 2:

The carbon content of the samples (40–50%) should allow for the pyrolysis/gasification reactions. Average oxygen content (35.9%) seems also favourable. The carbon to oxygen ratio of the raw material stream would facilitate the formation of carbon monoxide under optimal conditions. The measured amounts of H would be processed into H_2, constituting the second main combustible fraction of syngas. The pyrolysis/gasification of food waste might produce some undesirable products. Highly corrosive, toxic gases like hydrogen sulphide (H_2S) – formed from the sulphur compounds found in the feed – should be removed from the raw syngas stream prior to industrial utilization. Considering the low measured amounts of sulphur in the tested samples (<3%), only a minimal level of H_2S is expected to actually occur in the syngas. Another potential source of impurities is ammonia generated from the initial nitrogen content of the raw material. Once detected, this compound should also be removed from the syngas to prevent adverse, harmful effects.

The most commonly applied fuel for syngas production is coal. Comparing the ash content of coals (as given in the literature [6, 7]) to that of the tested food materials, 5 to 10 times lower values were obtained for the latter. Consequently, the expected amount of solid burning residues (slags) from the pyrolysis/gasification experiments is also estimated to be low.

Table 3 shows the ash content and compositional data obtained for vegetable residues generated during the food preparation processes. Percent moisture contents are illustrated in Figure 3.

Table 3

Ash content and elemental composition of vegetable residues (dry samples)

Samples	Elemental composition of dried samples, %m/m					Ash content, %m/m
	Nitrogen	Carbon	Hydrogen	Sulphur	Oxygen	
Withered cabbage	3.85	42,00	5.48	1.23	38.16	9.28
Dry garlic	2.28	42.20	5.90	0.76	42.69	6.17
Clementines peel	1.27	41.94	6.51	<100 ppm	47.39	2.89
Withered potato skins	2.32	42.09	6.23	0.42	44.55	4.39
Onion skins	1.68	25.28	4.92	0.70	60.93	6.49
Withered apple	0.34	39.33	6.69	<100 ppm	52.42	1.22
Withered carrot	1.41	40.32	4.84	0.29	47.30	5.84
Orange peels	0.91	44.00	6.15	<100 ppm	46.95	1.99
Banana peels	0.87	40.60	5.36	<100 ppm	43.75	9.42
Withered turnip	2.06	40.80	5.09	0.36	45.93	5.76
Kohlrabi peels	1.89	39.96	4.68	0.51	45.45	7.51
Capsicum leftovers	2.67	41.60	5.14	0.40	41.93	8.26
Withered lettuce	3.58	56.64	5.75	0.21	24.95	8.87
Cucumber peels	3.32	52.40	6.23	0.12	29.29	8.64
Radish peels	3.63	44.78	5.88	0.15	35.81	9.75
Average	**2.14**	**42.26**	**5.66**	**0.34**	**43.17**	**6.43**

As seen from Table 3, the average carbon content of food preparation wastes fell by 3.5% below the carbon measured for the food prepared. Yet, it was associated with higher oxygen content. The percent values of nitrogen and hydrogen were higher than for ready-made dishes, while significantly less sulphur was measured (0.34% on average). The ash content of the tested samples was twice as much as in Table 2.

Percent moisture content was about 15% higher for vegetable residues (food preparation wastes) than for prepared food material. The comparative results are represented in Figures 4 and 5.
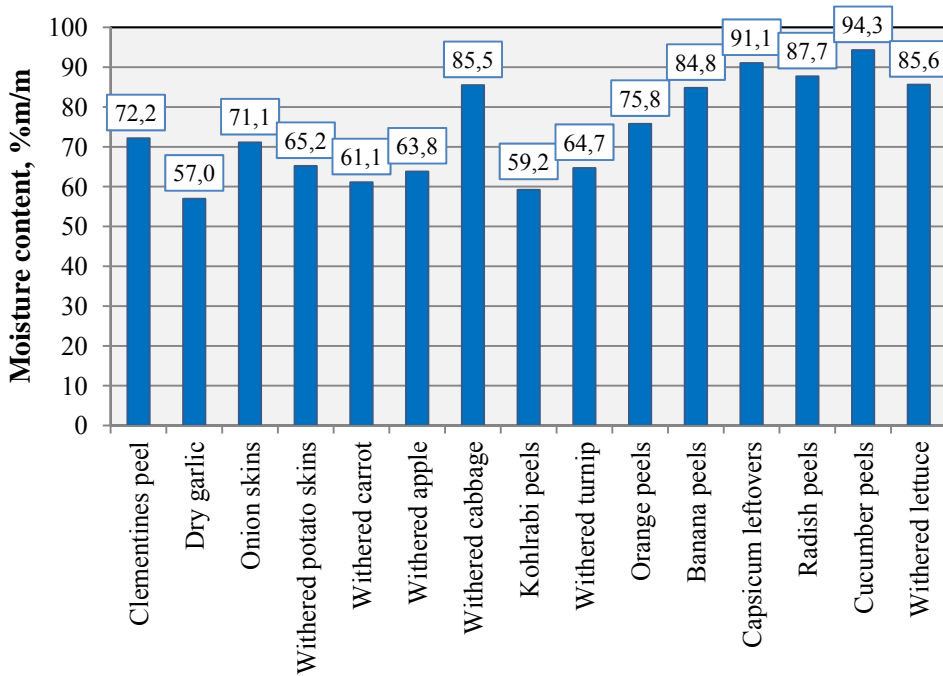
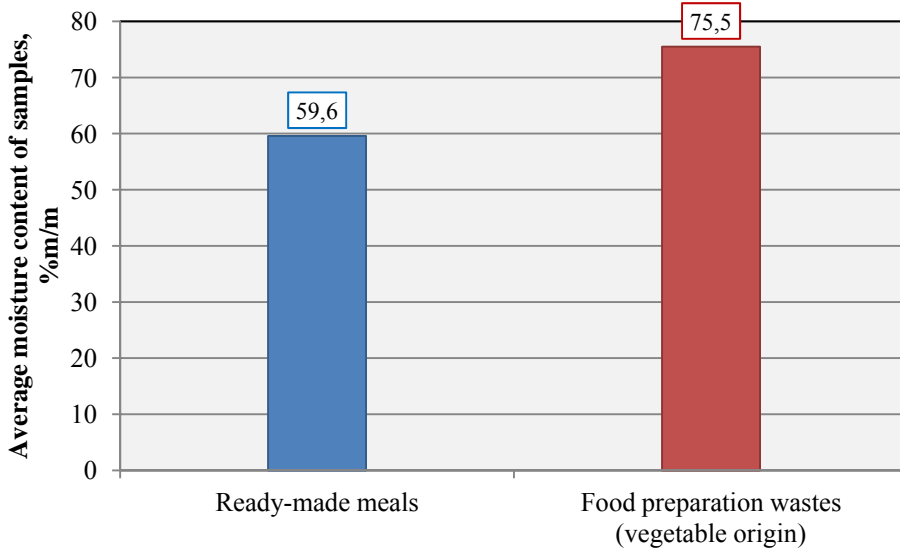*Figure 3. Percent moisture content of vegetable residues (from food preparation)*

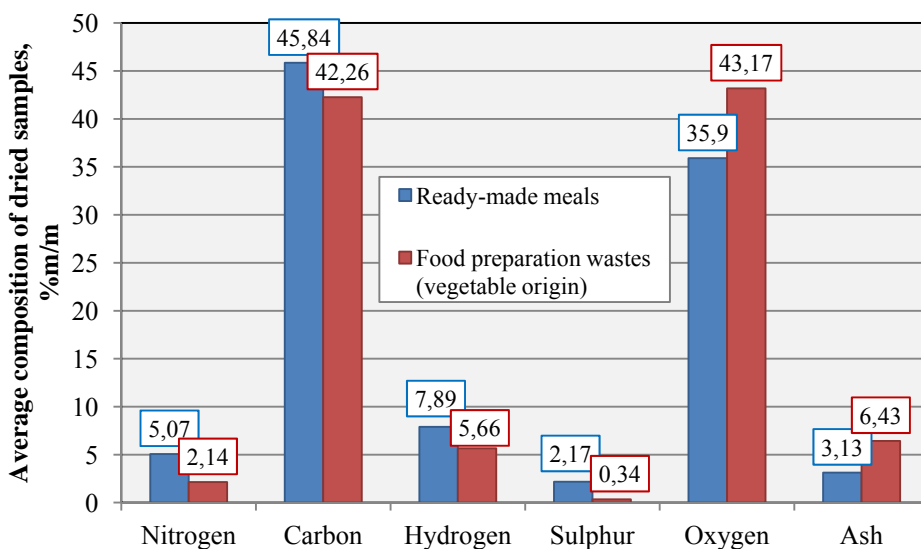*Figure 4. Average moisture content of ready-made meals and vegetable residues*

Figure 5. Average composition of ready-made meals and vegetable residues

Conclusion

Food wastes include any food substance that is discarded or unfit for human consumption, primarily generated by commercial establishments involved in the food supply chain, such as food processing plants, storehouses, caterers and retail premises.

This paper focuses on the study of canteen wastes. Canteen wastes come from a variety of sources:

- restaurants and cafeterias
- employee lunchrooms, and school canteens
- institutional and communal kitchens
- catering services, mobile catering
- kitchens of snack bars and fast food restaurants
- refreshment rooms

Proximate analysis was conducted to determine the elemental composition, moisture and ash content of ready-made dishes prepared on a daily base in a university canteen, and of food preparation wastes of vegetable origin.

Based on the results, both tested waste groups were found to meet the basic compositional criteria for syngas production. However, high moisture levels and limited feedstock availability justifies the need for economically advanced and technologically viable solutions, like the combined application of food waste and other material streams in the pyrolysis/gasification process. Complementary dry matter sources can be specified from the actual performance data of the pyrolysis/gasification experiments.

References

[1]   Erbert, Jessica: Syngas.
        http://syngastek.org/biocomposites/
[2]   Lindner–Bíró: *Tápanyagtáblázat*. 1998.
[3]   Nutritional values
        http://dieta-abc.hu/tapanyagtablazat.php
[4]   Nutritional values
        http://www.pharmindex-online.hu/diagnosztika-es-terapia/tapanyag-tablazat
[5]   European Commission: *Preparatory Study on Food Waste across EU 27- Technical report*. 2010.
        http://ec.europa.eu/environment/eussd/pdf/bio_foodwaste_report.pdf
[6]   Katona Zoltán: *Modern coal-fired power plants, tutorial*. Budapesti Műszaki és Gazdaság-tudományi Egyetem, 2011.
        http://energetika.13s.hu/pub/szeneromuvek/2%20eloadas%20sz%E9n%20%E9s%20t%FCzel%E9s.pdf
[7]   Szemmelveiszné dr. Hodvogner Katalin: Energy resources. Miskolci Egyetem Sokszorosító Üzeme, Miskolc, 1998.
        http://www.combustion.uni-miskolc.hu/oktatas/jegyzetek/energiahordozok.pdf

FULLY ELECTRIC VEHICLES IN PRACTICE

ALEX NEMES[1]–ZSOLT DOBÓ[2]–ÁRPÁD BENCE PALOTÁS[3]

There are already many forms of EVs (electric vehicle) from cheap to premium; from E-bikes to trucks; from demonstrational projects to practically usable cars. We have all heard about their pros, and cons when compared with ICE (internal combustion engine) cars. We are not going to list all these arguments, instead we highlight one of the most important thing: EVs need a different approach. It is possible to reach the same comfort level with an EV but this requires changes in our transportation habits: most importantly, one has to plug the car in right after use, not only when it's depleted. In this decade there will come a turning point, when the benefits will even out the disadvantages in general, and from then on, the ratio of conventional versus electric car usage will start to change. In many respects EVs tend to outperform ICE cars even today.
Keywords: zero emission, electric cars, battery electric vehicle, emission free transportation

Introduction

The market share of EVs is undoubtedly expanding, but we are still far from the number that would bring changes. Such changes could be the price drop of EVs owing to mass production or the positive environmental impact due to emission reduction. The intermittent nature of renewable energy sources sets new challenges, calling for highly efficient management systems of those sources. In addressing this problem, the beneficial utilization of additional storage resources come into view; thus the massive use of electric vehicles - particularly of vehicle-to-grid (usually referred as gridable vehicles or V2G) – can become a very relevant issue. In case of widespread EV usage, the total intake capacity of EV battery packs could facilitate electrical power system management [1]. Norway, with about 10,000 electric cars registered through December 2012, is the country with the largest EV ownership per capita in the world. Still today no more than 0,3% [2] of the cars has electric drive.

The main barrier in the EV market is undoubtedly the high price of Li-ion batteries. The trends are clearly visible: the prices are dropping from year to year. Some reports say [3], that by 2020 Li-ion battery prices will drop to the one-quarter of today's price.

People are usually concerned about the high prices of EVs and batteries. But do they calculate the consumption and maintenance costs of their ICE cars? Small-scale repeated disbursements like refueling or motor oil change, are less noticeable and means less of a burden for households/companies than a single but high payment. It is not an easy task to calculate the costs of a vehicle because of the differences in usage, vehicle category, the

---

[1] University of Miskolc, Department of Combustion Technology and Thermal Energy
   3515 Miskolc-Egyetemváros, Hungary
   alexnemes@gmail.com
[2] University of Miskolc, Department of Combustion Technology and Thermal Energy
   3515 Miskolc-Egyetemváros, Hungary
   zsoltdobo@gmail.com
[3] University of Miskolc, Department of Combustion Technology and Thermal Energy
   3515 Miskolc-Egyetemváros, Hungary
   palotas.arpad@uni-miskolc.hu

mechanical conditions of the cars, etc. Therefore, a valid comparison between ICEs and EVs is a though challenge.

In our article we summarize our experiences about EVs in practice, based on the research we have conducted for the automotive industry. Our perspective on EVs also comes from two vehicle conversion projects that we carried out. One of the car was a classical VW beetle with an 7,5 kW AC motor, the other is a Lada 2101, with an 11 kW DC motor.

1. Lada 2101 EV

Our first project started in 2012, with a sudden decision initiated by the Head of Institute Dr. Árpád Bence Palotás. At the Department of Combustion Technology and Thermal Management, an associate professor offered a "donor car" for conversion. The car was a classical Lada 2101 model from 1977. These models don't have servo braking, which makes them slightly uncomfortable to drive, but makes our work much easier. In the absence of comfort electronics (e.g. servo brakes, power steering, AC) the range of the EV could be higher. For a start, we removed all the unnecessary parts: the original engine, the cooling system, the exhaust system, the gasoline pipes, the fuel tank, the generator and the starter motor. In the following step we constructed the battery cases.

The first test model was equipped with conventional lead-acid batteries. One of our battery packs consisted of 45 Ah capacity batteries by which the car could go only about 20 km. The next solution was 140 Ah capacity lead-acid batteries with a 70 km range. This latter pack added almost 400 kg to the car's mass. Since the electric motor needs 144 V, the twelve batteries were connected in series. As soon as we had the chance, we changed the rusty chassis to a better one (to a "new" one from 1986), and also the batteries. The new LiFeYPO4 cells were operating at 3.3 V, so the pack consisted of 48 pcs in order to supply the motor. After the last modification, the battery pack was housed in the place of the rear seats. As a result, the modified vehicle is able to transport only two persons at a time (the driver, and one passenger). By this solution, the trunk still remained usable for luggage, and the load of the axels didn't change much. The range (about 60 km) is lower than expected, probably because of the inefficient electric motor and other powertrain losses. The car is equipped with LiFeYPO4 batteries suitable for EVs. These batteries are robust, and do not tend to overheat, therefore they are an optimal choice for EV use. There are Li-ion based batteries which have higher energy density yet may suffer thermal runaway and cell rupture if overcharged, overheated or injured [4]. In extreme cases, these scenarios might even lead to combustion.

The electric motor required a specific support, which needed unique design and construction. After the first tests we had faced a shaft coupling problem, which we managed to sort out later on with the modification of the original axis joiner. The nominal power of the original petrol engine was 44 kW, at 5600 RPM (Lada SOHC 1200 cm^3) and the maximal torque was 89 Nm at 3400 RPM [5]. In the lower RPM range the ICE has much less power. The built in electric motor has only 11 kW of nominal power, but even at zero RPM it can produce almost three times its nominal power for a short period of time. So, it is considered a dynamic car for city use. The top speed is also defined by the power and the maximal RPM of the motor, and since it's only 3500 RPM and 11 kW; the maximal speed is about 90 km/h.
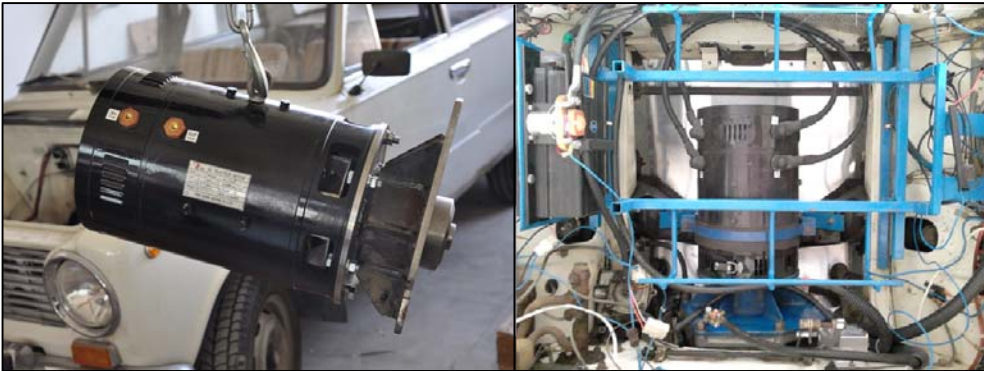
Figure 1. Lada 2101 and the 11 kW DC motor (left);
the built in motor with its supports (right)

The efficiency of our electric motor is more than 80–85%, which is still considered low in terms of electric drives. The ICE has about 20–30% efficiency, and the remaining energy dissipates in the form of heat. In cold seasons the heat loss from ICE can be used for heating the inside of the car, but for EVs, another solution has to be found, since there are no overheating parts. Still there is no heating system in our converted cars, but basically any electric heater with slight modification could do.

We installed a 5-speed transmission system (OEM part) in the car, so the drivetrain beside the engine, remained intact. The gearbox can be used in the same way as in the original car. Along with that, there is another operational option: owing to the different characteristics of the electric motor one can drive the car as an automatic, only using the brake and gas pedals in the fourth ratio. At red lights, no one has to concern about stalling, because there is no minimal RPM, neither any need for clutching.

A voltage converter was also placed under the hood. The original 12 V system had remained intact (windshield-wipers, headlamps, brake lights etc.), so in the absence of a generator this modification was necessary. Another small 12 V battery was also added to power the BMS system.

The BMS (battery management system) is a small, printed circuit, usually on the top of each battery. These devices are used to monitor the voltage and the temperature of each battery in order to avoid overheating, overcharging or discharging under a certain limit. There are feedbacks from the electronics through meters, and through an USB port. Another important action of the BMS is to balance the battery pack at the end of the charging procedure. Since the batteries are connected in series, the same current flows through every one of them, but the voltage may differ at the pins of each cell. When one of the cells (usually the one in the best condition) reaches the preset voltage value, the BMS takes it out from the charging chain, and continues charging the others. By this method, all of the cells in the pack reach the same voltage, regardless of their condition. Cell balancing is one of the most important thing, to preserve the consistency of the batteries [6].

Above the motor there is the automatic charger specified for Li-ion batteries. It communicates with the above mentioned BMS system, and has variable power output. Strangely it has maximum of 5 kW input on single phase! In order to exploit the maximal performance of the charger, we changed the plug to an AC (three-phase) 3X32 A

connector. Still only one phase is being active, but now we are able to connect the unit to a high performance socket. There is also a converter cable which allows us to plug the charger in any conventional, single-phase 230 V socket if we reduce the performance below the capability of the specific network (usually to 2 kW).

2. VW Beetle 1300 EV

Our second car conversion project started in May, 2013. The base was an original VW 1300 from 1969. Considerable metalwork and a complete paintjob was needed, since the model had rusty parts. VW Beetles are quite popular targets for conversion, therefore we have found a complete EV conversion kit for the car, and ordered it from the US. The kit consisted of a 7.5 kW AC motor, a motor controller (including the inverter), a converter for the 12 V system, a motor mounting system, cables, and several smaller gadgets.

In this case too, the original drivetrain remained intact; we placed the electric motor at the same spot where the ICE had been. Since the rotation direction of the new motor can be changed with a switch, the use of the gearbox is only optional, still we kept it. The car has the original 4-speed transmission, but in practice only the second and the fourth gear is used.

Figure 2. 9 LiFeYPO4 batteries in the trunk (left); 15 cells behind the rear seats (left)

This vehicle is able to regenerate the kinetic energy into the batteries. In this case, the wheels rotate the main-shaft via the gearbox and the electric motor works as a generator. The force of the generator-mode can be adjusted, and also switched off.

Regeneration of the break horsepower in favor of range extension could be a great improvement, but it would entail a set of other serious modifications. It would need the alteration of the brake system, which we didn't want to change, for authorization issues. Stopping the vehicle that weights more than one ton in a short period of time would release a huge amount of energy, which should be stored immediately. The batteries couldn't handle such a sudden energy shock, so an ultra-capacitor [7] would be required for absorption.

Since the vehicle is run by a 72 V motor, we installed 24 batteries, and connected them in series. There are nine 300 Ah LiFeYPO4 cells in the front and 15 more behind the rear seats (Figure 2). One cell weights about 10.5 kg [6]; with this pack the weight of the vehicle increased to 1040 kg (measured data), which is not considered high among today's cars.

The Beetle has a 3 kW charger, and a conventional 230 V connector, so it can be basically plugged in anywhere, where there is electricity. If the power grid is obsolete or in poor condition, the input of the charger can be reduced to avoid the overloading of the fuse.

Neither the motor nor the charger requires active cooling, however after the first tests we have noticed the overheating of the motor controller. In case of controller overheating, the software regulates the power output so the motor receives less and less current with rising temperature. As a solution, we installed a custom active cooler, which turned out to be oversized - a bigger passive one would have been sufficient.

Summary

At the University of Miskolc our small team of two PhD students for EV conversions led by Prof. Palotas was formed. It started as a hobby project and was originally financed from the savings from other R&D projects at the Faculty of Materials Science and Engineering. Later on (over the years) the projects attracted direct and indirect subsidies, which helped the Department and the University. Our three member ad-hoc team designed all the steps necessary to convert the two old gasoline powered passenger cars to fully electric ones.
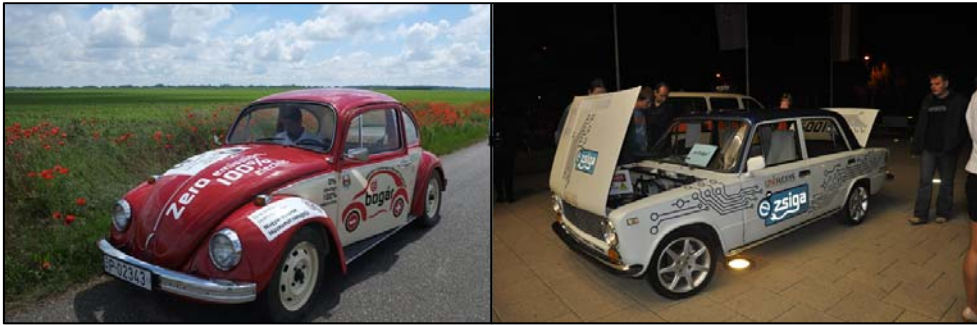

Figure 3. VW Beetle EV at the traditional Rákóczi race, and the Lada 2101 EV at an exhibition

A summary of the technical data can be seen in the Table 1. These specifications are the most important characteristics of an EV. All other vehicle related data can be looked up in the vehicle's original data sheet, since we did not modify the chassis, the 12 V system, the brakes, the suspension, and the drivetrain.

Table 1

Lada 2101 EV, and VW 1300 EV specifications:

Specifications	Lada 2101EV	VW 1300 EV
Electric motor	11 kW – DC – 144 V	7,5 kW – AC – 72 V
Battery type	90 Ah LiFeYPO4	300 Ah LiFeYPO4
Number of batteries	48 pcs	24 pcs
Total energy in battery pack	14 kWh	24 kWh
Battery pack weight	150 kg	250 kg

Charger performance	Variable, max. 5 kW	Variable max. 3 kW
Top speed	90 km/h	130 km/h
Range	60 km	160 km
Vehicle net weight	1080 kg	1040 kg
Charging time (from 0–100%)	80 min.	8 h
Passengers (with the driver)	2	4

The range of the Lada 2101EV turned out to be less than we expected. This may be due to the low efficiency of the electric motor and drivetrain losses. Based on our practical experiences, both of the cars are perfectly usable for everyday transportation. The average range necessary per day (in Hungary) is about 36 km [7], which can be covered with ease using the vehicles. Once the cars are completed, the maintenance costs are minimal, and the cost per km is about the one-third of those of ICE cars. All equipment required for EV car conversion are available at the stores, and the procedure can be carried out without a professional repair shop.

The authorization of converted vehicles is very difficult. In compliance with the European standards, several tests and experts opinions are required for traffic verification, which could triple the price of conversion. We have managed to use and test the vehicles with a temporary number plate, which entails several limitations like a defined set of drivers and a fixed number of uses.

There are public concerns about the higher risk of accidents due to noiseless operation, but in practice this is not a real problem. Modern ICE cars with appropriate exhaust-, and insulation systems have the same noise level as EVs. Our converted cars are far from confirming the general assumption that electric cars could be slow and circumstantial. These are fast cars, relaxing to drive, and enjoyable to look out of to see the curious faces from the pavements.

Acknowledgment

References

[1]   Moralis, Hugo: Evaluation of the electric vehicle impact in the power demand curve in a smart grid environment. *Energy Conversion and Management,* vol. 82, pp. 268–282, 2014.

[2]   E. V. I. *Global EV Outlook,* 2013. [Online]. Available: http://www.iea.org/publications/ globalevoutlook_2013.pdf. [Accessed 20 04 2014].

[3]   See, K.: Driving down costs in Lithium ion batteries for the electric vehicle market. Lux Research, 11 2012. [Online]. Available: http://energystoragejournal.com/driving-down-costs-in-lithium-ion-batteries-for-the-electric-vehicle-market/. [Accessed 10 05 2014].

[4]   Spotnitz, R.–Franklin, J.: Abuse behavior of high-power, lithium-ion cells. *Journal of Power Sources,* vol. 113, no. 1, pp. 81–100, 2003.

[5] zsiguli.hu, Lada típusok műszaki adatai. [Online]. Available: http://zsiguli.hu/ index. php? action =cikk&id=129. [Accessed 13 05 2014].

[6] Yinjiao Xing, E. W. M. M.: Battery Management Systems in Electric and Hybrid Vehicles. *Energies,* vol. 4, pp. 1840–1857, 2011.

[7] Dixon, Juan W. M. O. E. W.: *Regenerative Braking for an Electric Vehicle Using Ultracapacitors.* Catholic University of Chile, [Online]. Available: http://web.ing.puc.cl/~ power/paperspdf/dixon/42a.pdf. [Accessed 18 05 2014].

[8] Power, G.: *EV-power.eu - 300 Ah Li-ion batteries on stock.* [Online]. Available: http://www.ev-power.eu/Winston-300Ah-1000Ah/WB-LYP300AHA-LiFeYPO4-3-2V-300Ah.html. [Accessed 15 05 2014].

[9] KSH: *A lakossági közösségi és egyéni közlekedési jellemzői.* Statisztikai tükör, 2012. [Online]. Available: http://www.ksh.hu/docs/hun/xftp/idoszaki/pdf/lakossagikozlekedes12.pdf. [Accessed 14 05 2014].

WILLOW-BASED MIXED FEEDSTOCK FOR PELLET FUEL PRODUCTION

CSABA PÓLISKA[1]–SÁNDOR NAGY[2]–ROLAND CSEH[3]

The aim of this work was to produce high-quality pellet fuel from preselected biomass raw materials (i.e. Swedish willow species domesticated as energy crops; agricultural/food processing by-products). First, the combustion parameters of the respective energy willow species and of the biomass by-products were determined. Based on the results, one specific willow type and two of the by-products were selected as raw materials for pellet production. Preliminary calculations anticipated the technical availability of a potentially high-quality standard fuel.
Keyworlds: energy crops, pellet, alternative energy sources

Introduction

Pelleting is one of the most expensive ways of producing solid fuels from renewable resources. The energy demand of the process is relatively high, it takes 10–15% of the net energy content (net calorific value) of the pellet product itself. The question obviously arises: what makes pelleting viable?

While solid biomass fuels can be made cost-effective through the minimization of secondary processes, pellet production is complex and labour-intensive. For technical reasons, pellet fuels cannot be directly burnt even in high-temperature continuous energy systems (power stations, cement plants etc.) without a certain degree of fuel preparation. At small-scale discontinuous plants, controlled combustion is a necessary precondition for optimal operation. Smaller size and discontinuous operation makes the control of pellet-fuelled systems more difficult.

The size and shape of pellets is advantageous for relatively energy-efficient small-scale and medium-scale residential combustion equipments. Pellet storage requires about one-third of the net storage space of wooden chips, which is otherwise a relatively space-efficient fuel. Thus, the net energy content relative to storage space and material volume can be maximized, which is an important factor in designing heating systems e.g. of detached/semi-detached houses. Considering the ease of transport, the simplicity and convenience of fuel feeding (refill and dosage), there is no substantial difference between modern gas-fuelled and pellet-fuelled systems. On the other hand, safety risks related to storage and use are much lower for pellet than for gas.

Despite the relatively high price of pellets (47 to 95 HUF), pellet-fuelling is a competitive option for small-scale and medium-scale high-performance energy systems. When comparing the cost-efficiency of pellets and non-pelleted fuels, current and expected

[1] University of Miskolc, Department of Combustion Technology and Thermal Energy
    3515 Miskolc-Egyetemváros, Hungary
    tuzcsaba@uni-miskolc.hu

[2] University of Miskolc, Institute of Raw Material Preparation and Environmental Processing
    3515 Miskolc-Egyetemváros, Hungary
    ejtnagys@uni-miskolc.hu

[3] University of Miskolc, Department of Combustion Technology and Thermal Energy
    3515 Miskolc-Egyetemváros, Hungary

market trends sould be considered, with special respect to steadily increasing fossil fuel prices. Today, pellet-based energy production is globally on the rise – though with considerable differences between the local economies and their capacity to adapt to the change.

Pellets combustion largely contributes to the utilization of biomass wastes, residues and by-products, thus to the reduction of GHG-emissions (particularly of CO_2) [1].

Heating pellets are cylindrical-shaped fuel products of a few millimeters length and diameter, primarily made from dried and compressed wood waste. Pellets combustion implies the burning of a natural, renewable-based biofuel that is free of artificial additives or chemical adhesives. (Wood shavings are usually held together by lignin, which is an organic constituent of wood). During the pelletizing process, the wood raw material is demoisturized in order to improve heat performance and to achieve smooth burning [2]. The technical specifications of pellets (dimensions, composition, raw materials, moisture and ash content etc.) are regulated by international standards.

Two main types of pellets can be distinguished:

- wood pellets: made from compacted heartwood sawdust and other wastes from sawmilling
- grass pellets (also called agri- or agropellets, non-woody pellets): made from herbaceous crops (straw, corn, energy grass, sunflower husk, chaff etc.)

The basic difference in the combustion parameters of the two is ash content. While wood pellets typically have an ash content of max. 1%, grass pellets yield 3–10% of ash – due to the variety of raw materials. This partly derives from the technology of crop harvesting, whereby considerable amounts of extraneous matter (dust, sand, dirt) get commingled with the plant parts. The net calorific value (lower heating value) of non-woody pellets varies over a wide range, and the raw materials are often mixed for better compressibility (biomass blending) [2].

1. The pellet production technology

1.1. Pre-treatment of the raw material

In case the moisture content of the raw material exceeds 15% m/m, preliminary drying is required. Proper drying is a key factor for production control and quality assurance. The total energy input of the production process largely depends on the initial moisture content of the biomass. Over 14–15% wetness, pelletizing is almost impracticable [3].

Upon arrival to the plant, the raw biomass regularly contains undesirable substances (stone, metals etc.). Extraneous matter is removed by magnetic separation or other cleaning techniques (e.g. sifting) prior to industrial processing. This step is best to be implemented before feed milling and refinement (pulverization). Next, the clean raw material is crushed and milled in a single- or double-step process – depending on the size and heterogenity of the feed components. The ultimate aim is to obtain fine biomass powder with uniform particle size (0.5–1.5 mm is typically required for pelleting) [3].

1.2. Pelleting

Pellets are commonly prepared with no external binding agents added. Preferably, lignin is used as a "natural glue" organically found in the wood material. In case of low lignin

content, however, some kind of cohesive substance or adhesive can be blended with the feedstock to facilitate pelletization and increase product density. Another method of quality improvement is the homogeneous mixing of by-products or the use of special biomass blends. The commingling e.g. of straw with pine bar, sawdust or wax improves compactness. Hardness, density and low moisture content are the most important pellet properties to be controlled [4].

Before actual extrusion, the feed mix is preconditioned with about 70 °C water-spraying. In some pelletization techniques, 1–2% hot water steam is used for preconditioning. During the heat-up process, the lignin content of the feed gets released, which contributes to the rearrangement of plant fibres. Thus, the pulverized biomass containing the plasticized lignin enters directly in the compression area of the pellet die (see Fig. 1). Here, the feedstock surpasses to the pelletizing chamber (i.e. the die-roller assembly) and gets pushed through the die holes by rotating press rollers. Once the pelletized material extrudes from the die holes, another dose of biomass mash enters the pellet die to be compressed by the rollers [3].
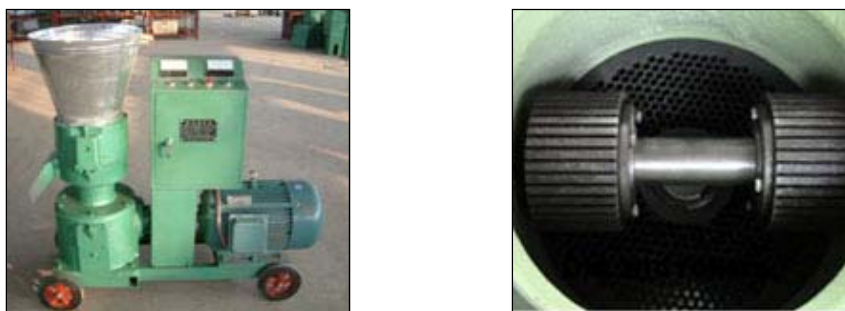
Figure 1. Pelleting equipment and the compression area of the pellet die

The factors influencing the quality and material properties of the final product are:
- the type and quality of the feedstock; pellet die compression ratio and the compression capacity of the pelleting press; die retention time (the specific time required by the feed spread on the die holes to bind together and form pellets); other intermittent processes,
- the friction and transmissivity of the pellet die,
- the surface properties of the press rollers and the pellet die (e.g. relief pattern),
- die hole geometry and L/D ratio (effective length [L] divided by the hole diameter [D]),
- the effective length of the die (the die thickness that actually performs work on the feed, thus determines the thickness of the material squeezed through the holes),
- compression ratio and rotational speed.

Feeds can be pelleted either in flat or in ring die mills. Complex, high-yield industrial pellet mills mostly apply rotating ring dies. Once the feedstock is introduced in the pelletizing chamber (mill drum or rotating drum), one or more rollers press/squeeze the material through the holes of the die at a defined compression rate. Then, the exposed pellet columns are torn up or crashed by a cutter (located on the other side of the die). Both types of pellet mills are supplied with differently patterned dies. Depending on the relief pattern

of the die (i.e. die thickness and hole size), pellet products of various length and diameter can be produced. The typical pellet diameter size is 6–8 mm [3–5].

The die and the rollers have supreme quality requirements, so that they would withstand extreme impact and wear. Besides material quality, compression ratio and the proper dosing of the feedstock are also decisive factors in production control. The ultimate aim is to reach high yield with low mechanical abrasion (i.e. of the mill assembly).

The compression process takes place at very high temperatures. Pressure rates are adjusted to feedstock type and other technical indicators. Generally, the higher the hardwood-content of the pelletized material is, the higher pressure rate is required for processing [3].

1.3. Cooling and packaging

The pellets exit the chamber in slightly plastic state at temperatures around 90 °C. A belt conveyor transports the pellets into a cooler. Air is pulled through the system to cool, dry, and harden the pellets making them resistant to spoilage and breakage. Thereby dust formation potential also gets reduced. Finally, the pellets are discharged into a shaker which functions as a fines and dust removal system. (Fines and dust are byproducts left from the pelleting process.) The finished products are either stored and sold bulk or packaged separately for sale. The residual particles recycled by the fines and dust collection system are redirected into the pelletization unit [3].

1.4. Pellet standards

In Hungary, wood pellets are qualified according to the European Standard (ENplus for fire pellets) and the certification scheme implemented in Germany – specifically:

- DIN 51731 "Pellets produced from untreated wood – HP 5",
- ÖNORM M 7135 "Pellets produced from untreated wood or untreated bark, pellets and briquettes – HP1",
- EN 14961-2: Solid biofuels – Fuel specification and classes – Part 2 – Wood pellets for non-industrial use.

2. Applied materials

The following section provides a detailed description of the raw materials used as biomass resources for pellet production.

2.1. SRC (Short Rotation Coppice) willow

Salix is a large genus of about 400–500 species of deciduous trees and shrubs (osiers) found primarily in the temperate zone of the Northern Hemisphere. Most willow species tolerate frost fairly well, therefore they are easy to cultivate in regions where winter is cold.

The purpose-bred varieties of Salix are suitable for energy cropping in short rotation coppice (SRC) systems. SRC planters propagate high-yield, fast-growing hybrids like Salix viminalis (common osier or basket willow), Salix x smithiana (typically white willow), and Salix x dasyclados. Compared to other woody perennials (e.g. poplar), willows produce the highest number of shoots per stool when coppiced (due to fast tiller development). Shrubby

Viminalis clones exhibit rapid gowth and high yields in short rotation cycles (2–3 years). Tree-shaped species like Salix alba or Salix rubens have longer growing periods and become viable for harvesting in 5 to 10 years from coppicing – peak biomass occurs in the first 3–5 years of vegetation, though.

With proper timing and under optimal conditions, vigorous willow clones can be effectively propagated from woody stem cuttings (up to 100%). Plant regeneration from stool-shoots (or soboles) subsequent to harvesting is also satisfactory (see Fig. 2).

The establishment of SRC willow plantations is most viable in Hungarian wetland regions where inland water or groundwater-fed seasonal ponds preclude traditional crop cultivation – i.e. in the floodplains of rivers Tisza, Kőrös, Szamos, Bodrog [6]. Fertile plateaus – e.g. alluvial terraces and riverside meadows currently under arable crops – are also ideal for energy crop cultivation, due to extremely high soil productivity and high yield potential [7], [8], [9]. The breeding and plantation of willow clones for biomass energy is long since a proven method. Special cultivars are easy to propagate vegetatively (stem cuttings are ready to sprout roots), give a fast coppicing response (high growth rate) and produce stable yields every 2–3 years over generations [10], [11].
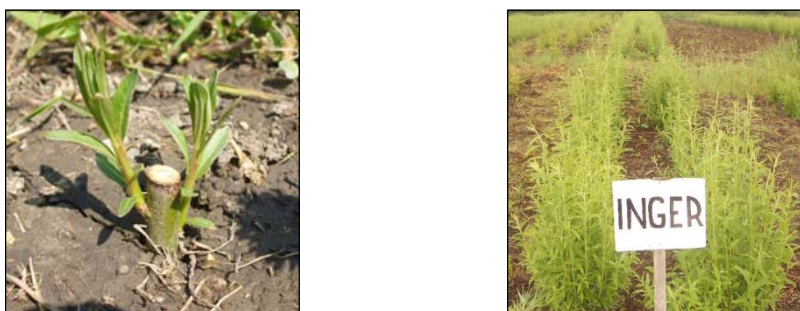
Figure 2. Propagation of SRC energy willow: mature stem cuttings and plantation stock (SW Inger)

In this study, three purpose-bred SW Salix varieties (SW Inger, dry soils; SW Tora and Sven, miscellaneous soils – each are available in Hungary) were selected as target species for the pelleting experiments.

Europe's largest SW seeds plant breeding station, Lantmännen SW Seed (run by Lantmännen Agroenergie AB, Sweden), looks back to more than 30 years of experience. Originally engaged in the selective cultivation of native species, Swedish professionals are now specialized in the targeted breeding of SRC willow crops by ways of genetic crossing and marker-assisted breeding. The ultimate aim of these techniques is to produce fast-growing, disease and pest-resistant plants with frost/drought tolerance and high biomass output. Today, Swedish willow clones are the most productive (show the best performance) of all European Salix varieties developed for energy cropping.

The following Swedish SRC willow clones are available in Hungary: Inger, Tordis, Tora, Torhild, Sven, Jorr, Gudrun, Olof and Doris. Laboratory and field testing by domestic researchers has shown the excellent performance and high adaptility of these willows to new ecological environments (compared to other European varieties). Due to environmental reasons, the hybrids Doris and Olof are nationally declared non-eligible, since these are the progenies of a Siberian basket willow (Salix viminalis), which is a non-native species in

Hungary. For the protection of domestic woodland, all promoters of exotic species are excluded from the beneficiaries of industrial forest plantation subsidies (in line with Hungarian forest resource management policiesy). Nonetheless, the domestication of Doris and Olof cultivars is not forbidden. Five other species, Tora, Tordis, Torhild and Sven prefer moderately wet habitats (with no slack water or residual waterbodies). Under such circumstances, these willows produce optimal dry matter yield. Sven exhibits good salt resistance, thus it is a potential candidate for root-zone waste water treatment. Inger is distinguished by its favourable properties like drought tolerance and high biomass output. Owing to the early start of the vegetation period, this domesticated clone has an outstanding capacity for weed suppression. Early bud burst is complemented with good frost tolerance: buds and shoots do not get damaged by mild winter frosts to 3 °C below zero. Inger cultivars can be harvested as soon as in November, before they enter into the phase of dormancy. The wetness of the freshly cut biomass is 44–52%. (Subsequent to harvest, four to six weeks of drying is necessary to reach the moisture level [<35%] required for cost-efficient transport). Yield stability is the most impressive trait of Inger. It is based on the good eco-adaptability of the clones to local environmental volatilities (e.g. drought, seasonal floods or inland water) [12].

2.2. Nutshell

As a by-product, cracked nutshell is extremely hard, firm, sharp-edged, non-perishable and retains quality over an extended period of time. It is neither toxic nor in any ways harmful or dangerous to human health; it does not cause adverse effects if swallowed or rubbed into the skin. Nutshell is non-reactive with either basic or acidic media. The woody shell consists of a solid superstructure of cellulosic fibres, where lignin and hemicellulose function as filling and binding materials. Nutshell waste is reutilizable, organic and biologically neutral, it naturally decomposes [13].

Characterized by low moisture content and fairly high heating value (18–20 MJ/kg), nutshell is considered a valuable biomass source.

2.3. Corn stover

Worldwide, corn stover is increasingly being harvested as a feedstock for biomass fuel production. The energy use of corn stover provides an economic benefit (i.e. a new source of income) for inland corn grain farmers and contributes to the commitment of the individual states to reach renewable energy targets. In present-day agricultural practice, however, corn stover is generally left on the fields to protect the soil from erosion and deflation, facilitate water retention and provide nutrient supply (soil fertilisation) [14].

In Hungary, corn stover is the second largest source of vegetable by-products (after straw). About 90% of the total amount of corn growing by-products is stalks and leaves (corresponding to an energy content of about 90 PJ per year). Specially equipped combines (forage choppers) are used for the cutting, shredding and baling of corn stover. A great obstacle to viable harvest, storage and industrial processing is the wetness of the raw material. The moisture content of freshly cut corn stover ranges from 30 to 70%, therefore special treatment and storage is required to avoid maintenance difficulties and/or quality deterioration [8]. Cost-efficient commercial drying techniques, which would facilitate the conversion of crop residues into biofuel are not yet available.

Supposing that the stored biomass has an optimal moisture content of 12–20% m/m, the lower heating value of the fuel amounts to 13–14 MJ/kg, which is an attractive combustion parameter.

2.4. Sunflower seed shell

Sunflower shells is the residues remaining from the commercial hulling and separation of harvested sunflower seeds. If heating properties are considered (low moisture content, high calorific value), this biomass gives an outstanding feedstock for bioenergy production [9]. Sunflower seed shells is generated as a co-or by-product from the food processing industry (particularly by vegetable oil refining), therefore, with proper bilateral cooperations between the production partners, it is easy to "collect" and is regularly available in large quantities. Even in Hungary, there are several good examples of successfully installed pellet-fuelled heat recovery equipments fed exclusively by sunflower hull pellets, mostly operating in vegetable oil refineries or other small-scale plants. The state-of-art systems, however are not entirely free of operational problems.

3. Methods

As described in the previous section, the research samples were obtained from a variety of sources, including short rotation wooden perennials from energy plantations, agricultural by-products and industrial wastes. Before pelleting, the combustion parameters of these raw materials were tested. The methodology and the test results are presented below.

3.1. Ultimate analysis

Elemental or ultimate analysis encompasses the quantitative determination of the basic chemical constituents (carbon, hydrogen, sulphur, nitrogen and oxygen) found in organic substances. The chemical composition of fuels is a key factor in calculating higher and lower heating values (HHV/LHV), estimating actual heating performance and optimizing the combustion process for the respective feed.

Carbon-, hydrogen- and oxygen-content primarily define the combustion properties and thermal behaviour of fuels. Percentages of nitrogen and sulphur are, on the other hand, associated with environmental impacts and corrosion risks.

There are several methods available for the determination of chemical composition. Most of these include the thermal conversion (i.e. the complete oxidation) of the fuel samples and the componental analysis of the flue gas formed from the process. In this study, a Carlo Erba EA 1108 type elemental analyser (with a software-based data acquisition system) was used for the measurement of the C-, H-, N- and S-content in the respective fuels – in line with the principles and methodology suggested by the international standards (ISO, DIN, CEN).

3.2. Moisture

When testing biomass samples, two forms of moisture are a matter of interest: intrinsic moisture – the one contained without the influence of weather – and extrinsic moisture, which is influenced by weather conditions during harvesting.

Total moisture content (W_t) can be determined with single-step and double-step methods, the latter including raw and hygroscopic mass measurements. In this study, a single-step drying method (oven-dry method) was chosen for the determination of total moisture contained by the fuel samples – as recommended in the respective standard (standard No. 24000-23-1977 by MSZ). The final results were calculated with the following formula:

$$W_t = \frac{m_1}{m} \cdot 100 \text{ , \% m/m} \tag{1}$$

where
m_1 weight loss (of the sample) on drying, g;
m the initial weight of the sample, g.

3.3. Ash content

Ash is the solid burning residues left from the complete combustion of a fuel. It comes from the mineral components and other inorganic matter originally present in the fuel.

Three measurements were executed for each fuel sample, following the protocol provided in the Standard Analytical Method No. MSZ ISO 1171. This test method covers the determination of ash (A), expressed as the percentage of residue remaining after dry oxidation in closed chamber at 815±10 °C (with prefixed, constant air flow rate). All results are reported relative to the oven dry weight of the sample, according to the formula:

$$A = \frac{m_3 - m_1}{m_2 - m_1} \cdot 100 \text{ , \% m/m} \tag{2}$$

where
m_1 the weight of the crucible, g;
m_2 the initial weight of the crucible and the sample together, g;
m_3 the weight of the crucible and the ash produced, g.

3.4. Determination of higher heating value (HHV) and lower heating value (LHV)

Calorific tests were performed using a Parr 6200 type calibrated isoperibol oxygen bomb calorimeter. The higher heating values (energy equivalent values) of the tested fuel samples were automatically computed by the data processing system. The principle of the measurement was based on a substitution procedure in which the heat obtained from the sample was compared with the heat obtained from combustion of a similar amount of benzoic acid (as standardizing material) whose calorific value was known. Measurements were obtained by burning the representative samples in high-pressure oxygen atmosphere within a metal pressure vessel or "bomb". The energy released by this combustion was absorbed within the calorimeter and the resulting temperature change within the absorbing medium was noted. The heat combustion of the sample was calculated by multiplying the temperature rise in the calorimeter by a previously determined energy equivalent (or heat capacity) determined from previous tests with a standardizing material. Corrections had to be applied to adjust these values for the heat transfer occurring in the calorimeter, as well as for the side reactions which are unique to the bomb combustion process.

$$HHV = \frac{V(t_m - t_0 + c) - \Sigma b}{G}, \text{ kJ/kg} \qquad (3)$$

where:

V   heat capacity of the bomb (relative to water), J/°C;

t_0 initial temperature of the measurement, °C;

t_m final temperature of the measurement, °C;

c   correction factor for heat transfer between the calorimeter and its environment, °C;

Σb   standard deviation or summated heat value from external processes (side reactions), J;

G   sample weight, g.

In the calculation of V and Ho, the Regnault–Pfaundler method was applied to determine the proper correction factor for heat transfer, [c].

Three experiments were developed for each sample to secure data reproducibility. For the determination of the lower heating value (net heating value), the following formula was used (as given by the pertinent standard):

$$LHV = HHV - 24{,}49278 \cdot \left(9 \cdot H + W_t\right), \text{ kJ/kg} \qquad (4)$$

where

HHV   higher heating value (as defined above), kJ/kg;

H   weight percent hydrogen in the sample (as specified by MSZ 24000/11), % m/m;

W_t moisture content of the samples ("total moisture" for wet samples, "0" for dry samples), % m/m.

4. Results and discussion

4.1. Ultimate analysis

The results obtained from ultimate analysis are shown in Table 1. Out of the three main components of solid fuels (carbon, nitrogen, oxygen), two were measured (C, N).

Table 1

Ultimate analysis data for SRC willow and biomass wastes

Sample	C-content wet % (m/m)	H-content. wet % (m/m)	N-content wet % (m/m)	S-content wet % (m/m)
SW Inger	47.81	6.46	0.18	<0.01
Tora	47.96	6.63	0.22	<0.01
Sven	49.37	6.83	0.13	<0.01
Nutshell	50.94	6.67	0.71	<0.01
Corn stover	46.98	6.29	0.21	<0.01
Sunflower seed shell	47.45	6.32	1.25	<0.01

The wet biomass samples contained about 47.4–50.9% m/m of C; 6.2–6.8% m/m of H and 0.1–1.2% m/m of N. The sulphur-content stayed below the lower limit of detection

(0.01%). Most values fell approximately in the same range, with a prominent difference observable in the high percentage of N in sunflower seed shells.

4.2. Proximate analysis

For reasons of reproducibility, three experiments were performed on each fuel sample. The results are presented in Table 2 (the values are the mean averages of 3 measurements).

Table 2

Proximate analysis data for energy crops and industrial wastes

Fuels	Moisture (% m/m)	Ash (% m/m)	HHV (MJ/kg)	LHV (MJ/kg)
SW Inger	39.64	0.63	19.23	16.83
Tora	39.33	0.65	18.51	16.09
Sven	37.66	0.64	18.94	16.51
Nutshell	12.76	1.12	18.93	17.15
Corn stover	17.35	6.51	16.70	14.89
Sunflower seed shell	13.15	2.54	18.75	17.04

As seen, the total moisture content of the tested SRC willow and biomass samples tend to vary over a wide range (12.76–39.64% m/m). Moisture is a critical parameter in designing suitable combustion technologies and proper combustion units tailored for these fuels. Note should be taken that the respective willow samples were tested within 1 week from cutting, without any kind of pre-treatment. This accounts for their exceptionally high initial moisture content. On the other hand, all other biomass sources were relatively dry, even corn stover contained moisture to less than 20% m/m.

SRC willow is proven to yield very low amounts of ash when burnt. Thus, it is the prime source for pellet production. The ash content of other biomass sources is largely dependent on material composition. Degradable dry matter content indicates whether the given raw material can be effectively admixed with the feedstock to make high-quality pellets. Based on the results, the applicability of corn stover is not convincing.

SRC willows are characterized by uniformly high HHV. Out of the tested biomass waste samples nutshell and sunflower seed shell were found to have satisfactory HHVs for quality pellet fuel production.

4.3. Hypothetical pellet mixtures

Of the tested biomass resources, SW Inger (SRC willow), nutshell and sunflower seed shells (biomass by-products) were selected as potential applicants for experimental biofuel pelleting (relatively low moisture and ash content).

Prior to the actual experiments, hypothetical pellet mixtures were compiled from the data measured for the distinctive constituents. The mixture rates with the calculated fuel characteristics are presented in Table 3. The table was used as a tool in the preliminary selection of the best possible mixture with the most optimal combustion parameters.

Proximate analysis data for the hypothetical pellet mixtures

Fuels	Moisture (% m/m)	Ash (% m/m)	HHV (MJ/kg)	LHV (MJ/kg)
90% m/m SW Inger + 10% m/m Nutshell	36,952	0,679	19,2	16,86
80% m/m SW Inger + 20% m/m Nutshell	34,264	0,728	19,17	16,89
70% m/m SW Inger + 30% m/m Nutshell	31,576	0,777	19,14	16,93
60% m/m SW Inger + 40% m/m Nutshell	28,888	0,826	19,11	16,96
90% m/m SW Inger + 10% m/m Sunflower seed shell	36.991	0.821	19.18	16.85
80% m/m SW Inger + 20% m/m Sunflower seed shell	34.342	1.012	19.13	16.87
70% m/m SW Inger + 30% m/m Sunflower seed shell	31.693	1.203	19.09	16.89
60% m/m SW Inger + 40% m/m Sunflower seed shell	29.044	1.394	19.04	16.91

While most hypothetical mixtures are characterized by relatively low ash content (>1%), the addition of excessive amounts of sunflower seed shell to the feedstock results in a drastic increase in ash production. Higher heating values invariably stay above 19 MJ/kg, which is considered very good.

Conclusions

The ultimate aim of this research is to produce high-quality pellet fuels from SRC energy willow and biomass by-products. In the first step, the combustion analysis of three SW *Salix* clones and three distinctive biomass materials was performed. Considering (low) ash content and (moderately high) heating value, the results obtained for nutshell and sunflower seed shells seem most promising. With regard to the combustion properties of the hypothetical pellet mixtures, nutshell appears to be the preferred choice. The high oil content of this biomass might even contribute to the compactness and density of the pellets.

Based on the reported data, the availability of nutshell and sunflower seed shell resources is virtually unlimited. In 2011, more than 24 tonnes of nutshell wastes were generated by industrial producers in Hungary. This quantity represents a year of poor agricultural performance (when merely half of the expected yields were actually harvested) due to extreme summer heat and drought. Given the steady expansion of domestic walnut plantations and assuming a normal year, the estimated total amount of nutshell waste may reach 48 tonnes per year.

The next research step involves the preparation and testing of various pellet mixtures. Combustion analysis would be completed with ash characterization (compositional data,

ash fusion characteristics) in order to provide data for the pelleting industry, including pellet stove manufacturers.

Acknowledgements

References

[1]   Fenyvesi L.–Ferencz Á.–Tóvári P.: *A tűzipellet*. Cser Könyvkiadó és Ker. Kft., 2008.
[2]   A CARBOROBOT Kft. honlapja, www.carborobot.hu/HU/fűtőanyagok/Pellet.htm
[3]   Az ECOTEQ Kereskedelmi és Tanácsadó Kft. honlapja, http://brikettalo.hu/pellet-gyarto-gepek/pelletalok/a-pelletgyartas-technologiai-lepesei.html
[4]   Domonkos L.: *A pellet felhasználása.* www.globalstone.hu
[5]   Thompson, Jena L.–Tyner, Wallace E.: Corn stover for bioenergy production: Cost estimates and farmer supply response. *Biomass and Bioenergy,* 62, 166–173, 2014.
[6]   Bárány G.–Csiha I.: Kivezető út vagy zsákutca. *Erdészeti Lapok*, CXLII. évfolyam, 4. szám, 2007.
[7]   Borhidi A.: *Magyarország növénytársulásai*, Akadémiai Kiadó, Budapest, 2003.
[8]   Bokodi L.: Energiafűz mint megújuló energiaforrás, *Agrárium*, A magyar Agrárkamarák Lapja (Agrár és Piacgazdaság) 17. évfolyam, 3. szám, 2007.
[9]   Kondor A.: Adatok az „energia fűz" (Salix Viminalis L.) gyomszabályozási lehetőségeiről. *Agrártudományi Közlemények*, (26) Különszám, 2007.
[10]   Robertson, A. W.–Khail M. A. K.: *Conifers for Biomass production.* Vol. I and II. Forest Energy Program. Canadian Forestry Service and I. E. A., 1984.
[11]   Lukács G. S.: *Energiaerdő*. Mezőgazdasági Kiadó, Budapest, 1989.
[12]   A Holland Alma Kft. honlapja, www.hollandalma.hu
[13]   Orosz Péter: *Könyv a dióról.* http://dioskonyv.bionuss.eu/
[14]   Bai, A.–Lakner Z.–Marosvölgyi B.–Nábrádi A.: *A biomassza felhasználása*. Szaktudás Kiadó Ház, Budapest, 2002.

MICROREACTORS: A NEW CONCEPT FOR CHEMICAL SYNTHESIS AND TECHNOLOGICAL FEASIBILITY
(Review)

JUDIT NÉMETHNÉ-SÓVÁGÓ[1]–MÁTÉ BENKE[2]

Nowadays, continuous flow techniques for the execution of chemical reactions in microreactors have come to the front. The advantages of these revolutionary new reactor types are: the quick and effective mixing of the reagents, more effective heat transfer comparing to the classical chemical reactors, short reaction time, very small reagent quantities used for the synthesis (which is quite important for reaction optimization), the regulation of the main reaction parameters (flow rate, residence time, pressure, temperature) with very high accuracy, the simple and quick adjustment of optimal reaction conditions. Furthermore, the reactor scale can be increased in an easy way – through the parallel building of the microreactor chips – in order to enlarge production capacity.
Keywords: continuous flow chemistry, microreactor, organic synthesis, micro-process technology, process intensification

Introduction

The microreactor technology has attracted a great deal of attention as an enabling tool for novel reaction development and scale-up. The use of microreactor devices make it possible for synthetic chemists and process engineers to perform reactions with an unprecedented control over mixing, mass- and heat-transfer, safety, reaction residence time and other process parameters, which results in enhanced reproducibility. In addition, they allow the practitioner to utilize extreme reaction conditions, which are far from the common laboratory practice (e.g., high temperature, pressure, and reactant concentration), in a safe and reliable fashion. In microreactors the reaction rates can be accelerated by orders of magnitude and the reaction times shrink from hours to minutes and seconds.

This compilation focuses on the process chemistry potential of continuous flow microreactor technology based on a literature review, and presents the construction of a Syrris Asia type liquid phase micro-reactor, which was purchased by (the University of Miskolc for) our Department last year.

1. The Basics of Flow Chemistry

Flow chemistry (sometimes referred to as plugflow, microchemistry, or continuous flow chemistry) offers exceptional benefits over synthetic techniques to research and development chemists. In flow chemistry, the reagents are continuously pumped through the reactor and the product is continuously collected, as seen in Figure 1.

---

[1] University of Miskolc, Institute of Chemistry
   3515 Miskolc-Egyetemváros, Hungary
   kemjutka@uni-miskolc.hu
[2] University of Miskolc, Institute of Chemistry
   3515 Miskolc-Egyetemváros, Hungary
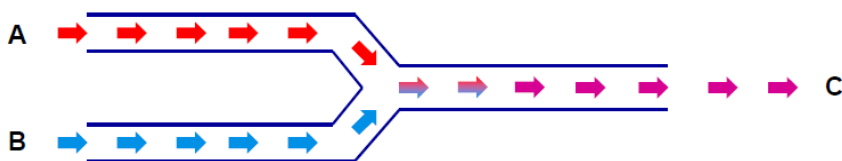
Figure 1. The principle of flow chemistry

The mixing process can basically rely on two principles, namely diffusion and convection. Diffusion between short distances, establishing high concentration gradients was initially the most frequently applied principle by simply making the channels themselves smaller and smaller. Soon, the limits of that strategy, also in terms of robustness (fouling) and costs (complex microfabrication), became obvious. In recent years, various methods were developed to overcome these limits by diffusion mixing, all of them based on the induction of secondary-flow (convective) patterns which are superposed on the main flow, often in the vertical direction to the flow axis. This includes recirculation patterns, chaotic advection and swirling flows. Convection is effective for mixing, since it serves to enlarge mixing interfaces. Convections of 'gross' mass portions can be used at a much larger scale to 'stir' complete chamber volumes, e.g. by ultrasound, through electrokinetic instability or by acoustic means. At high Reynolds numbers, turbulent mixing can be utilized; however, this is often not practicable, as it implies the achievement of unrealistically high flow velocities. The few special equipment known to use turbulence rely either on free-guided flows or guide liquid flow through meso-scale channels [1].

The following section covers some of the basics of flow chemistry. The principles of a traditional batch reactor and a continuous flow microreactor are compared in Figure 2 [2].

Figure 2. The principle of a traditional batch reactor vs. a continuous flow microreactor

Due to the reduced length scale of microstructured process equipment, the transfer lengths are short and precisely defined, and the areas are small, but high surface-to volume ratios and tiny volumes dominate everything. This provides many opportunities for experts to handle chemical and process engineering issues at the microstructure level. Small channels allow short transport lengths for heat and mass transfer.

This results in high transfer rates, as expressed – for diffusive mass transfer with the mean transport length – from the Einstein-Smoluchovski equation (Eq. 1)

$$x^2 = 2Dt \qquad\qquad (Eq.\ 1),$$

where x is the diffusion length, t is the diffusion time, D is the diffusion constant.

The transport length by diffusive mixing in gases (D = $10^{-5} - 10^{-6}$ m²/s) and in liquids with low viscosity (D = $10^{-9} - 10^{-10}$ m²/s) is displayed over the corresponding time in Figure 3.
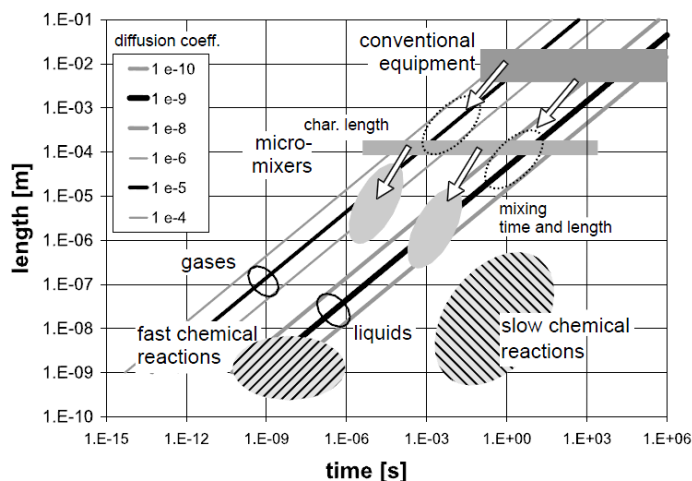
Figure 3. Characteristic length and time scales for mixing in microstructured devices together with chemical reactions [3]

Conventional equipments have typical geometries in the range of centimeters and produces fluid structures in the range from 100 μm to 1 mm. The corresponding diffusion times is in gases slower than approx. 1 ms and in liquids in the range of 1 s. Microstructured devices with typical length scales from 100 μm to 1 mm provide fluid structures with length scales of approx. 1 μm. These small fluid structures lead to mixing times shorter than 100 μs in gases and approx. 1 ms in liquids. This is the main reason for the enhanced selectivity and high yield of chemical reactions in microreactors. The length scaling often coincides with a time scaling of the relevant processes. In general, the shorter the length, the shorter the characteristic time for transport processes, and the higher the transformation frequencies will be. With properly designed micromixers and an adjustment of the component concentrations, the selectivity of a complex reaction can be increased dramatically. Mixing

time is only one criterion for an optimal chemical reaction, another is the scale of fluids residence time within the device [3].

1.1. Key Principles of Flow Chemistry (regarding to Syrris Asia Micro reactors)

1.1.1. Flow rate, residence time, reactor volume and production rate

In a flow reactor the residence time of the reagents in the reactor chip (i.e. the amount of time that the reaction is heated or cooled) is calculated from the volume of the reactor and the flow rate (Eq. 2).

$$Residence\ time = \frac{Reactor\ Volume}{Flow\ Rate} \qquad (Eq.\ 2)$$

Therefore, to achieve a longer residence time, it is possible to pump more slowly and/or use a reactor with increased volumes. For example, if two reagents are flown into a 1 ml glass microreactor at 0.25 mL/min flow rate each (see Figure 4), residence time can be calculated as follows.
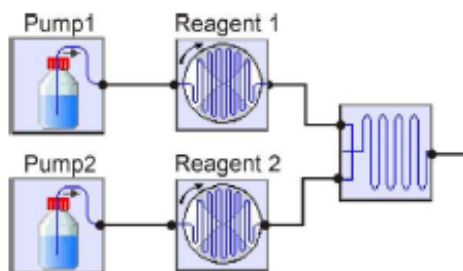
Figure 4. Two reagent are flown into a glass microreactor [2]

The combined flow rate (Eq. 3) is defined as:

$$Combined\ flow\ rate = 0{,}25\,\frac{ml}{min} + 0{,}25\,\frac{ml}{min} = 0{,}5\,\frac{ml}{min} \qquad (Eq.\ 3)$$

According to equation (2) the Residence Time (Eq. 4):

$$Residence\ Time = \frac{1\ ml}{0{,}5\,\frac{ml}{min}} = 2\ min \qquad (Eq.\ 4)$$

If we would like to change the residence time e.g. to 8 min, two options are available:
- to slow down the flow rates to 0,0625 ml/min each, or
- to increase the reactor volume to 4 ml.

The microreactors are able to operate with reaction times from a few seconds to a few hours. For the same given residence time one can either choose to use a larger reactor (and therefore larger flow rate) or a smaller reactor (and therefore smaller flow rate). The key difference is that with a large reactor more material will be synthesized in a given time. In practice, for example Asia systems can be used to syntesize mg to kg quantities in 24 hours (depending on reaction time and concentration).

1.1.2.   Diffusional Mixing in Microreactors

In Asia type liquid phase microreactors the reagents do not mix by turbulence (as in a round bottom flask or jacketed reactor), instead the reagents mix by diffusion. Because the distance across the chip reactor channel is approximately 200 μm, the time taken for reagents to completely diffuse is in the order of seconds. At typical Asia system flow rates this corresponds to less than 10 mm of flow along the reaction channel. The total length of the chip reactors is approximately 1 m. As diffusion time is proportional to the distance squared (Eq. 1), therefore, over short distances the diffusion is rapid. The process scheme can be seen in Figure 5 [2, 4].
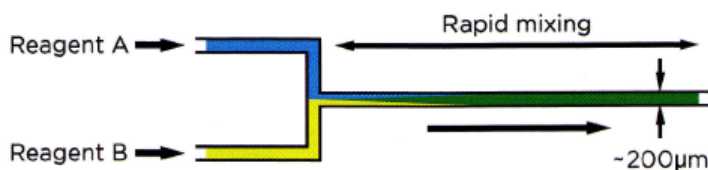
Figure 5. Diffusional mixing in microreactors [2]

1.1.3.   Pressure

When a liquid flows through a „tube" (as in the reactor) there is an inherent resistance to its flow. This resistance or (backpressure) is dependent upon a number of physical factors. Thus, smaller reactor cross section, longer reactor length, higher flow rates and more viscous liquids all generate higher backpressure. The microreactor chips used by Asia system are specifically designed to generate low backpressure.

There is a possibility to use Pressure Controller in Asia System up to 20 bar. This allows reactions to be performed at temperatures much higher than the atmospheric boiling point of test fluids, enabling faster and often cleaner, higher yielding reactions. Typically, solvents can be heated 60 to 150 °C above their boiling points. The Arrhenius rate law tells us that reactions are two times faster for every 10 °C rise. Using the Arrhenius rate law reaction rate increases of the order of 1000-fold are possible (100 °C rise = 2x2x2x2x2x2x2x2x2x2 = over 1000x faster).

Applying pressure in the microreactor also suppresses the evolution of gases. This is also beneficial, because if gas bubbles are formed, they can propel the reaction mixture out of the reactor, leading to uncertain residence times.

1.1.4. *Temperature*

Flow chemistry makes it possible to achieve faster reactions because:
- it is much easier to pressurize flow reactor,
- higher pressures enable higher temperatures,
- higher temperatures result in faster reaction rates.

Due to a higher surface area/volume ratio, flow reactors enable better heat transfer and therefore better temperature control [5]. The surface area-to-volume ratio of the reaction mixture in an Asia reactor is 1000 times greater than in a round bottom flask. Reactions cool down or heat up are extremely rapid (faster than a microwave). Moreover, by pressurising, flow reactors can operate at temperatures above the typical boiling point of liquids, offering additional adventages for process chemistry investigation.

1.2. *Process intensification, production flexibility*

The intensification of chemical processes targeting the effective use of raw materials and energy implies the miniaturisation of chemical reactors. Microstructured reactors (MSR) are systems with a well-defined structure of channels with an internal diameter in the range of 10–500 μm [6]. Due to the small diameters of the channels and the high specific surface area of microreactor (in the order of 10, 000–50, 000 m^2/m^3 [7]), high heat transfer performance can be achieved with heat transfer coefficients up to 25,000 $W/(m^2K)$ [8]. Moreover, the heat exchanger is often integrated within the reactor allowing for an efficient control of the highly exothermic or endothermic reactions. In the case of multiphase systems, the specific interface is also drastically increased in comparison with traditional reactors. The specific interfacial area of multiphase systems can be obtained in the range of 5000–30, 000 m^2/m^3 [8]. Therefore, microreactors allow an intensification of the reactions as shown by Lomel et al. for the case of organometallic synthesis [9]. Other important characteristics of MSR include narrow residence time distribution and easy scale-up, with inherent reactor safety [10, 11].

The accompanied large increase in productivity is a further cornerstone in making micro-process technology a competitive concept as opposed to the economics of scale, practised since decades in production chemistry aiming to increase the vessel size more and more. Different from the content provided in a number of recent reviews, certain compilations focus on the process chemistry potential of superheated processing, working out a methodology for novel processing conditions and the evaluation of the resulting data. [8, 9]

An increase in the throughput of microreactors is achieved by a numbering-up approach, rather than scaling-up. In this case, the functional unit of a microreactor, e.g. a mixing structure, is multiply repeated. Fluid connection between these units can be achieved by using distribution lines and flow equipartition zones. Numbering-up widely guarantees that the desired features of a basic unit are kept when increasing the total system size. In an ideal case, the measuring devices for production reactor and for process development become similar, being composed of identical units. In addition, a larger number of units results in higher flexibility in adapting the production rate to varying demand since, at least in principle, a certain number of systems can be switched off or further systems may be simply added to the production plant. A plant design based on a large number of small reaction systems can, again at least in principle, be modified to

perform a variety of reactions by changing the piping network, i.e. the plant may be adapted to the synthesis of various substances using microreactor modules like a "LEGO" system. This flexibility may be supported by a considerably broader range of operating conditions of a microreactor compared with a macroscopic system [8]. A simplified scheme illustrating scale-up versus numbering-up strategies can be seen in Figure 6.
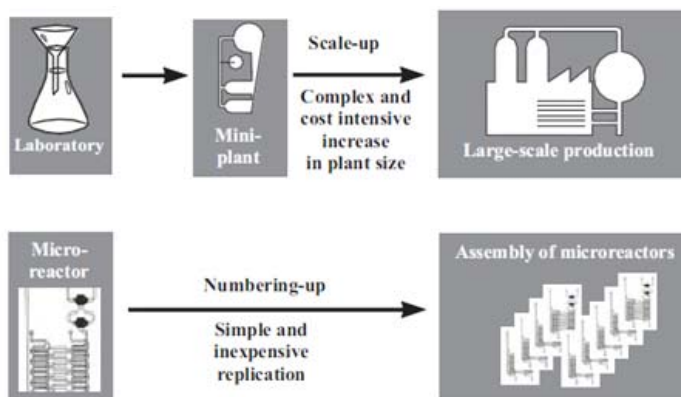

Figure 6. Simplified scheme of scale-up versus numbering-up strategies [8]

2. Types of microreactor

2.1. The SYRRIS ASIA type microreactor [2]

The liquid phase SYRRIS Asia microreactor system offers a variety of flow chemistry modules and systems making it an ideal option for both beginners with modest budgets and experts who demand the utmost functionality of the devices. As the basic construction of the respective type of microreactor system had been purchased for the Chemical Department of the University of Miskolc, an Asia 110 microreactor system is shown below (see Figure 7).

Figure 7. Asia 110 Flow Chemistry System [2]

The main parts of the microreactor system include:
- Asia Microreactor: a chemically resistant, transparent and robust flow reactor for solution phase chemistry, which offers a wide temperature and pressure range. The design results in extremely fast and reproducible mixing, rapid heat transfer and minimized back pressure due to flow.
- Asia Syringe pumps: this part offers two ultra smooth, chemically resistant, continuous flow channels with wide flow rate ranges and built-in pressure sensors.
- The Asia Chip Climate Controller provides quick and accurate temperature control from –15ºC to +150ºC without the need for a circulator or water cooling.
- The Asia Pressure Controller allows reactions to be pressurized up to 20 bar. This enables temperatures far in excess of the atmospheric boiling point of the solvent, and therefore an increase in reaction rate.

All the modules can be controlled by the intuitive twist and click knobs and data such as flow rate, pressure and temperature is displayed on the front panels. By entering data such as reaction time and reactor volume, the pumps automatically control the flow rate and indicates when the reaction is available for collection. Safety features include an automatic leak check and a safety shutdown for the case of over-pressurization of the system.

2.2. Other types of the microreactors

Depending on the application focus, there are various suppliers and commercial development entities to service the evolving market.

The Hungarian ThalesNano Inc. has developed gas phase microreactor types for hydrogenation (H-Cube, H-Cube Midi), ozonization (O-Cube), and other reactors, which suitable for other specific chemical reactions (X-Cube X-Cube Flash) [12]. The newest member of H-Cube series of hydrogenation reactors was developed as a safe, powerful and affordable reactor intended to bring back hydrogenation to the everyday educational curriculum and research process.

Hydrogenation is one of the most important reactions in chemical synthesis, but the hazardous nature of hydrogen has restricted its use. These microreactors have already eliminated the dangers associated with hydrogenation through the use of in-situ hydrogen generation and the handling of pyrophoric catalysts by filling them in sealed catalyst cartridges. This technology has been adopted by the leaders in the pharmaceutical, flavour and fragrance, fine chemical and agrochemical industries.

In case of Vapourtec microreactors four different adjustable temperature zones can be adjusted till 250 ° C. Recently the cooling is also solved even at –70 ° C. In this system maximum 50 bar pressure can be achieved. The reactor made of stainless steel, but it can be replaced by copper. The standard Vapourtec system controls temperature by blowing air around the reactor within the reactor manifold. Hot air is used to raise the reactor temperature, ambient air is used to cool it. With the new cooled reactor module, a dry ice heat exchanger is used to generate chilled nitrogen which is used to cool the reactor down to the low temperatures required. No external recirculating chiller is required, and the reactor temperature set point is completely programmable. Vapourtec has also developed the UV-150, a pioneering photochemical reactor that will lead to more efficient, precise, consistent, safe and scalable photochemical synthesis offering potential routes for novel compounds and building blocks together with possible new manufacturing processes [13].

Further significant representative of the microreactor technology is Chemtrix [14], Uniqsis [15], Corning [16] and the swedish Alfa Laval [17].

3. Examples for applied flow chemistry, application areas of microreactors

3.1. Phase transfer reactions in microreactor

The formation mechanism of slug and parallel flow was studied and the mass transfer performances of two flow patterns were compared by A. L. Dessimoz et al [18]. In order to define the reaction conditions and to design a microreactor system for a specific chemical transformation, detailed knowledge of the hydrodynamics in the microchannels is necessary. Controlled hydrodynamics allow the operator to decrease the pressure drop, to improve the mass transfer and to facilitate the product separation from the reaction mixture. The common modes of interface in the case of liquid–liquid two-phase flow are "slug flow" (Fig. 8A) and "parallel flow" (Fig. 8B). In the case of slug flow, two mechanisms are known to be responsible for the mass transfer between two fluids: (a) internal circulation takes place within each slug and (b) the concentration gradients between adjacent slugs lead to diffusion between the phases. In the case of parallel pattern, the flow is laminar and the molecular transfer between the two phases is supposed to occur only by diffusion [19, 20, 21].
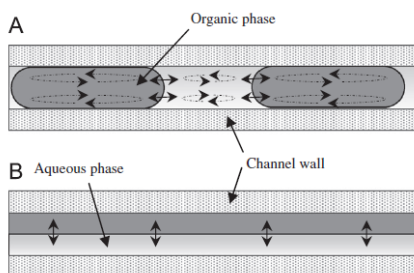
Figure 8. Types of liquid-liquid two-phase flow patterns in glass microreactors:
A: slug flow, B: parallel flow

3.2. Pharmaceutical researching

To develop a new generation of drugs, pharmaceutical companies need to be able to synthesise and screen novel chemicals with enhanced speed. A new technology that would enable a cost-neutral step change in the number of potential drug candidates would provide a distinct competitive advantage. Therefore the use of microreactors can facilitate substantial progress in slective drug testing. Indeed the miniaturisation of chemical reactors offers many fundamental and practical advantages of relevance to the pharmaceutical industry, who are constantly searching for controllable, information-rich, high-throughput, environmentally friendly methods of producing products with a high degree of chemical selectivity [22, 23, 24, 25].

3.3. Synthesis of organic and the hazardous compounds

A further research area is associated with organic chemistry, regarding organic chemical synthesis in microreactors. Microchannel reactor was used, for example, for the fast synthesis of acetic acid esters, including methyl acetate, ethyl acetate, *n*-propyl acetate and *n*-butyl acetate, etc [26, 27, 28, 29].

In addition, continuous technology enables the generation and immediate use of unstable or hazardous intermediates as well as the combination of many reactions in series to achieve multistep synthesis.

3.4. Solid phase and catalytic reactions

Despite the several favorable attributes of microflow reactors, the continuous use of solids remains challenging. The introduction of solids into a flow reactor is particularly difficult, since most pumps function poorly, even with small particulates, which in turn can result in channel clogging. Although the use of solids in flow has been the topic of a number of recent papers, they have focused on overcoming the challenges associated with the introduction and suspension of solid reagents and starting materials. An area that has received less attention is the continuous use of solid catalysts (and catalyst precursors) that only partially or slowly dissolve into or react with the solution [30, 31]. Recent developments in microreactor technology (MRT) are reviewed within the context of discovery, the development and commercialization of catalytic systems. Emerging trends and drivers for development of pilot plants and scale-up methods for the next generation of multiphase catalytic processes are presented by Patrick L. Mills et al. [32].

3.5. Microreactors in Refineries and the Energy Industry

Microreactors can be used in the refinery and energy sectors too. The acid-catalyzed esterification and transesterification reactions suitable for biodiesel production from high acid value oils face the problem of long reaction time. Peiyong Sun et al. developed a two-step process for fast acid-catalyzed biodiesel production from high acid value oil in a microstructured reactor [33].

The primary research efforts in the energy field are focused on fuel processing as a (potential) hydrogen source, mostly for distributed consumption through fuel cells. Catalyst development, along with reactor design and testing for the reforming and removal of carbon monoxide through water-gas shift, preferential oxidation, selective methanation and membrane separation are therefore under investigation. An increasing number of integrated complex micro-fuel processors has been developed for a large variety of fuels. The synthesis of liquid fuels, namely Fischer-Tropsch synthesis or methanol and dimethylether production from synthesis gas and biodiesel production is another emerging topic [34].

3.6. Miniaturised Total Analytical Systems in the biomedical field

Great research effort in the field of micro-scale devices has been made in the analytical field. One of the main aims of this kind of research is to develop a miniaturised total analytical system (μ-TAS). Optimally, such devices would automatically perform sampling, sample preparation, separation, detection and data processing in a fully-integrated manner.

In addition to the advantages of high, automated throughput and low reagent consumption with increased safety of operation resulting from low reagent quantities, these devices offer potential as remote controlled systems, which can be placed in inaccessible locations for the continuous monitoring of chemical or enviromental processes. To date the most popular area of μ-TAS research has been in the biomedical field [25].

3.7. Industrial application

In relation to the process intensification, two reactions, namely the Swern–Moffatt oxidation and the Claisen rearrangement, are discussed in detail by Volker Hesse et al. As a practical reaction example with industrial guidance of a running European Project on the epoxidation of vegetable oils, the new methodology is exemplified beyond the level of the organic chemists' descriptions given so far [35].

Summary

To conclude, microreactor chemistry is emerging and involves a promise to become a novel method on which to build a new chemical processing technology. With this device, comparable process conditions can be realized in the laboratory – allowing to optimize many parameters and conditions quickly – and in the production plant, with high flow rates and controllable safety requirements. The first experimental results from the industrial plant are expected to give reasonable reproducibility comparable to the laboratory plant. The equal-up design strategy and the consequent implementation of microstructures in the reactors easily allow for the enhancement of the throughput of the devices from laboratory- to production-scale without the risks and costs of the conventional scale-up procedure. In the near future, microstructured plants will help to yield laboratory data and information on the process and the plant, which can be directly transferred to the production plant. The established scale-up procedure with advanced simulation tools can successfully combine the miniplant with the pilot plant, and thus abridge one or two development phases. „This leads to an easy scale-up procedure, a more cost-efficient process development, and a shorter time-to-market period, however, the goal should be to use as many microstructures as necessary, whilst being economical, and to build them to a scale that is useful and manageable" [3].

The integration of microstructured devices with sensing and actuating elements, resembling the "macro world", will be one of the key issues for future development.

According to these information and in posession of an Asia liquid phase microreactor system, our research team in the Chemical Institute initiated scientific researches regarding the investigation and optimisation of liquid phase chemical synthesis – such as eserification reactions – in microreactor.

Acknowledgement

References

[1]   Hessel, Volker–Löwe, Holger–Müller, Andreas–Kolb, Gunther: *Chemical Micro Process Engineering Processing and Plants*. Wiley-VCH, 2005.

[2]   www.syrris.com/flow-products (download on Aug 20, 2014)

[3]   Kockmann, Norbert: *Transport Phenomena in Micro Process Engineering*. Springer, 2008.

[4]   Hessel, Volker–Löwe, Holger–Schönfeld, Friedhelm: Micromixers–a review on passive and active mixing principles. *Chemical Engineering Science* 60 (2005) 2479–2501.

[5]   Vörös, A.–Baán, Z.–Hermecz, I.–Mizsey, P.–Finta, Z: Mikroreaktorok alkalmazása szerves kémiai reakciókban. *Magyar Kémiai Folyóirat – Közlemények*; 117. évfolyam, 1. szám, 2011.

[6]   Löwe, H.–Ehrfeld, W.; State-of-the-art in microreaction technology: concepts, manufacturing and applications. *Electrochimica Acta* 44, 3679–3689. 1999.

[7]   Jahnisch, K.–Hessel, V.–Löwe, H.–Baerns, M.: Chemistry in microstrutured reactors. *Angewandte Chemie,* International Edition 43, 406–446, 2004.

[8]   Ehrfeld, W.–Hessel, V.–Löwe, H.: *State of the art of microreaction technology*, Microreactors: New Technology for Modern Chemistry. Wiley-VCH, Weinheim. pp. 1–14. 2000.

[9]   Lomel, S.–Falk, L.–Commenge, J. M.–Houzelot, J. L.–Ramdani, K.: The microreactor. A systematic and efficient tool for the transition from batch to continuous process. *Transactions of the Institution of Chemical Engineers, Part A, Chemical Engineering Research and Design,* 84, 1–7, 2006.

[10]   Kiwi-Minsker, L.–Renken, A.: Microstructured reactors for catalytic reactions. *CatasisToday*, 110, 2–14, 2005.

[11]   Schouten, J. C.: *Advances in Chemical Engineering Microsystems and devices for (Bio)Chemical Processes,* Vol. 38., Elsevier, 2010.

[12]   www.thalesnano.com (download on Aug 20, 2014)

[13]   www.vapourtec.co.uk (download on Aug 20, 2014)

[14]   www.chemtrix.com (download on Aug 20, 2014)

[15]   http://uniqsis.com (download on Aug 20, 2014)

[16]   http://corning.com (download on Aug 20, 2014)

[17]   http://www.alfalaval.com (download on Aug 20, 2014)

[18]   Dessimoza, Anne-Laure–Cavinb, Laurent–Renkena, Albert–Kiwi-Minskera, Lioubov: Liquid–liquid two-phase flow patterns and mass transfer characteristics in rectangular glass microreactors. *Chemical Engineering Science,* 63. pp. 4035–4044 (2008)

[19]   Burns, J.R.–Ramshaw, C.: The intensification of rapid reactions in multi phase systems using slug flow in capillaries. Lab on a Chip, 1, 10–15, 2001.

[20]   Dummann, G.–Quittmann, U.–Gröschel, L.–Agar, D. W.–Wörz, O.–Morgenschweis, K.: The capillary-microreactor: a new reactor concept for the intensification of heat and mass transfer in liquid–liquid reactions. *Catalysis Today,* 79–80, 433–439, 2003.

[21]   Kashid, M.N.–Gerlach, I.–Goetz, S.–Franzke, J.–Acker, J.F.–Platte, F.–Agar, D.W.–Turek, S.: Internal circulation within the liquid slugs of a liquid–liquid slug flow capillary microreactor. *Industrial and Engineering Chemistry Research*, 44, 5003–5010, 2005.

[22]   Watts, Paul–Haswell, Stephen J.; *Chemical Synthesis in Microreactors*. Microengineering in Biotechnology, Methods in Molecular Biology 583, Ş Humana Press, a part of Springer Science + Business Media, LLC 2010

[23]   Zhang, Ying–Chan, Hon Fai–Leong, Kam W.: Advanced materials and processing for drug delivery: The past and the future. *Advanced Drug Delivery Reviews*, 65 (2013) 104–120.

[24]   Stouten, Stefan C.– Wang, Qi–Noël, Timothy–Hessel, Volker: A supported aqueous phase catalyst coating in micro flow Mizoroki–Heck reaction. *Tetrahedron Letters*, 54 (2013) 2194–2198.

[25]   Fletcher, Paul D. I.–Haswell, Stephen J.–Pombo-Villar, Esteban–Warrington, Brian H.–Watts, Paul–Wong, Stephanie Y. F.–Zhang, Xunli: Micro reactors: principles and applications in organic synthesis. *Tetrahedron*, 58 (2002) 4735–4757.

[26]   Yao, Xingjun–Yao, Jianfeng–Zhang, Lixiong–Xu, Nanping: Fast Esterification of Acetic Acid with Short Chain Alcohols in Microchannel Reactor. *Catal Lett*, (2009) 132:147–152.

[27]   Lau, W. N.–Yeung, K. L.–Martin-Aranda, R.: Knoevenagel condensation reaction between benzaldehyde and ethyl acetoacetate in microreactor and membrane microreactor. *Microporous and Mesoporous Materials*, 115 (2008) 156–163.

[28] Kulkarni, A. A.–Zeyer, K. P.–Jacobs, T.–Kaspereit, M.–Kienle, Achim: Feasibility studies and dynamics of catalytic liquid phase esterification reactions in a micro plant. *Chemical Engineering Journal,* 135S (2008) S270–S275.

[29] Wirth, Thomas: *Microreactors in Organic Synthesis and Catalysis*. Wiley-VCH, 2008.

[30] Opalka, Suzanne M. –Longstreet, Ashley R.– McQuade, D. Tyler: Continuous proline catalysis via leaching of solid proline. *Beilstein J. Org. Chem,* 2011, 7, 1671–1679.

[31] Tseng, Chih Heng T.–Paul, Brian K.–Chang, Chih-Hung–Engelhard, Mark H.: Continuous precipitation of ceria nanoparticles from a continuous flow micromixer. *Int J Adv Manuf Technol,* (2013) 64:579–586.

[32] Mills, Patrick L.–Quiram, David J.–Ryley, James F.: Microreactor technology and process miniaturization for catalytic reactions – A perspective on recent developments and emerging technologies. *Chemical Engineering Science*, 62 (2007) 6992–7010.

[33] Sun, Peiyong–Sun, Juan–Yao, Jianfeng–Zhang, Lixiong–Xu, Nanping: Continuous production of biodiesel from high acid value oils in microstructured reactor by acid-catalyzed reactions. *Chemical Engineering Journal*, 162 (2010) 364–370.

[34] Kolb, Gunther: Review: Microstructured reactors for distributed and renewable production of fuels and electrical energy. *Chemical Engineering and Processing*, 65 (2013) 1–44.

[35] Hessel, Volker–Cortese, B.–Croon, M.H.J.M.de: Novel process windows – Concept, proposition and evaluation methodology, and intensified superheated processing. *Chemical Engineering Science*, 66 (2011) 1426–1448.

POLARIZATION CHARACTERISTICS OF TIN ELECTROREFINING IN CHLORIDE SOLUTIONS

GERGELY B. TÓTH[1]–MASAHITO UCHIKOSHI[2]–TAMÁS KÉKESI[3]

The refining electrolysis of tin in HCl media is a smart way to process valuable secondary resources produced by the use of tin-based soldering materials in the electronic industry. However, the structure of the cathodic deposit implies certain difficulties in continuous operation and the anodic processes also need clarification. We have focused on the kinetic behavior of the technically pure tin cathode and anode by performing potentiodynamic experiments in solutions of various Sn and HCl concentrations under stationary conditions and by applying varied stirring intensities. The presented diagrams demonstrate the critical influence of ion transport on the electrode processes, which determine the properties of cathodic morphology and anodic dissolution.

Keywords: tin refining, polarization, electrolysis, deposit structure, anodic dissolution

Introduction

An increased amount of scrap of higher tin concentration is generated from lead-free materials in the soldering technology used in the electronic industry. A novel and flexible method of processing the valuable scrap, usually containing tin metal and a few percent of silver and copper is hydro-electrometallurgical refining in aqueous solution, which offers the additional advantage of producing high purity tin in one step [1].

Acidic solutions are used for this purpose rather than alkaline ones, since their operation does not require high temperature, and the cathodic deposition takes place from divalent tin ions instead of tetravalent species, thereby consumes half as much electricity. Sulfuric acid based systems require expensive components and additives [1]. Hydrochloric acid solutions offer high solubilities [2] at low acid concentrations and higher stability in the absence of expensive additives. Furthermore, chloride salt crystals adhering to the cathode metal removed from the cell are eliminated during the final melting step. On the other hand, rough cathodic deposition structure still causes difficulties. The electrode processes are also hindered by chloro-complex formation [3]. When the crystals get in touch with the anode, short circuit arises and anodic slime directly contaminates the product. Organic inhibitors (glue, β-naftol, gelatin) have little effect on this system [3]. The application of periodically interrupted (PIC) or reversed (PCR) currents can provide an alternative for influencing the crystal structure [4]. Another practical approach is electromechanical systems applied for the cyclical compression of the cathodic deposit [5]. These

---

[1] University of Miskolc, Institute of Metallurgy and Foundry Engineering
 3515 Miskolc-Egyetemváros, Hungary
[2] Tohoku University
 Sendai, Miyagi, Japan
[3] University of Miskolc, Institute of Metallurgy and Foundry Engineering
 3515 Miskolc-Egyetemváros, Hungary
 kekesi@uni-miskolc.hu

methods are more efficient than organic inhibitor addition, but the implied sophisticated techniques cause technical difficulties at the industrial level. Therefore, the conditions of cathodic deposition and anodic dissolution should be optimized for possible applications in the industrial electrorefining of tin.

The basic structural type of the deposit is determined by the inhibition of the neutralized atoms to build into the structure of the cathode and by the overpotential [6]. The former is usually controlled by organic additives and the latter is represented qualitatively by the ratio of the current density and the concentration of the relevant metallic ions, as represented in Fig. 1.

(FI: Field oriented isolation, BR: Base reproduction, UD: Unoriented dispersion,
Z: Twin crystals, FT: Field oriented texture)

Figure 1. Types of polycrystalline cathodic depositions and orientations obtained at various overpotentials and inhibition intensities [6]

However, deposition morphology also depends on ion transport, since the concentration of the ions available at the cathode surface at a given current density depends on the supply by diffusion. Thus, potentiodynamic studies with solutions under various agitation rates are needed to find the most suitable conditions to get denser and finer cathodic deposits. The examination of the anodic process also bears importance, not just for the effect on the overall efficiency but also because the types of ions produced at the anode may influence the characteristics of cathodic deposition. The principally active species are the divalent tin ions, but the

$$Sn(IV) + Sn = 2 Sn(II) \qquad (1)$$
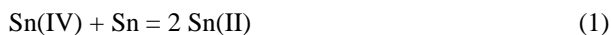
reaction can modify the shape of the deposited crystals and interfere with the principal cathodic process.

1. Experimental procedure

The potentiodynamic experiments were run with 1 and 2 M HCl solutions of 5–30 g/dm^3 Sn concentrations in 5 mV/0.5 s potential steps at room temperature. Short steps were applied mainly in the cathodic direction because of the rapidly changing conditions at the electrode surface. A glass adapter ending in a Luggin-capillary of ~ 1 mm diameter connected a saturated calomel reference electrode (SCE) to the center of the active working electrode surface. A computer with the IEMEAS 1.06 software recorded the current, supplied by an Electroflex EF 435C Potentiostat. The recorded potential values corresponded to the set program, however the actual working electrode potential was measured by a precision desktop multimeter, then manually recorded. The experimental setup is shown in Fig. 2.
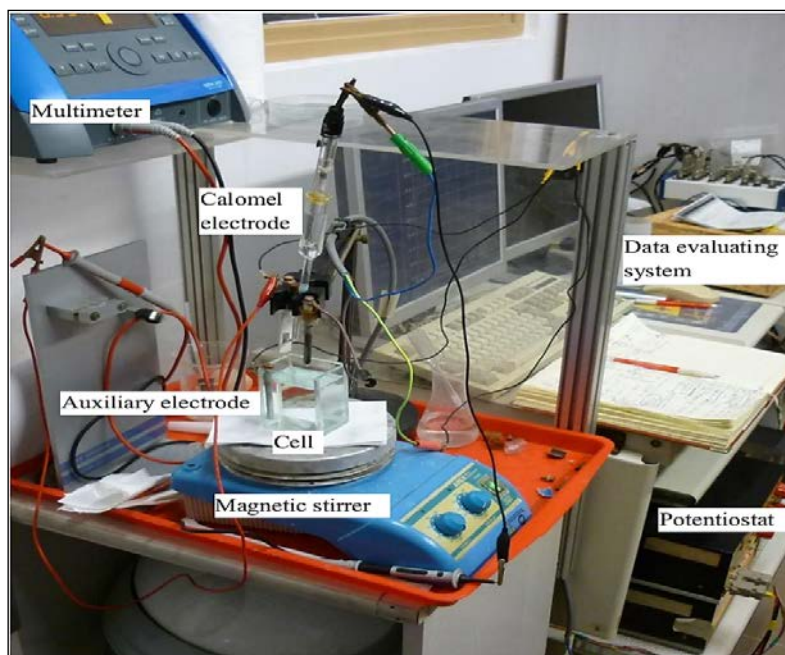
Figure 2. The apparatus used for the potentiodynamic experiments

Tin chloride solutions with at least 1 mol/dm^3 of HCl in the background would remain stable on the long run, if strong oxidative conditions are excluded [1, 7]. Lower acid concentrations have been shown to be sensitive to hydrolysis. Therefore, applying 2 mol/dm^3 of HCl may provide further improved solution stability and anodic dissolution, yet also entails a higher corrosion of the equipment and increased costs.

Measurements were performed with pure tin electrodes and also with 2 or 9% lead containing anodes. The solutions contained 1 and 2 mol/dm^3 of HCl and 0, 2.5, 5, 10, 20

and 30 g/dm^3 of Sn, respectively. Tin concentration was monitored with iodometric method and corrected whenever necessary. Sn(II) was the dominant oxidation state in the electrolyte solutions. The stirring speed was set at 0, 100, 200, 350, 500, 650 and 800 rpm. After and during each run, photographs were taken of the surfaces of the working electrodes. An extensive set of data with large spread was collected from about 1000 experimental runs and evaluated with Microsoft Excel with the help of algorithms developed in Microsoft Visual Basic.

In terms of cathodic measurements, it was hardly possible to construct the conventional overpotential-current polarization charts, due to the specific properties of the tin electrode in acid solutions. The depletion of tin ions at the active surface or the formation of loose deposit structures required special methods of evaluation based on the plots of the collected potential and current results against time and on the relevant images of the deposits.

2. Experimental results and discussion

Our results have been presented in uniform diagrams. The plotting area is headed by titles of the form: **X**(g)–**Y**(M)–**Z**(r), where **X** stands for the tin concentration (g/dm^3), **Y** gives the HCl concentration in (mol/dm^3) and **Z** indicates the stirring speed (1/min). The plotted currents density (*j*) is apparent, as it is expressed for the initial geometric surface area of the working electrode. The presented images of working electrode surfaces correspond to the relevant diagrams. Filled squares (■) denote apparent current density, filled triangles (▲) show the actual potential and empty circles (○) demonstrate the potential values defined by the program.

2.1. Cathodic deposition

Cathodic currents and potentials are considered negative, however the verbal discussion refers to the absolute values of these without repeatedly mentioning it. Figure 3*a* demonstrates that current density started rising steeply with a solution of 5 g/dm^3 Sn and 1 M HCl, along with the potential, but in a few seconds the tendency reversed and the value of the limiting current was reached.
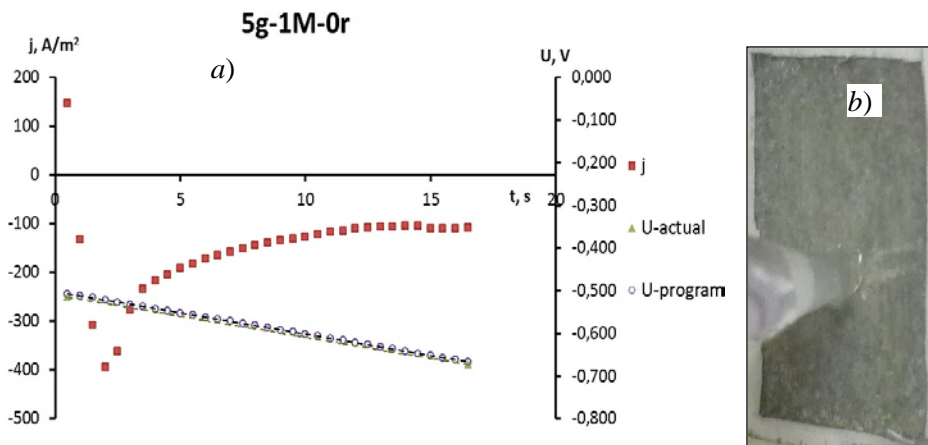

Figure 3. Potentiodynamic investigation in stationary solution of 5 g/dm^3 Sn, 1 M HCl

As the potentiostat shifts the potential from equilibrium in the cathodic (negative) direction, the resulting cathodic partial current density (i_{red}) of the

$$Sn^{2+} + 2e^- \Leftrightarrow Sn \tag{2}$$

electrode process varies according to the expression:

$$i_{red} = -2Fc_{Sn^{2+}} B \exp\left(-\frac{\varepsilon_{red}^{\neq} - \alpha_{red} 2F \eta_{akt}}{RT}\right) \tag{3}$$

where α_{red} is the charge transfer coefficient of the reduction step at the cathode, B is a kinetic constant, $\varepsilon_{red}^{\neq}$ is the activation energy of the cathodic reaction, F is the Faraday-constant, η_{akt} is the activation overpotential, R is the universal gas constant and T is the temperature [8]. The initial rise of the current is soon followed by a sharp decrease in Fig. 3 because the concentration of the active species ($c_{Sn^{2+}}$) on the cathode surface drops. This phase is followed by a flat section corresponding to the limiting current, determined by a stabilized surface concentration at the cathode supplied by the ion transport from the bulk solution.

Using as high as 30 g/dm³ Sn concentration, like in Figure 4*a*, that the initial current is followed by a short limiting current range of relatively high observed value. The limiting current density (i_{lim}) of the cathodic process can be expressed as:

$$\left| i_{lim} \right| = 2FD \frac{c_b}{\delta} \tag{4}$$

where D is the diffusion coefficient and δ is the diffusion layer thickness of the doubly charged active species of c_b bulk concentration. Accordingly, these limiting values are found approximately proportional to the tin concentration in the examined 5, 10, 20 and 30 g/dm³ Sn solutions.
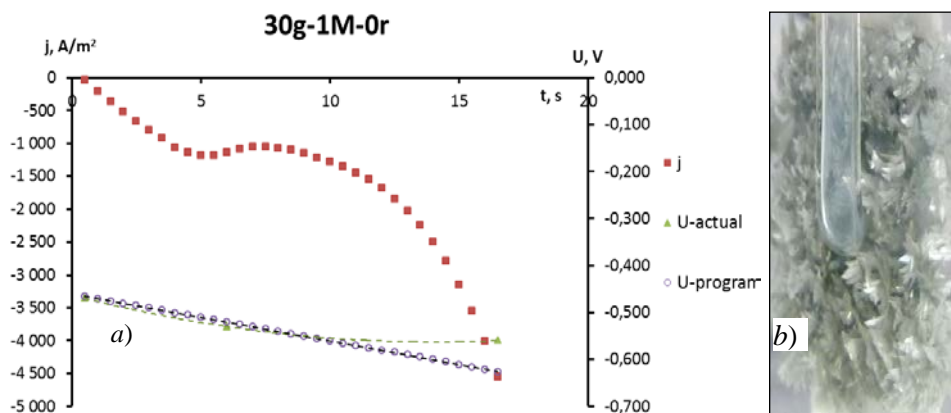

Figure 4. Potentiodynamic deposition in stationary solution of 30 g/dm³ Sn, 1 M HCl

However, at higher Sn concentrations, faster growing crystals tend to stick out of the diffusion layer and soon terminate the limiting range. This results in a second phase of current increase. With the loose morphology of the deposited metal and the dendrites growing distinctly, the actual cathode surface is greatly extending, especially at the beginning of the electrolytic process. Thus, the current – i.e. the plotted apparent current density – may increase more intensively than the effective current density. After the first few seconds, the potentiostat was obviously unable to increase the current with the proper pace required by the potential steps. The potential is controlled through an Ayrton-circuitry, which increases the current as long as the required potential is attained. As the surface area grows rapidly, higher current is required to reach the potential values according to the program. Therefore, the actual potential will lag behind the programmed value. This phenomenon, together with the current curve profile, clearly indicates the development of unfavorable deposit morphology. The long dendrites formed in this process are demonstrated in Fig. 4*b*.

If the tips of the crystals reach the anode surface, short circuits arise and particles from the anode slime may cause the contamination of the cathodic product. These conditions are to be avoided by enhancing the ion transport and reducing the tin concentration in the bulk solution, thus reducing the drop of tin concentration at the cathode surface.

A comparison of Figs. 5 and 4, demonstrates that by lowering the tin concentration (to ~5 g/dm^3) in the bulk solution and applying vigorous stirring one can significantly improve the conditions and a dense – acceptable – deposit structure can be obtained.
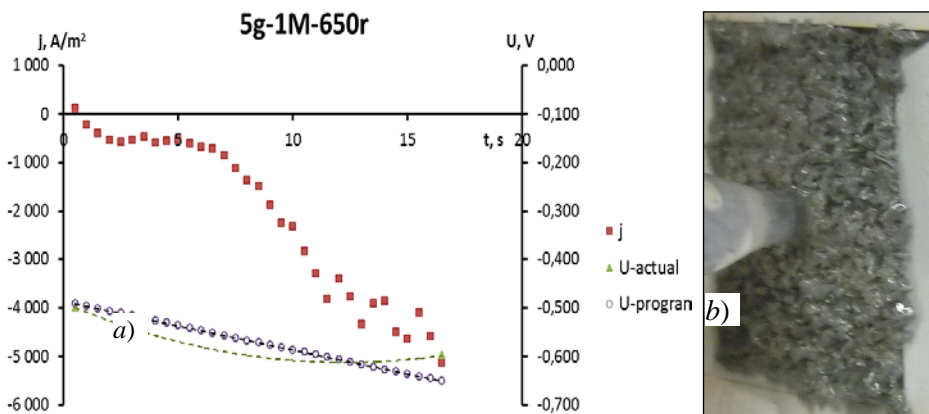
Figure 5. Potentiodynamic deposition in stirred (650 rpm) solution of 5 g/dm^3 Sn, 1 M HCl

As the crystals are less protruding, the current is not growing progressively with the potentiodynamic steps. A comparison of Figs. 3 and 5 demonstrates the significance of ion transport enhancement in a low tin concentration electrolyte. As the supply of ions to the cathode surface is more abundant, the crystals are not protruding far from the substrate and the surface is more evenly covered. However,

Fig. 6 shows that increased tin concentration and the maintainance of vigorous stirring cannot provide favorable conditions.
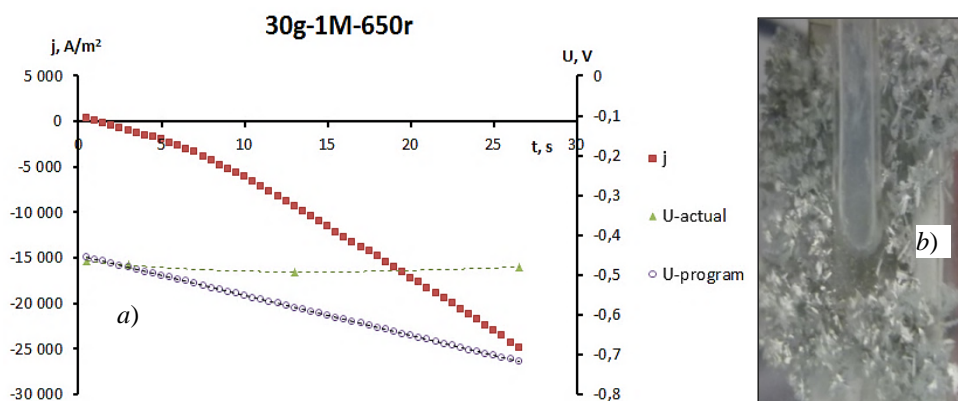
Figure 6. Potentiodynamic deposition in a stirred (650 rpm) solution of 30 g/dm³ Sn, 1 M HCl

Increased tin concentration allows for the growth of relatively large crystals, while the agitation of the solution cannot force deposition at sites between the long dendrite arms. Under these conditions the structure of the deposit became so rough and the actual cathode surface so large, that the current can be increased with very slight increase in the potential.

2.2. Anodic dissolution

Figure 7 shows the noticeably high current values measured in the vigorously stirred (650 rpm) solution of 10 g/dm³ Sn and 2 M HCl concentrations. We can see the thin slime layer appearing as a result of the high currents reached in short time. The potentiostat again, proved to be unable to produce the required potential steps – by the Ayrton-circuitry.
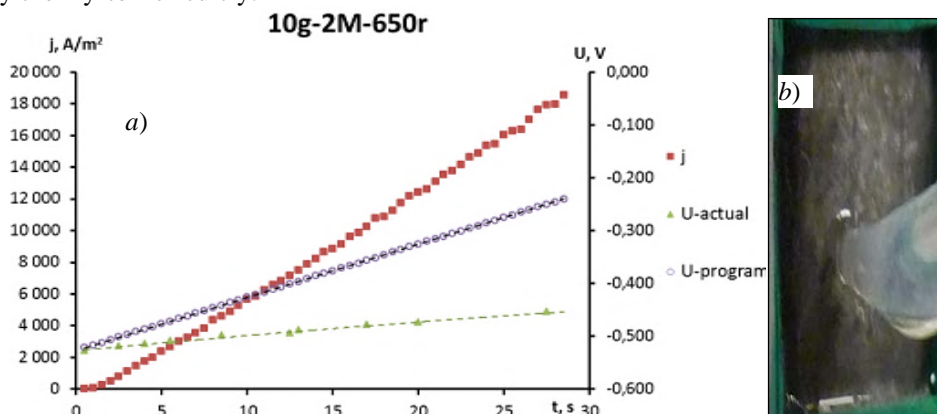
Figure 7. Potentiodynamic dissolution in a stirred (650 rpm) solution of 10 g/dm³ Sn, 2 M HCl

The anodic process could be examined with the surface of the working electrode left practically unchanged, therefore, standard type polarization curves could also be constructed from the results, as shown in Fig. 8.
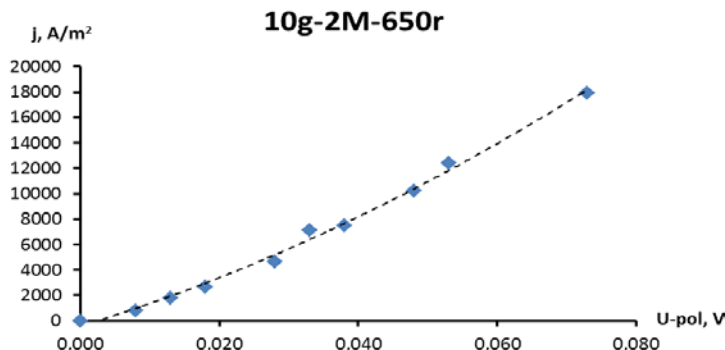
Figure 8. Anodic polarization curve in a stirred (650 rpm) solution of 10 g/dm^3 Sn, 2 M HCl

Raising the tin concentration to 20 g/dm^3 but omitting the agitation gives different results, as shown in Fig. 9*a*. The anodic current drops with the appearance of crystals (Fig. 9*b*) that block the anode surface. On the other hand, under these conditions the potentiostat can follow the programmed potential steps through the Ayrton-circuitry. During anodic dissolution, a concentrated layer of tin solution forms at the anode surface, particularly without stirring. After a certain time, the solubility of tin is reached, and a white tin chloride coating occurs (Fig. 9*b*) on the electrode, which was seen dissolving when stirred. Despite the surface cover formed in the stationary electrolyte, the rate of anodic dissolution might increase again at higher potentials. These conditions are, however, unfavorable because of the formation of Sn(IV) – according to Eq. (1) –, which can re-dissolve the tips of the cathode crystals and impede deposition, whereby hydrogen evolution might occur at the cathode surface.
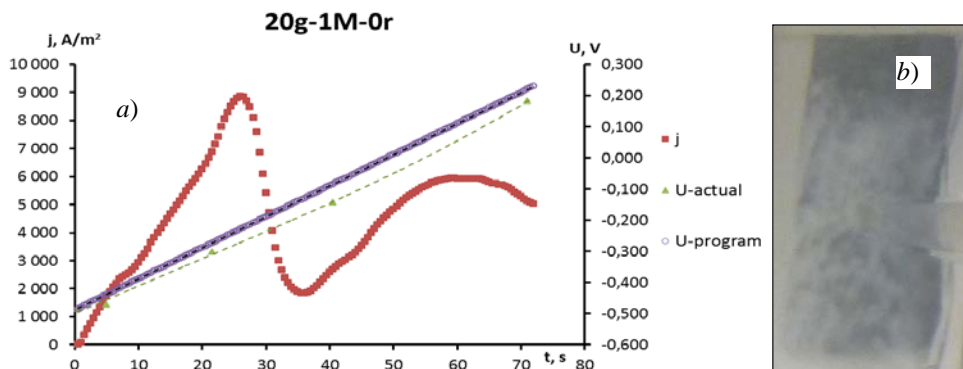
Figure 9. Anodic process in a stationary solution of 20 g/dm^3 Sn, 1 M HCl.

Examinations have shown that the change of the HCl concentration in the 1–2 mol/dm^3 range has virtually no effect on either the anodic or the cathodic process. With higher (20 g/dm^3) tin concentration in the solution, the introduction of vigorous stirring resulted in a continuous dissolution of the anodically polarized working electrode in a wide potential range, as shown in Fig. 10.
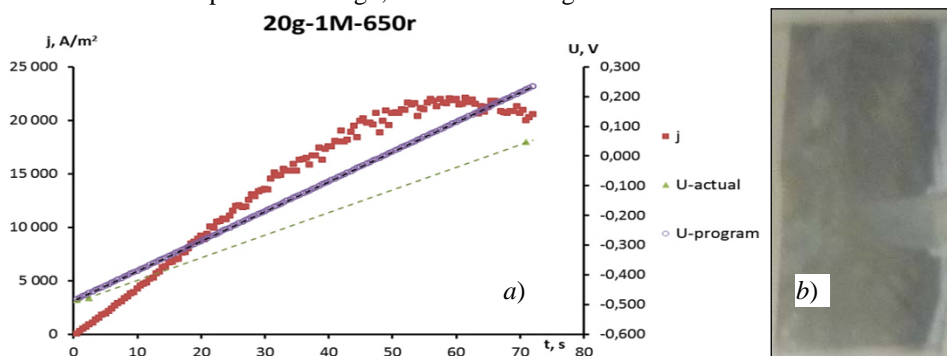
Figure 10. Anodic process in a vigorously stirred (650 rpm) solution of 20 g/dm^3 Sn, 1 M HCl

The dissolution of the anode is facilitated by lower tin concentration in the electrolyte. In comparison with Figs. 7 and 10, Fig. 11 demonstrates a fast increase in current density during the potentiodynamic run, while the potential is lagging behind the programmed steps.
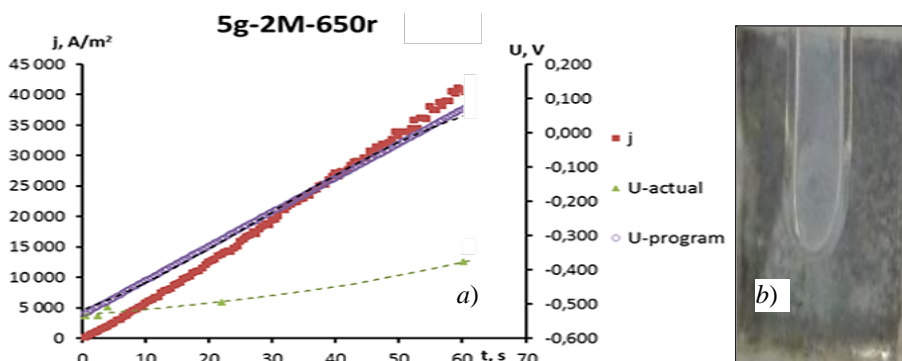
Figure 11. Anodic process in a vigorously stirred (650 rpm) solution of 5 g/dm^3 Sn, 2 M HCl

Despite the low concentration of tin in the bulk solution and the application of vigorous stirring, some precipitation of tin chloride could still be observed at the surface of the working electrode due to the extremely high anodic currents.

Since lead alloying may influence the dissolution of the anode, it has also been investigated. As compared to the pure tin anodes, lead content in the 2–9 % range was found to reduce the current density at similar overpotentials. Figure 12 shows

that by approximately 140 mV anodic overpotential (reached within 30 s from the start), the anodic current density was ~ 12 kA/m^2, whereas with pure tin anode (Fig. 11) it was about 18 kA/m^2 and the potentiostat generated ~ 50 mV anodic overvoltage at this point.
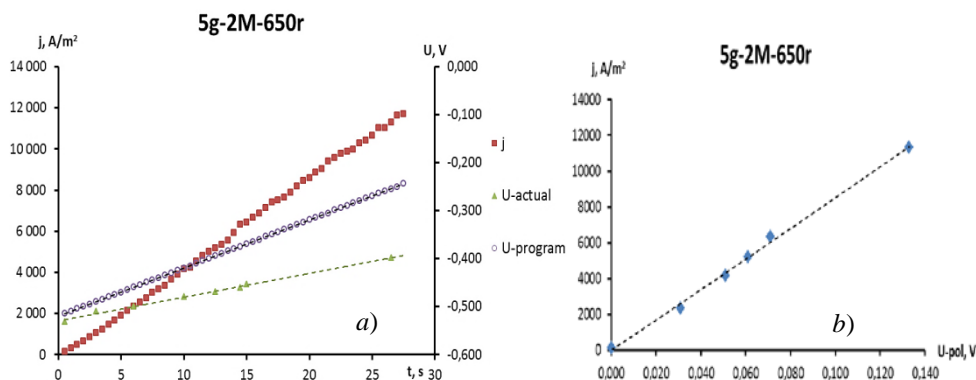
Figure 12. Dissolution and polarization of the Sn-9%Pb anode in vigorously stirred (650 rpm) solution of 5 g/dm^3 Sn, 2 M HCl

The alloyed anodes also produced a higher rate of precipitation at the anode surface due to the lower solubility of lead in the tin chloride – HCl solutions. Significantly higher anode potentials cause the formation of Sn(IV) ions at lower anodic current densities than with pure Sn electrodes, thus the cathodic process will also be adversely affected.

Conclusions

The potentiodynamic study of the cathode and anode processes highlighted the significance of tin concentration in the 5–30 g/dm^3 range, whereas the HCl concentration in the 1–2 mol/dm^3 range seemed to have little effect on the processes. The rough dendritic structure of the cathodic deposit reflects a slow ion transport in the electrolyte coupled with a fast electron transfer at the electrode surface. In order to avoid the formation of long protruding dendrites, the drop in tin concentration at the cathode surface has to be reduced. The deposit thus obtained can be relatively dense though easily removable from the substrate. Anodic dissolution also favors low tin concentration in the solution. Dissolution can be hindered by higher than 10 g/dm^3 tin concentrations in the bulk solution, and the oversaturation of the surface layer might produce chloride precipitates. Lead alloying noticeably deteriorates the conditions of anodic dissolution, for the required overpotential increases and the lower solubility of the lead species enhances the precipitation of chloride crystals at the anode surface. According to the interpretation of the potentiodynamic experimental results, the practical implementation of tin electrorefining in the chloride system is recommended at low tin and moderate HCl concentrations in an efficiently agitated electrolyte with controlled anode potential to avoid Sn(IV) formation. Although the crystals deposited at the cathode may not form a compact

deposit, the uneven growth of protruding dendrites can be suppressed through properly selected working conditions.

Acknowledgement

References

[1]   Rimaszéki, G.–Kulcsár, T.–Kékesi, T.: Application of HCl solutions for recovering the pure metal from tin scrap by electrorefining. *Hydrometallurgy,* 125–126 (2012) 55–63.
[2]   Stephen, H.: *Solubilities of inorganic compounds*, Vol.1, Pergamon Press, Oxford (1963).
[3]   Rimaszeki, G.–Kulcsar, T.–Kekesi, T.: The characteristics of electrolytic refining of tin soldering scrap in hydrochloric acid solutions. *Proc. 50th Annual Conference of Metallurgists – Waste Proc. and Recycling – VI,* Ed. Rao, et al., Montreal, Canada. 2–5 Oct. 2011, 137– 145.
[4]   Kulcsár, T.–Dobó, Zs.–Kékesi, T.: The Effect of Micro-impulse Current on the Morphology of Tin Electrodeposited from Chloride Solutions. *Materials Science Forum*, 752 (2013) 294–303.
[5]   Dobo, Zs.–Kulcsár, T.–Rimaszéki, G.–Kékesi, T.: *Programozott katódtömörítéssel és áram-vezérléssel működő berendezés forrasztási ónhulladék elektrolitos raffinálására és eljárás a megvalósításra*. Patent HU201100722-A2. 10-860957.*Szabadalmi Közlöny*, 14, 2012. 387–388.
[6]   Winand, R.: Electrocrystallization. *Hydrometallurgy,* 29 (1992) 567–598.
[7]   Rimaszéki, G.–Kulcsár, T.–Kékesi, T.: Investigation and optimization of tin electrorefining in HCl solutions. *J. Appl. Electrochem.* 42 (2012) 573–584.
[8]   Erdey-Grúz, Tibor: *Elektródfolyamatok kinetikája*. Akadémiai kiadó, Budapest, 1969.

ENERGY TAXATION: NOTES ON THE UNSETTLED LEGAL BACKGROUND OF A BIOMASS-BASED HEATING PLANT

ÉVA ERDŐS[1]–ORSOLYA RÓNAI [2]

Energy policy has always formed an integral part of EU legislation. In its new ('Europe 2020') economic-environmental strategy, the Community clearly sets the directions for the enhancement of an inclusive, advanced economy through technological innovation and a sustainable competitive energy policy relying to a great extent on renewable energy sources. Sharing the global concerns about declining fossil fuel resources (particularly of oils stocks), the European Union has multiplied its efforts to boost the establishment of a sustainable energy system based primarily on renewable energy. To meet this end, a radical shift is required – both in the Union's joint energy policy and in the behaviour of market actors (whether they be multinational companies or individual consumers). The range of applicable tools include financial, legal, political and social incentives, among them regulatory schemes already introduced in the Community's mid-term development strategy. From the standpoint of Financial Law, this paper primarily focuses on the implementation of these in the energy taxation regime.

Directive 2003/96/EC on energy taxation laid the foundations for the restructuring of the Community framework for the taxation of energy products and electricity. Since the time the Directive was adopted (27 October 2003), a number of ambitious policy objectives have been defined to tackle the challenges posed by climate change, declining energy supplies, market imbalances and related social problems. Therefore, substantial amendments to the 2003 Directive became necessary and inevitable.

In the light of the general criticism made by the Commission to the European Parliament and the Council, some of the most problematic questions of the Energy Taxation Directive are elaborated on in the following sections. Then, a case study is presented to give a closer look on taxation-related problems of sustainable energy use through the practical example of a biomass-based district heating system in its social context.

 Keywords: biomass, energy policy, energy tax directive, heating plant, renewable energy sources

Introduction

Rapidly dwindling fossil fuel reserves urge for a global shift to renewable energy sources (at the highest speed possible and to the highest achievable rate). Modern lifestye has been built upon the consumption of fossil energy, preeminently on oil, the diminishing resources and growing production costs of which definitely have negative consequences in several areas of life. Living costs are on the rise, casting serious doubts on the long-term capability of societies to finance their energy needs. These concerns have lead the decision-

---

[1] University of Miskolc, Faculty of Law, Department of Financial Law
   3515 Miskolc-Egyetemváros, Hungary
    jogerdos@uni-miskolc.hu
[2] University of Miskolc, Faculty of Law, Deák Ferenc Doctoral School
   3515 Miskolc-Egyetemváros, Hungary
   drronaiorsolya@gmail.com

makers of the EU to redefine the Community's energy policy and revise the Energy Taxation Directive issued in 2003.

The joint decision to overhaul the existing system of measures fully accorded with the opinion of the European Economic and Social Committee (hereinafter EESC) saying: "However painful it may be in short term, the price message conveyed by high levels of taxation on motor fuels has prepared European energy consumers for inevitable shortages and restrictions by promoting energy investment and economy efforts, the attractiveness and development of renewables, resistance to oil stocks…"

The proposed revisions to the Directive (Directive 2003/96/EC) aimed at creating incentives to promote sustainable development, preserve the environment, protect internal markets and stimulate market growth. It provides legal and financial tools to reduce labour-associated costs and budgetary deficits.

The correlation between energy taxation and renewable energy resources is made explicit in the cited EESC document.

This study was inspired by a multidisciplinary research[3] conducted since 2011 at the University of Miskolc with the joint participation of experts, professors and research professionals (from the fields of Materials Science and Technical Engineering, Humanities and Law) within the framework of a SROP[4] project. The aim of the two-year-long project was to develop a biomass-based district heating system in a small Hungarian settlement (Csernely) in Borsod-Abaúj-Zemplén county. Project feasibility analysis involved a detailed examination of the legal background and of the pertinent regulations of the national Civil Law. Solutions to potentially unsettled issues were suggested wherever necessary.

This explains for the dual structure of this paper: closely related to Financial and Community Law, the first part deals with recent modifications to the EU Energy Taxation Directive (in fact, to the whole taxation regulation scheme); the second part explicates a number of unsettled legal issues associated with the implementation of the mentioned biomass-based heating system in Csernely (Hungary).[5]

1. The EU energy taxation scheme and its revision

1. 1. Hungary's role in the development of the energy sector – before the 2004 accession

Within general process of legal harmonisation from the 1990s, the Hungarian Parliament has restructured and amended its national energy legislation. The general aim of regulatory reforms was to modernize the existing infrastructure of energy production and to encourage market competiton. To that end, most of the energy sector underwent privatisation.

Market positions are decisively influenced by energy prices. At the European level, increased competitiveness can be reached through the integration of national energy

---

[3] Erdős Éva is being a member of an interdisciplinary research team at the University of Miskolc (Faculty of Law, Civil and Political Sciences Institute) since 2011.
[4] This research was carried out as part of the TAMOP-4.2.1.B-10/2/KONV-2010-0001 project supported by the European Union, co-financed by the European Social Fund.
[5] Related to the project see also the special edition of *Magyar Energetika* 2012, in particular: OLAJOS István. A csernelyi biomassza fűtőmű-projekt jogi problémái. *Magyar Energetika*, 2012. Special Ed. pp. 20–24.

markets into a single, unified internal market. As regards the EU roadmap on the opening of national energy markets, two Directives have been adopted in 1997 and 1998, allowing for the free flow of electricity and gas between the Member States. The removal of trade restrictions on electricity in 2004 was soon followed by the liberalisation of the gas market. The strategic objectives towards a smart, sustainable and resource-efficient society include the rationalisation of energy use and the promotion of progress in energy savings. Top priority is given to the increased consumption of renewable energy forms (solar, hydro- and wind power, biomass, geothermal energy). Hungary has committed itself to follow this direction, reflecting the principles of energy saving and efficiency improvement in its energy strategy of 1999 (targeting the adjustment of national efficiency indices to the European average).

Preceding the year of Hungary's accession to the EU, the Community's share of renewable energies in gross final energy consumption reached slightly more than 6%, with a 14% share in the electricity sector. Directive 2001/77/EC, adopted on 27 September 2001, made it an imperative for the Member States to meet the targets of 12% and 22% to 2010, respectively.

In Hungary, the share of renewables in the national energy mix amounts to 3.6%, with a percent rate slightly hiher than 0.6 in the electricity sector. These figures are indicative of the country's limited potential on renewable energy use. At present, the largest contribution is made by hydropower generation, though there is considerable progress in biomass utilization and wind power technologies. A special biodiesel programme has been launched by the Ministry responsible for environmental sustainability and resource management.

During the period of 1998 to 2002, Hungary was actively involved in the Community Programmes targeting increased environmental awarness, the greening of economy and non-technological action on energy efficiency. A number of Hungarian stakeholders (companies, business enterprises, research institutions) committed themselves, in joint projects, to complete the developmental objectives drawn up in SAVE I–II and ALTENER framework programmes for intelligent energy use.

With the adoption of Directive 2003/96/EC, the Council of the European Union established minimum taxation rates for energy products (including coal, mineral oils, natural gas and electricity from renewable and non-renewable sources) – mandatory from 2004.

The joint demand for an EU-level consolidation of national taxation regimes and for the creation of a unified regulation scheme on energy taxation has long been on the agenda of the Community's energy policies. Nonetheless, the lack of common consensus and the conflict of interests between the Member States made it impossible to arrive at unanimous decision. Finally, it became obvious that the question was to be settled before the 2004 EU enlargement – partly to avoid market distortions caused by the low taxation rates applied by the newly joining States, partly to prevent endless negotiations with the increased number of participants (25 then 27). Directive 2003/96/EC came out as a compromise solution, setting minimum levels (instead of fixed rates) of taxation to be imposed on energy products by all Member States (including those who previously objected the proposal). Even with a number of allowances made (e.g. the application of partial or total exemptions or reductions, transitional periods provided for the implementation of measures etc.), the Directive was a crucial milestone in the harmonisation of national energy taxation systems at the EU level and it paved the way for the newly joined Member States to modernise and restructure their regulation schemes.

In order to guarantee the undisturbed functioning of the internal market, new Member States – among them Hungary and Slovakia – were allowed a transition period to adjust to the defined minimum levels (until no later than 2007).

If applied efficiently, taxation measures create proper legal incentives to realize the energy objectives of the EU. Considering that energy consumption accounts for more than 79% of global GHG (greenhouse gas) emissions, it seems reasonable that in the Europe 2020 strategy, the Member States are required to set national targets for improved energy saving and a cleaner, highly energy-efficient economy.[6]

1.2.   Directive 2003/96/EC (Energy Taxation Directive) – a brief review

In accordance with the relevant provisions laid down in the Articles of Directive 2003/96/EC adopted in 27 October 2003 in Luxembourg, the Member States shall impose taxation on energy products and electricity. For the purposes of the Directive, the list of taxable products are presented according to codes of the Combined Nomenclature. The range of energy products exempt from taxation is likewise specified. The Directive sets minimum levels of taxation to be imposed on energy products and electricity by the Member States, allowing the Member States, though, to exceed these fixed rates. The level of taxation is defined as "the total charge levied in respect of all indirect taxes (except VAT) calculated directly or indirectly on the quantity of energy products and electricity at the time of release for consumption" (Article 4, Paragraph 2).

A list of cases is specified by the Legislator in which the Member States, under fiscal control, may apply differentiated rates of taxation with respect to the minimum levels of taxation prescribed by the Directive and provided that they are compatible with Community law. Such cases are e.g. when the differentiated rates are directly linked to product quality; or particular uses like: local public passenger transport (including taxis), waste collection, armed forces and public administration, disabled people or ambulances (Article 5).

Member States can also freely give effect to exemptions or reductions in the level of taxation a) directly or b) by means of differentiated rate, or c) by refunding all or part of the amount of taxation (Article 6).

Article 7 and Table A of Annex I. determines the minimum levels of taxation applicable to motor fuels. As regards the scheduled implementation dates, from 1 January 2004 the minimum rate is EUR 2.6 (per gigajoule gross caloric value), which is left unchanged by the recast Directive in effect from 2010.

Minimum taxation levels applicable to products used as motor fuels for industrial and commercial purposes such as agricultural, horticultural or piscicultural works and forestry; stationary motors; plant and machinery used in construction, civil engineering and public works; vehicles intended for use off the public roadway or which have not been granted authorisation for use mainly on the public roadway are referred to as a separate item in Article 8. The reference value for natural gas (used as motor fuel) is EUR 0.3 (per gigajoule gross calorific value)[7].

---

[6]   Communication from the Commission to the European Parliament, the Council and the European Economic and Social Committee: 'Smarter energy taxation for the EU: proposal for a revision of the Energy Taxation Directive'. COM (2011) 168 final. *OJ/L/C 24/70, 2012.1.28.*

[7]   Table B of Annex I, Directive 2003/96/EC.

Heating fuels are also treated as a distinct category, with fixed minimum rates set. Thus, natural gas (for non-business use) is being charged EUR 0.15 (per gigajoule gross calorific value) and EUR 0.3 (per gigajoule gross calorific value) for business and non-business uses, respectively.[8] A separate Article (Art. 9) pertains to Member States, which from 1 January 2003 have been authorised to apply a monitoring charge for heating gas oil. These States may continue to apply a reduced rate of EUR 10 per 1000 litres for the respective product until repealment (of the authorization) by the Council for the prevention of trade distortion between Member States. As considers 'business use', it is identified in the Directive as "use by a business entity, which independently carries out, in any place, the supply of goods and services, whatever the purpose or result of such economic activities" (Article 11; Paragraph 1). Mixed uses are also regulated.

For those Member States who have not adopted the euro, provisions are set out for the consistent conversion of national currencies (i.e. the value of euro in national currencies to be applied to the value of the levels of taxation is being fixed once a year).

Member States shall exempt certain activities from taxation under conditions which they shall lay down for the purpose of ensuring the correct and straightforward application of such exemptions (and of preventing evasion, avoidance or abuse). These activities are, e.g.:

- energy products and electricity used to produce electricity and electricity used to maintain the ability to produce electricity;
- energy products supplied for use as fuel for the purpose of air navigation other than in private pleasure-flying;
- energy products supplied for use as fuel for the purposes of navigation within the Community waters (including fishing), other than private pleasure craft, and electricity produced on board a craft.

Without prejudice to other Community provisions, Member States may apply (under fiscal control) total or partial exemptions or reductions in the level of taxation. The exemption or reduction provided for the products may be granted under a multiannual programme by means of an authorisation (issued by an administrative authority to an economic operator) for more than one calendar year. The exemption or reduction authorised may not be applied for a period of more than six consecutive years. This period may then be renewed.

Provided the minimum levels of taxation are respected on average for each business, Directive 2003/96/EC retains the flexibility of tax rates on heating fuels (i.e. energy products used for heating or for other purposes determined by the Directive). Reference is made to the event of taxation rate change. In such cases, stocks of energy products already released for consumption may be subject to an increase, or a reduction of the tax. Member States may refund the amounts of taxation already paid on contaminated or accidentally mixed energy products sent back to a tax warehouse for recycling. (Articles 22–23)

The Directive coments on energy products released for consumption in a Member State, contained in the standard tanks of commercial motor vehicles and intended to be used as fuel by those same vehicles, as well as in special containers, and intended to be used for the operation, during the course of transport, of the systems equipping those same containers. These shall not be subject to taxation in any other Member State. (Article 24)

---

[8]   Table C of Annex I, Directive 2003/96/EC.

Article 25 is binding in a specific way inasmuch as it obliges Member States to inform the Commission of the levels of taxation (which they apply to the products listed in Article 2) on 1 January each year and following each change in national law. Member States shall inform the Commission about the measures taken in certain situations (such as tax exemptions, tax reductions, tax differentiation and tax refunds), which might constitute State aid and therefore have to be notified to the Commission (Articles 25–26).

Adopted by 15 Member States, the Directive entered into force on the day of its publication (31 October 2003) in the Official Journal of the European Union. The fact that the Energy Taxation Directive has been effective for more than 10 years properly justifies the need for revision.

1.3. Energy policy within the EU, renewable energy sources, the definition of 'biomass'

In fact, no explicit legal basis for the EU energy policy existed until the Treaty of Lisbon came into force (on 1st December 2009). Article 3 of the EC Treaty (TEC – Treaty Establishing the European Union) granted only for a limited scope of action in energy affairs. The lack of definitive contractual authority, however, did not preclude provisions for 'the establishment and development of trans-European networks of energy infrastructure' (as laid down in Article 170 = ex Article 154 of TEC).

In Article 194 of the Consolidated Version of the Treaty on the Functioning of the European Union, the following aims are defined for the Union's policy on energy:

- to ensure the proper function of the energy market;
- to ensure security of energy supply in the Union;
- to promote energy efficiency and energy saving and the development of new and renewable forms of energy[9]; and
- to promote the interconnection of energy networks,

with special regard for the need to preserve and improve the environment.

The Commission identified three target areas where urgent action is necessary, such as:

- to reduce the EU's energy dependency from non-EU sources,
- to ensure more competitive prices for energy products, and
- to enforce the realisation of environmental aspects in energy markets.[10]

The realization of these aims are impeded by the reluctance of the Member States to take coordinated actions and delegate their competence to the European Union to decide on energy prices, on the exploitation of domestic energy sources and other related energy policy issues.
Several EU Directives have been issued with the aim to promote cleaner and more effective energy technologies and to boost the utilization of alternative energy forms.[11] Within the

---

[9]   Renewable energy sources are e.g.: solar, wind, wave, tidal, geothermal, hydropower, biomass energy, methane from coal mining, energy products developed from fuel cells.
[10]   KRAMER, Ludwig.: *Az Európai Unió környezeti joga*. Dialóg Campus Kiadó, Budapest–Pécs, 2012, p. 377.
[11]   See: KRAMER, Ludwig: (2012) pp. 322

framework of "Intelligent Energy Europe" programme (from 2006), a range of financial instruments has been provided in support of renewables, energy efficiency and energy used in transport. Non-EU States were invited to jointly participate, thus, the average annual funding amounted to about 3 million EUR per State.[12]

In 1997, a White Paper on renewable energies was adopted by the Commission, targeting the massive penetration of renewables (from 6% to 12%) to 2010 in the Union's gross internal energy consumption. The overall political objective would obviously require a major input from the Member States, including a series of fiscal and financial measures like the differentiation of the prices of fossil and non-fossil fuels, product category labelling system, advanced research and development, financial support to eco-energy etc.

Still before 2001 and with reference to Article 194 Paragraph 1 of the TFEU, the Commission submitted a proposal for a Directive on the promotion of electricity produced from renewable energy sources, which was finalized and adopted in 2001 by the Council.[13] The provisions and regulations laid down in the Directive were to be implemented in the national legal orders of Member States no later than 27 October 2003. In order to ensure the increased market penetration of electricity produced from renewable energy sources, the Member States were required to set national indicative targets for consumption.[14]

For the assessment (by the Commission) of the progress made by the Member States in achieving national indicative targets, a report should have been published every 2 year (which included an analysis of success in meeting the national indicative targets and which indicates to what extent the measures taken were consistent with the national climate change commitment.) The Directive allowed Member States to use different mechanisms to support renewable energy sources at national level (e.g. green certificates, investment aid, tax exemptions or reductions, tax refunds and direct price support schemes). To facilitate trade in electricity produced from renewable energy sources, the guarantee of origin of such electricity was declared necessary.

The notion of biomass was defined by the Directive as:
"the biodegradable fraction of products, waste and residues from agriculture (including vegetal and animal substances), forestry and related industries, as well as the biodegradable fraction of industrial and municipal waste" (Article 2, Paragraph b) of directive 2001/77/EC).

Directive 2003/30/EC on the promotion of the use of biofuels or other renewable fuels for transport was likewise adopted in 2003. It gave conferred specific adventage on gaseous or liquid propellants produced from biomass for use in transport. To that end, the Directive obliged the Member States to set national indicative targets for the increased penetration of renewable sources (against petrol and gas) in gross domestic energy consumption. (i.e. A target of reaching a 5.75% share of renewables in the transport sector by 2010 was established.) The Member states were expected to report on the measures implemented every two year.

---

[12]   KRAMER, Ludwig (2012) pp. 323.
[13]   Directive 2001/77/EC of the European Parliament and of the Council on the promotion of electricity produced from renewable energy sources in the internal electricity market. *Official Journal of the EU,* 2001. 283/pp. 33.
[14]   KRAMER, Ludwig: (2012) p. 323.

The two directives were modified by a single new document issued in 2009 (Directive 2009/28/EC on the promotion of the use of energy from renewable sources)[15]. The new Directive established mandatory national targets for the share of renewables in gross final energy consumption and fixed the percent of energy generated from biofuels or renewable-based fuels in transport. The term 'energy from renewable sources' was defined (with reference to Directive 2003/54/EC) as: "energy from renewable non-fossil sources, namely wind, solar, aerothermal, geothermal, hydrothermal and ocean energy, hydropower, biomass, landfill gas, sewage treatment plant gas and biogases."

The definition of 'biomass' was further specified as: "*the biodegradable fraction of products, waste and residues from biological origin from agriculture (including vegetal and animal substances), forestry and related industries including fisheries and aquaculture, as well as the biodegradable fraction of industrial and municipal waste*" (Directive 2009/28/EC)[16].

Under Directive 2009/28/EC[17] on the promotion of the use of energy from renewable sources, a mandatory target of a 20% share of energy from renewable sources in overall Community energy consumption by 2020 and a mandatory 10% minimum target were to be achieved by all Member States for the share of biofuels in transport petrol and diesel consumption by 2020 (Paragraph 9 of Preliminaries to Directive 2009/28/EC).[18] Considering the fact that by 2005, only a minority of European states managed to increase their share to 15%[19], even today, the 20% target seems somewhat too optimistic. To ensure that the mandatory overall targets are reached, the Member States are required to establish a national renewable energy action plan and work out a forecast document (i.e. an indicative trajectory including information on sectoral targets and annual implementation reports). In case a Member State fails to meet the indicative trajectory within a period of two years, it was required by the Directive concerned to submit an amended national renewable action plan to the Committee (with the necessary and proportionate measures for improval) (Article 4). The Member States were given freedom to chose the most effective tools compliant with the objectives referred (and with the Community legislation). Directive 2009/28/EC has been criticised for the lack of specified penalties or sanctions imposable on Member States who do not implement the provisions set out in the regulation. In terms of enforcement, only vague references are made to Article 258 of TFEU (Treaty on the Functioning of the European Union) – which can hardly be considered satisfactory.[20]

As it is clearly outlined in the Commission Communication of 28 January 2012 (entitled 'Smarter energy taxation for the EU: proposal for a revision of the Energy Taxation Directive'), the EU itself has a series of demanding, legally binding climate and energy

---

[15] Directive 2009/28/EC of the European Parliament and the Council on the promotion of the use of energy from renewable energy sources. 2009 *OJ/L*/140/p. 16. & Ludwig KRAMER (2012) p. 324.

[16] Directive 2009/28/EC Article 2 Point e) *The term biomass is the same as the one in Directive 2003/96/EC (Article 16, Paragraph 1.) 'Biomass' means the biodegradable fraction of products, waste and residues from biological origin from agriculture (including vegetal and animal substances), forestry and related industries including fisheries and aquaculture, as well as the biodegradable fraction of industrial and municipal waste.*

[17] Directive 2009/28/EC.

[18] Kramer, Ludwig: (2012) p.324.

[19] E.g. Denmark, Estonia, Latvia, Austria, Portugal, Romania, Slovenia, Finland, Sweden. Ludwig Kramer: (2012) p. 324.

[20]   KRAMER, Ludwig: (2012) p. 325.

targets to be met by 2020. These are spelled out in the Europe 2020 Strategy defining the challenges that Europe is facing for the next decade, in economic, environmental and social areas and setting as a priority sustainable growth resulting in a more resource efficient, greener and competitive economy. Th strategy includes the commitment to bring energy taxation more closely in line with the EU's energy and climate change objectives.[21]

1.4. Smarter energy taxation for the EU: proposal for the revision of the Energy Taxation Directive

The new direction in the EU energy policy is clearly reflected in the Commission's repeated criticism on the Energy Taxation Directive.[22] In order to define the most problematic points of ETD, the Commission submitted a proposal for revision in 2011. The Directive was found to be defective inasmuch as it disregarded (i.e. failed to represent) the sustainability approach and gave false incentives, setting minimum target rates for energy products used as propellants (motor fuels) or heating fuels for electricity generation. The minimum rates were to apply to the volume of the energy product consumed.
The aforementioned problems raised a number of related issues, such as[23]:

- The current minimum rates based on the volume of energy products consumed do not reflect the energy content or the CO_2 emissions of the energy products, leading to inefficient energy use and distortions in the internal market.
- They also create incentives that are contradictory to the EU energy and climate change goals, as, for instance, they promote the use of coal as heating fuel.
- As regards to motor fuels, lower minima for diesel further reinforce the natural advantage that diesel has over petrol due to its higher energy content.
- These rates also discriminate against renewables, which are in principle taxed at the rate of the conventional fuel which they replace even though their energy content is lower.
- Moreover the current minima do not create a level playing field for business consumers, because, in practice, economic operators can be better off compared to others depending on the energy source they use.
- From an energy policy point of view, the Energy Taxation Directive provides no incentive or even price signal to promote alternative energies and encourage consumers to save energy. With taxation based on volume, ethanol is effectively the most heavily taxed energy product today. The same goes for energy sources used for heating, where coal is currently the least taxed energy source.
- From the point of view of the single market, Member States currently might not tax CO_2 emissions as such as they would like because it could put their business at a

---

[21]   Communication from the Commission to the European Parliament, the Council, and the European Economic and Social Committee: 'Smarter energy taxation for the EU: proposal for a revision of the Energy Taxation Directive'. COM (2011) 168 final. *OJ/L/C 24/70, 2012.1.28.*
[22]   Communication from the Commission to the European Parliament, the Council, and the European Economic and Social Committee: 'Smarter energy taxation for the EU: proposal for a revision of the Energy Taxation Directive'. COM (2011) 168 final. *OJ/L/C 24/70, 2012.1.28.*
[23]   Note that the date of reference of the following statements is 2011.

disadvantage or induce consumers to buy their fuel in lower tax Member States leading to revenue loss.

- This will encourage the consumption of energy sources emitting less CO_2 and reward more energy efficiency, in line with and supporting EU climate and energy policies. (Energy products with high energy content, such as diesel, LPG and compressed natural gas will continue to be attractive, but they will ultimately compete on fairer grounds, without an additional subsidy from taxation.)

2. Legal problems associated with the construction of a biomass-based district heating system in Csernely

Under Article 15 of Directive 2003/96/EC on energy taxation, biomass might be made tax exempt. Member States may apply (total or partial) exemptions or reductions in the level of taxation to biomass-related uses (as specified in the relevant paragraphs of the Directive).[24] Differentiated rates of tax can be charged on biomass-containing energy products, while electricity generated from biomass (or from products produced from biomass) can be fully exempted. Note should be taken, however, that a) the exemption or reduction in taxation resulting from the application of the reduced rates laid down in the relevant paragraphs may not be greater than the amount of taxation payable on the volume of the products referred to in the same paragraphs present in the products eligible for the reduction (Article 16, Paragraph 2); and b) the exemption or reduction in taxation appled by Member States shall be adjusted to take account of changes in raw material prices to avoid over-compensating for the extra costs involved in the manufacture of the products referred to in the aforementioned paragraph (Article 16, Paragraph 3).

As regards the possibility of applying a level of taxation down to zero, from 31 December 2012 it was to be repealed by the Commission. As a part of a multiannual programme authorised by an administrative authority prior to 31 December 2012, Member States may still apply the exemption or reduction after 31 December 2012 until the end of multiannual programmes (i.e. for a period no longer than six consecutive years). The respective period may not be renewed.[25]

The application of tax exemptions or reductions (as set by the Directive) would largely contribute to the feasibility of the Csernely project. Otherwise – as it is apparent from the example of Hungary's first biomass-based local district heating system implemented in Pornóapáti[26] – the costs of energy might get so high that local inhabitants would rather choose to disconnect from the system.

---

[24] See the presentation of NAGY Zoltán, entitled: Adómentességi kérdések az energia adózás területén" – at the conference on 'Sustainable Natural Resources' ('Fenntartható természeti erőforrások'). 12 October 2012. Published in: Jogtudományi tanulmányok a fenntartható természeti erőforrások témakörében (szerk. Csák Csilla), Miskolci Egyetem, Miskolc, 2012. pp. 131.

[25] Directive 2003/96/EC Article 15.

[26] In 2003, a heating plant of 5 MW capacity was put into operation in Körmend, covering about 70–75% of the energy needs of the town (via a district heating network). Approximately 2000 households and some public establishments are supplied from this plant. 6 tons of biomass per year is used for the operation of the plant, which is provided from the wood by-products of the small regional firms. A heating plant of 715 MW performance is operating in Szombathely, which generates electricity for heating and hot water for 2000 households. The first Hungarian biomass-heating plant was opened in

2.1. The advantages of biomass-based local heating

Prior to the enumeration of pending legal questions associated with the implementation of the Csernely project, the most decisive advantages of biomass-based district heating is demonstrated through the practical example of Pornóapáti, Hungary. Heating with biomass allows for the elimination of severe negative impacts made by fossil fuels on the environment. In this way, excess CO_2 emissions can be reduced to zero and considerable reductions can be achieved in atmospheric PM (particulate matter) concentrations.

Given the example of Pornóapáti, biomass combustion resulted in a substantial decrease in the annual amount of solid combustion residues produced from residential heating. Compared to 116 tonnes per annum of hazardous ash and slags left from conventional heating (i.e. with coal and wood), only 22 tonnes (per annum) of wood ash is obtained from biomass burning, most of which is recycled. The regeneration potential of biomass adds to the sustainability aspects of this fuel against other sources of energy – with special regard to fossil fuels, the finite stocks of which pose an increasing challenge to long-term global energy production. Another advantage of biomass-based district heating is the relative independence of the local community of the country's energy supply. Since electricity is obtained from locally generated woodchips and other biomass products, heating services and hot running water can be provided in-situ by the local supplier. This guarantees for stable, low-level prices (with no exposure to energy price fluctuations in the national/international markets) and for the retainment of the money invested in the region.

The operation of a biomass-fuelled heating plant can be considered as an economic driver in the creation and maintenance of workplaces. Local workforce is involved in income-generating activities, such as logging, chipping, transport and production. Social cohesion is further strengthened via the common concept of the plant as a joint property of the local community.[27]

Biomass basically derives from agricultural practice and woodworks. The feedstock material ranges from lower-quality by-products of logging and wood processing (chippings, cuttings, sawdust) to cultivated energy crops. In Hungary, about 1.5 million m[3] of cuttings (brown- and greencuts) are left in the forests, which is nearly 20% of the total harvested amount of wood. Hungary still has considerable unexploited potentials of biomass production. The estimated amount of economically harvestable woodstock is 4 million m[3] per year, of which only a limited ratio is actually extracted.[28]

High capacity biomass-fuelled boilers in Pornóapáti typically operate at a maximum flow temperature of 95 °C with a circulating water amount of 32.5 m3/h. A cabinet-like heating unit consisting of a heat exchanger and a circulating pump is being installed in the individual consumers' homes. The system is automatically controlled and equipped with an RMS module (remote monitoring system). The biomass feedstock is basically sawdust and

the autumn of 2005 in Pornóapáti. It was modelled on an Austrian commercial plant, however it functions less effectively.
Source (10 April 2012): http://fenntarthato.hu/epites/leirasok/települes/esettanulmany/pornoapati-falufutomu
27   Source (10 April 2012):
http://fenntarthato.hu/epites/leirasok/települes/esettanulmany/pornoapati-falufutomu
28   35.6 PJ is the energy content of the respective amount of wood. Source (10 April 2012):
http://fenntarthato.hu/epites/leirasok/települes/esettanulmany/pornoapati-falufutomu

organic woodchips (or other ligneous material unsuitable for industrial use) deriving from the adjacent wood processing plant. The boiler system supplies a network of 97 households and local establishments.

The Csernely project is generally based on the same model as the described heating system in Pornóapáti. There are, however, locally arising problems which need site-specific solutions. On the other hand, The Pornóapáti example does have its own weak points which sould preferably be avoided when actual construction/implementation takes place.

2. 2. Unsettled legal issues related to biomass-based district heating

There is sufficient resources (forest stands) available in Csernely to provide for heating wood supply. In theory, the continuity of supply could be maintained from biomass plantations established in the adjacent non-cultivated lands. In practice, however, the majority of these lands (estates) belong to unknown owners who moved abroad long before and thence have supposedly deceased. The unsettled legal status of these owners cause problems in the proceedings of succession and impede the lease of lands (by the proprietor) to the local government.

Under the given conditions, the following process shall be followed pursuant to Act XXXVIII of 2010 on probate proceedings:

a) Unknown heirs[29]:

In case personally identifiable information is partially or totally unavailable, the interested party is referred to as ʿunknown heir' and shall be served with summons to the probate proceedings via notification published by the Notary Public. Therein, the applicant is called upon to present his/her Claim Against the Estate to the Notary Public within 30 days from delivery of notification. Provided that within the respective period no valid claims against the estate concerned (in the probate) is being filed and the interested party neither applies for the estate concerned nor appears in the Probate Court, any further claim by the applicant shall be ignored by the Court. In case no other legal heir (or distributee) is known, the State of Hungary shall be entitled to the estate as distributee (under Article 599, Paragraph 3 of the Hungarian Civil Code). Under these conditions, a Public Notice shall be issued by the Notary Public, addressing any interested persons, who apply as claimants against the estate concerned, to present their claims ot file their petitions to the Notary Public within 30 days from publishment of the notice. At the same time, the Notary Public shall notify the State of Hungary (of entitlement to the estate) by submitting the same notification at the same time to the competent authority acting on behalf of the State. If within the period of 30 days, no claims or petitions are filed by interested parties, the Notary Public attests the entitlement and provides for the distribution of the estate to the State of Hungary.

Delivery of notifications are registered in the official computer records of the Hungarian Chamber of Civil Law Notaries. The data included in the public register are provided on request as ordained by the pertinent regulations. Any petitions submitted by persons other than the adressee (recipient) of the document delivered by notification shall be treated with

---

[29]   Act XXXVIII of 2010. Article 63, Paragraphs 1–2 and Article 64.

due discretion. Under such restrictions, information can be provided/disclosed to public or administrative authorities if it is necessary for the performance of their statuary duties or to the petitioner if it is necessary for the exercise of rights conferred by law to the respective person. In any case, the parties shall establish a legitimate interest therefor.

Conclusively, in case of unknown heirs, the State of Hungary shall be entitled as owner of the estate which can thereon be made subject of lease or sale to the local government (for purposes of wood logging or of the plantation of biofuel crops).

b) Heirs with whereabouts unknown:

Such cases are covered in Articles 58 and 59 of Act XXXVIII of 2010 on probate proceedings:

Delivery is effected by public notice in case the habitual residence of the interested party is unknown or registered in a State where delivery is not assisted. Notification shall be effective for 15 days from publication (by the Notary Public), delivery is considered accomplished at the end of this period. Legal implications to the public notice are effectuated upon entry in the official register of the Hungarian National Chamber of Civil Law Notaries. Notices are published via the publicly accessible electronic register of the National Chamber available free of charge for all citizens. The document to be delivered through public notification is to be posted on the notice board in the Office of the competent local authority of the last known address or (in abscence thereof) the place of residence of the interested party or (in abscence thereof) in the Office of the Notary Public responsible for the probate procedure. If within a fixed period from publication no application is made and provided that no other legal heir is known, the estate shall be distributed to the heir with whereabouts unknown.

The status of 'heirs with whereabouts unknown' is a source of legal and administrative problems in that these persons can be identified and entered as owners (of the property concerned) in the Land Register (or Estate Registry), yet cannot be located and contacted by the local authority as lessee. Following the entry of the owner in the Land Register (or Estate Registry), application for lease shall follow/falls under a different procedure.

Another critical issue affecting all municipalities with biomass-based heating systems is the unsolved problem of "goods-for-service" transactions, namely the exchange of harvested biomass (woodchips) for district heating services. Under Act CXXVII of 2007 on Value Added Tax, neither payment allowances nor exchange transactions of this type are authorized. Within the general provisions laid down in the pertinent regulation, the price of woodchips harvested by the local inhabitants can in no way be included in the heating costs. On the other hand, district heating services, thus the production of heat from renewable energy sources are (among other goods and services) subject to a reduced VAT rate as listed in Schedule No. 3 to Act CXXVII of 2007. This means that the VAT to be charged on district heating services from biomass-based heating plants is 5% (instead of 27%) of the taxable amount – which is financially advantageous for the Csernely project. Woodchips provided on a regular base for commercial purposes is regarded by the rule as commercial activity, therefore it is subject to/falls under normal VAT rates (27%). The two transactions concerned, namely local biomass supply and local district heating fall within the terms of 'supply of goods and services' under the Act on VAT, and are therefore

excluded from the category of exchange transactions. Given the above, the supply of woodchips in Csernely can not contribute to the reduction of heating costs.

The next recurrent problem to renewables-based district heating systems is the official pricing of connection fees.[30] Administrative prices are a tool for price control and are assigned a positive role in market regulation, nonetheless, they add to the costs of renewables-based services. This could be overcome by the authorisation of lower price rates for energy provided from renewable sources. The pursuant Law allows for that option.[31] The application of administrative prices mean the direct intervention of pricing authorities in market price conditions. In such cases, the price of goods and services listed in the Annex(es) of the pursuant Act are maximized by the pricing authorities – allowing, though, for the application of lower prices. In case minimal price rates are set by the authorities, these shall be regarded as reference rates in contracting. Given that the target rates (for connection fees) are fixed regardless of the fuel source, the regulation applies for biomass-based heating systems as well. In terms of connection fees, the aforementioned regulations might adversely affect competitiveness. If administrative prices imposed on district heating are too high, it might avert consumer preferences to the use of conventional fuels (gas, wood, coal). Obviously, any increase in the consumption of fossil fuels is undesirable and avoidable, since it exerts further environmental loads and directly counteracts the sustainability goals set in the Community's long-term strategy.

Conclusions

The Csernely project (on the establishment of a biomass-based local heating system) is a progressive step towards a cleaner, sustainable future economy. It is a justified demand on the part of the stakeholders that the legislation applicable to the implementation of the project be consistent with the strategic objectives of the Europe 2020 programme and give preference to activities and investments targeting the market uptake of renewables and advanced innovative technologies. This paper gives a non-exhaustive overview of legal problems arising from inconsistencies in the regulatory framework the investment project should comply with. In order to better assess the expected positive and negative impacts of

the enterprise and to evaluate the major legal-economic drawbacks, comparisons are drawn to a similar project already realized in Pornóapáti. By identifying the critical points and suggesting possible solutions to these, the authors try to contribute to the success of the decision-making process.

Acknowledgements

---

[30] See Act LXXXVII of 1990 on the determination of prices. The charges imposed on natural gas systems are set by administrative pricing, just like the charges on electricity. See also Article 103 of Act XL of 2008 on the supply of natural gas.

[31] See Articles 7 to 18 of Act LXXXVII of 1990. If administrative prices are fixed in a contractual transaction, prices higher than the highest price and prices lower than the lowest price cannot be legitimately applied.

References

[1] OLAJOS István: A csernelyi biomassza fűtőmű-projekt jogi problémái. *Magyar Energetika*, 2012, Special Issue 20–24.

[2] *Communication from the Commission to the European Parliament, the Council, and the European Economic and Social Committee: Smarter energy taxation for the EU: proposal for a revision of the Energy Taxation Directive*. COM (2011) 168 final. *OJ/L/C 24/70, 2012.1.28.*

[3] Annex I., Table B. Directive 2003/96/EC.

[4] Annex I., Table C. Directive 2003/96/EC

[5] KRAMER, Ludwig: *Az Európai Unió környezeti joga.* Dialóg Campus Kiadó, Budapest–Pécs, 2012, 321–325, 377.

[6] Directive 2001/77/EC of the European Parliament and of the Council on the promotion of electricity produced from renewable energy sources in the internal electricity market. *Official Journal of the EU*, 2001. 283 pp. 33.

[7] *Directive 2009/28/EC of the European Parliament and the Council on the promotion of the use of energy from renewable energy sources.* 2009 *OJ/L*/140/p. 16.

[8] NAGY Zoltán: Adómentességi kérdések az energia adózás területén. Conference proceeding in the conference of „A fenntartható természeti erőforrások." 12 October 2012, Miskolc In: *Jogtudományi tanulmányok a fenntartható természeti erőforrások témakörében* (szerk. Csák Csilla), Miskolci Egyetem, Miskolc, 2012.

[9] http://fenntarthato.hu/epites/leirasok/település/esettanulmany/pornoapati-falufutomu

[10] Act XXXVIII of 2010. Article 63 Paragraphs 1–2 and article 64.

[11] Act LXXXVII of 1990 on the determination of prices.

.